ScuDo
Scuola di Dottorato ~ Doctoral School
WHAT YOU ARE, TAKES YOU FAR

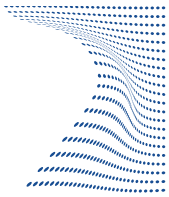

Doctoral Dissertation
Doctoral Program in Energy Enginering (33.th cycle)

Multiscale approach applied to fires in tunnels

Model optimization and development

Jesus Alberto Mejias Tuni
* * * * * *

Supervisors
Prof. V. Verda, Supervisor
Prof. E. Guelpa, Co-supervisor

Doctoral Examination Committee:
Prof. Tartarini, Paolo; Referee, Università degli studi di Modena e Reggio Emilia
Prof. Rein, Guillermo; Referee, Imperial College of London
PhD. Gissi, Emanuele; Corpo Nazionale dei Vigili del Fuoco
Prof. ; Politecnico di Torino
Prof. ; Politecnico di Torino

Politecnico di Torino
February 28, 2022

I hereby declare that, the contents and organisation of this dissertation constitute my own original work and does not compromise in any way the rights of third parties, including those relating to the security of personal data.

. . . . . .

Jesus Alberto Mejias Tuni
Turin, February 28, 2022

Summary

Tunnel fire simulations are a constant topic in the literature, where through CFD (computational fluid dynamics) simulations the distribution of the temperatures and other properties in a fire can be calculated, giving information capable of improving the performance of tunnel ventilation and emergency management systems, among others. But tunnels are domains difficult to simulate, due to their length, consuming high amounts of calculation time and resources. Still this disadvantage can be mitigated by using multiscale models.

Multiscale modelling are a kind of CFD simulation where the simulation is divided into two submodels, one to simulate in 3D and other in 1D. The 3D model simulates the more complex part of the domain, the zone close to the fire, and the 1D model simulates the distant areas, where the flow is almost homogeneous. The objective of using these two models together is to save calculation time, as 1D simulations take only a small fraction of the time consumed by 3D modelling, obtaining accurate results, as the 3D manages the more complex areas.

This work continues the development of a multiscale model that uses FDS as its 3D algorithm and Whitesmoke to calculate the properties distribution in the 1D part of the domain. The model exploits the best capabilities of each one of the two submodels and connects and compile them together in Fortran language.

The main goals of this thesis are to improve the multiscale model that has been in development in Politecnico di Torino in the last years. This improvement include: changes to the compilation to guarantee shorter calculation times, modifications to the boundaries to respect the conservation laws in the boundaries, changes to the exchange of data among the models to minimize perturbations due to their interaction and verification of the pressure calculating capabilities of the simulations.

The results of this work are divided among four chapters:

Chapter 3, shows the capabilities of the multiscale to reduce the calculation time needed to complete tunnel fire simulations. The tests in the chapter use a small theoretical tunnel as test case and simulate a small fire (2 MW). The tests results exhibit a simulation time reduction that is proportional to the percentage of the domain simulated into the 1D.

Chapter 4, Examines FDS tunnel fire simulations and compares them to Fluent and FDS heat source simulations finding that the pressure presented some inconsistencies.

An equivalent model was developed to calculate an accurate pressure field using the other properties provided by the FDS. The pressure results of this model where compared with the other reference simulations proving that the properties obtained from FDS were correct, but there was some source of error accumulating in the pressure.

Chapter 5, shows testing regarding the pressure model of the FDS. Reporting that changes in the pressure solver of the FDS were capable of giving better results to the simulations. Simulations modelling the Dartford tunnel were capable of demonstrating that using UGLMAT was capable of guaranteeing better pressure results across the tunnel

Chapter 6 includes multiscale simulations compared to a tunnel fire test in a 2600 meters long tunnel and FDS simulations in the Dartford tunnel.

In the first tunnel, the simulations show trends similar for all the measurements and maintain a low error for anemometer measurements and thermocouples 30 and 130 m away from the fire, demonstrating that the multiscale model is capable of reproducing a real life fire test.

In Dartford, the multiscale is compared to FDS simulations. The trends along the tunnel and in 5 sections of the tunnel are analyzed, showing the same behavior and values as the FDS curves, with low error in some regions of the tunnel, and pressure curves that were more steady than the ones observed in FDS. This tests confirm the capability of the multiscale model of simulating long tunnels without introducing important sources of error.

Acknowledgements

I would like to acknowledge the work of my supervisors, Vittorio Verda and Elisa Guelpa (advising me during my research and helping me when i got lost sidetracking), to my reviewers, Guillermo Rein and Paolo Tartarini (for their feedback on my work), and the rest of the committee (for letting me borrow a bit of their time for my dissertation). Also an special thanks to the people at NIST in Gaithersburg, among them, Randall McDermott, Marcos Vanella, Kevin McGrattan and Glenn Forney, who helped me in my stay at NIST and taught me a lot about research, physics and programming.

In a more personal note, I would like also to express my gratitude for my co-workers during this years. Sara Cosentino (Who started the work on this multiscale model), Alberto Pizzolato (A very nice and helpful workaholic), Ludovica Marincioni (An excellent partner at work and at the gym), Martina Capone (The best assistant teacher the world could have), Umberto Tesio (A Very talented researcher and memeologist), Giulia Mancò (Unsure of herself, but unBeelivably talented), Sofia Russo (A great source of reassurance and peace), Manfredi Neri (Excellent worker, capable of getting in other person Shoes), Elisa Guelpa (Another nice workaholic that also has an older sister vibe) and Vittorio Verda (An excellent supervisor, worker, runner, swimmer, cook, etc.).

I would like to dedicate this thesis to my family and coworkers that have always helped and supported me.

Contents

List of Tables

List of Figures

Chapter 1

Introduction

1.1 Fires in tunnels

A fire can be defined as ”an unwanted or uncontrolled combustion process characterized by heat release and accompanied by smokes, flames or glowing” according to the PIARC[55]. Fires in tunnels are exposed to a confined environment, increasing the amount of variables involved in the behavior of the flames. These variables include the fast heat feedback received by the fire from the gas and walls surrounding it (capable of rising the fire intensity), and the limited availability of oxygen (capable of increasing the health risks linked to incomplete combustion and the production of carbon monoxide).

The interest surrounding the fire and risk management in tunnels has grown over the last decades after terrible accidents have been seen in European tunnels, as the Gotthard tunnel (2011) [53], the Frejus tunnel (2005), and other tunnels around the world, as it is listed by the National Academy of Sciences [50]. The concern about this subjects should increase in the future considering the growing amount of kilometers of tunnels, as shown by De Mulder[18], and the rising quantity of vehicles circulating in Europe, as observed in the statistics presented by the European Automobile Manufacturers Association [3].

1.1.1 Review on Tunnel fire accidents

The concern focused in tunnel fires is centered in catastrophic events, as it was mentioned in the previous section. The data extracted from different sources regarding tunnel fires [50, 4, 36] are synthesized into the Table 1.1, showing some severe fire incidents in tunnels occurred in the last decades. The incidents shown are the ones considered more relevant, due to the amount of victims or damages they caused to the tunnel structure. In the table can be observed that the consequences of each tunnel fire differ substantially. Many factors influence the aftermath of tunnel fires, among the factors the stronger ones are the amount and type of vehicles (buses, sedans, tankers, cargo trucks, among others) involved in the accident, the amount of people present, the

tunnel infrastructure, the ease of access for the firefighters and the speed of response to the fire.

Year	Tunnel	Consequences
1949	Holland, USA	66 injured, more than 20 cars involved, serious tunnel damage.
1979	Nihonzaka, Japan	7 deaths and 2 injured, more than 160 cars involved in a 159 hours fire with serious tunnel damage.
1982	Caldecott, USA	7 deaths and 2 injured, 8 vehicles involved, and serious structural damage
1982	Salang, Afghanistan	more than 700 deaths in a tanker explosion in a tunnel transited by russian soldiers
1983	Pecorila, Italy	9 deaths and 22 injured, 10 vehicles involved and limited tunnel damage
1993	Serra Ripoli, Italy	4 deaths and 4 injured, 16 vehicles involved and limited tunnel damage
1999	Montblanc,France/Italy	39 deaths, more than 30 vehicles involved, resulting in the closure of the tunnel for 3 years
1999	Tauern, Austria	12 deaths and 49 injured, 40 vehicles involved and 3 months of tunnel closure.
2001	Gotthard, Switzerland	11 deaths , 25 vehicles involved and serious tunnel damages.
2003	Baregg, Switzerland	2 deaths and 21 injured, with 7 vehicles involved and serious damages to the tunnel
2005	Frejus, France/Italy	2 deaths and 21 injured, 4 cargo trucks involved, and consequent tunnel closure
2007	Santa Clarita, USA/Canada	3 deaths and 23 injured, more than 30 tractors involved
2010	Wuxi Lihu, China	24 deaths and 19 injured, involving 1 shuttle bus
2014	Yanhou, China	31 deaths, involving 2 tankers and other 40 vehicles

Table 1.1: Historic tunnel fire accidents of the last decades

The next subsections include the descriptions of the events in some of the tunnel fires in the Table 1.1, with information extracted from the PIARC publication [54].

Nihonsaka tunnel, Japan (1979)

The tunnel is composed of 2 unidirectional 2km tubes. The accident originally started as a rear-end collision that involved 4 trucks and 2 cars. The fixed deluge sprinkler

system installed in the tunnel was capable of controlling the fire, but after some time the contents of some of the trucks started catching fire, producing a fire that would require more than two days to be brought under control and approximately a week to extinguish. The semi-transverse ventilation system, present in the tunnel, was unable of exhausting enough smoke and gases to guarantee an optimum environment where the firefighters could work.

Caldecott tunnel, USA (1992)

The tunnel was composed at the time of 3 tubes of 1.1 km of length approximately. The fire occurred in the third and northernmost tube when a driver under the influence of alcohol lost the control of his car crashing against the tunnel and producing an incident with an empty bus and a gasoline tanker, with more than 30000 liters of gasoline. The emergency measures for the extinction of this fire took 75 minutes to start, and approximately 3 hours to extinguish the fire, due to lack of preparation and difficulty to find a source of water as the fire fighting connections in the vicinity where non-functional.

Mont Blanc tunnel, France/Italy (1999)

The tunnel is composed by a single tube with two lanes in each direction, with a length of 11.6 km. The fire started in a truck transporting 9 tons of margarine and 12 tons of flour that was in front of other 13 trucks also transporting goods. The trucks were at 6.5 km of distance from the french portal making it difficult for the fire-fighters to reach the fire, also losing two water tenders inside the smoke during the extinction labors. The ventilation in the tunnel worked at its maximum output, having the downside that it gave more oxygen to the fire to increase its heat output and increased the danger in the vicinity of the fire due to the smoke and temperatures. Some incompatibilities in equipment used by the firefighting services of the two portals and communication problems among the services were registered during this incident. In the end the tunnel was severely damaged and had to remain closed for 3 years.

Tauern tunnel, Austria (1999)

The Tauern tunnel is 6.4 km long, composed by one tube at the time of the fire. The fire started 800m away from the north portal where some roadworks where placed and a queue of cars and trucks formed. One articulated truck failed to stop and crashed against the queue, resulting in some cars instantly catching fire. Afterwards the fire would spread to a total of 16 trucks and 24 cars. The transversal ventilation system placed in the tunnel was used to keep the back-layering at bay, but after 15 minutes the fire release rate went over the capability of the ventilation system, the firefighters had to withdraw and then it took close to 17 hours to extinguish the fire, with damages to the tunnel and 16 trucks and 20 vehicles consumed by the fire.

Gotthard tunnel, Switzerland (2001)

Is a tunnel composed by one bidirectional tube 16.5 km long. The fire was caused by an inebriated driver in a articulated truck, as he steered his truck into the opposing direction lane causing a frontal crash with another truck driving in the contrary direction. The two vehicles caught fire which expanded to the fuel tank of both trucks and the cargo they were transporting. The load of one of the trucks consisted of car tires having as a consequence the release of heavy smoke through the tunnel. The fire managed to consume 7 trucks and the smoke produced by it took the life of 11 victims. It took 10 hours to control this fire, and caused severe damages to the tunnel ceilings and electrical installations.

Nowadays, the vast majority of the tunnel fire incidents are smaller events that are controlled with more efficacy due to the normative and safety measures that tunnels have incorporated with the passing of the years. Still, every fire has some potential to develop into a severe incident if they are not handled promptly or adequately.

1.1.2 Risks

The start of the tunnel fires are mainly the result of two types of incidents, a vehicle collision or the malfunction of a vehicle (or its load). The amount of risk linked to both of these scenarios changes from tunnel to tunnel, also increasing proportionally to the amount of traffic and the length of the tunnel.

Collisions

For collisions, the risks has been statistically calculated for the different parts of the tunnels [55]. PIARC studies indicate that the entrance area, the first 150 m of tunnel length, is the zone most likely to have incidents involving collisions among cars. Some factors that change the frequency of collisions are the tunnel configuration (bidirectional or unidirectional), the horizontal alignment (curves) and vertical alignment (inclination), number of driving lanes, etc. The influence these factors have is:

- The tunnel configuration effect makes the unidirectional tunnels more risky, as the drivers feel safer with no vehicles traveling in the opposite direction being prone to commit more mistakes while driving.
- The horizontal alignment affects the field of sight of the drivers, giving them a shorter time window to react to any eventualities in the road.
- The steepness, vertical alignment, seems to increase the risk as it lets the drivers go faster, rising not only the vehicles speed but also the speed differences among vehicles (in opposing directions).

- The number of driving lanes might have a negative effect if it promotes lane movement. This happens when the amount of lanes is reduced in the entrance of the tunnel, producing a funnel effect, or when there are too much lanes, allowing lane changing.

The number of collisions have been calculated based in the amount of vehicles that have used the tunnels multiplied by the length of the tunnel itself and are reported by PIARC [55]. Statistically the analyzed nations have approximately from 3 to 11 collisions for every hundred of millions of vehicles per kilometer. This would translate into approximately 1 to 2 collisions, yearly, at the Frejus tunnel or Mont Blanc tunnel, or 6 or more in the St. Gotthard tunnel (due its larger length and daily traffic), calculated with data extracted from Statista [63].

Vehicle Failure

The second main cause of incidents in tunnels are vehicle malfunctions, they can come from different failures in the automobiles. Like Engine Fires, Electrical malfunctions, braking systems fires, under-seat heaters failures, among others. According to data obtained from the National Academy of Sciences [50] malfunctions are far more frequent than vehicles collisions, being the origin of more than 2 thirds of the buses fires according to french data, 70% of fires involving trucks, among others vehicles.

Still, it continues to be difficult to quantify the frequency of fires in tunnels, a fire rate per amount of vehicles per kilometers of tunnels is approximated by PIARC in the manual [55]. The amount is around 10 fire incidents per every 10^9 vehicles per kilometer. This amount changes from country to country, because of the particularities of the tunnels and the evaluation of what can be considered a tunnel fire in each country. Evaluating the Frejus and others trans-alpine tunnels the amount of fire incidents statistically should be close to one incident every 10 years for the Frejus and Mont Blanc tunnels, and close to one every 2 or 3 years in the St. Gotthard Tunnel. These numbers justify the precautions and safety measures taken in the tunnels as Fire incidents are no so unlikely to happen in any moment.

1.1.3 Interactions with ventilation systems

Ventilation systems have different duties during the operation of a tunnel. The management of the clean and vitiated air of a tunnel is its function most of the time, maintaining the carbon monoxide, soot and nitrogen oxides levels under healthy margins. The second task of the ventilation systems is linked to the safety during emergency conditions. Safety measures oriented towards the prevention and control of tunnel fires can take different shapes, from fire detection cameras or linear heat detectors (fibrolaser) to fixed

extinction systems. But the most frequent and versatile emergency measure continues to be the use of the ventilation system of the tunnel, capable of managing the back-layering, smoke extraction, among others.

Ventilation systems for tunnels work based in two main approaches: Natural and Mechanical ventilation [68].

Natural Ventilation

The natural ventilation is the process of moving the air through the tunnel without direct mechanical assistance. The most common method to produce natural ventilation is by designing a tunnel with a pressure difference between the two portals produced either by a difference of temperature (climate) or height (geographic).

Another phenomenon that induces natural ventilation through a tunnel is the ”piston” effect. The ”piston” effect originates from the air flow pushed by the vehicles circulating through the tunnel and then it becomes more important if the dimensions of the tunnel cross section are similar to the vehicle dimensions. The ”piston” effect is more important in structures like train tunnels and less important in long roadway tunnels, because of the dimensions of the tunnel and the machines.

These two natural convection effects can be enough to maintain operative air velocities in tunnels, mostly if the tunnels are relatively short and if there is enough traffic through them. Still, it might not be enough to keep the required ventilation conditions for smoke control during fires, so the tunnels often add fans, or others mechanisms, to increase their ventilation capabilities.

Mechanical Ventilation

There are 3 kinds of mechanical ventilation systems when it comes to the method used to move the air through the tunnel.

Longitudinal systems, (A) in Figure 1.1, use fans and jet-fans to move the air along the longitudinal axis of the tunnel. Under regular conditions the longitudinal ventilation system produces a flow of air at a velocity that guarantees that the amount of contaminants in the air are not harmful to the health through the whole tunnel (where the area with the higher concentration of contaminants is the downstream portal of the tunnel). Under emergency conditions the fans can increase their output to guarantee adequate conditions, managing the back-layering length of the smoke and the heat intensity of the fire. The positioning of the fans has few essential requirements, first, the fans should be at least at 100 m of distance to the portals, and second, the fans should be placed with at least 50m of longitudinal distance among them.

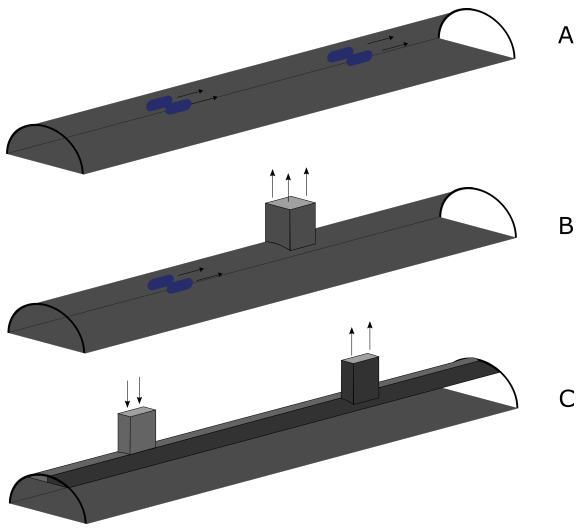

Figure 1.1: Tunnel ventilation types, A) longitudinal, B) semi-transversal, C) transversal

Transversal systems, (C) in Figure 1.1. These systems use air ducts, transversal to the tunnel tube, to extract and introduce air into the tunnel. These systems receive their denomination according to the amount of exhausted and inserted air that is handled, fully transversal systems handle the 100% of the exhaust and fresh air flow transversely, relaying minimally in the longitudinal flow of the air in the tunnel.

The last type of ventilation system are semi-transversal systems, (B) in Figure 1.1, these ventilation systems use air ducts to exhaust and insert fresh air into the tunnel, but not all the air is handled transversely. It can both use only air ducts or also use fans to handle better the air in the longitudinal direction of the tunnel. Some semi-transversal systems can even go further and change the amount of air that is handled transversely and longitudinally with extractions and fans that can change their output and direction according to the situation in the tunnel.

Regardless of the system type, ventilation systems are very important in the case that a fire breaks out inside a tunnel. Emergency management and the upgrade of existing fire control systems have been the object of numerous European projects, like Uptun (project to promote new measures to lower the probability of tunnel fires and their incorporation in existing tunnels) [28], SafeT (guidelines to prevent incidents and mitigate its effects)[60], VIRTUALFIRES (project to make a virtual fire simulator for training and performing fire safety and ventilation testing)[15]. These projects and the academic research, have incorporated progressively CFD as an aid to tunnel testing, which have proven useful to reduce the cost and increase the availability of tunnel tests.

1.2 Tunnel Fire Research

The research regarding tunnel fires relies in analytical models and in different tests that serve as a validation for the proposed researches. Still, the difficulty involved in making tests in real tunnels makes it necessary to introduce additional tools for the validation of the research. Therefore, different test methods have been implemented to aid the research, among them scaled tunnels and computational CFD models.

Fire modeling, using Computational Fluid Dynamics (CFD) is capable of replacing tests or complementing them with additional information. These models have been researched across the years, focusing on different topics as 1D models, monodimensional models that have as main objective the calculation of tunnel network fires and their interaction with ventilation, like MFIRE [8], SPRINT [61], FSSIM [23] and WHITESMOKE [16, 17, 12]. Also zone models, like BRANZFIRE [72] and CFAST [57, 41], where BRANZFIRE uses a zone model for fire in room corners and CFAST simulates zones linked to approximate more complex buildings.

Fire modeling has also focused in 3D simulations, with software capable of simulating complex fire scenarios, here we can mention FDS (Fire dynamics simulator)[30, 33], OpenFoam [25] and Fluent. Among these three software the first 2 are open source codes that can be modified freely (making it more accessible for the research community in general) and the last is a private software part of the Ansys package. These software have been used to simulate fire under different circumstances. Some examples are, Trouvé et al. [67] simulating confined fires using FireFOAM and FDS, also, Jenft et al. [39] where the extinction of confined fires, using mist sprinklers,was simulated using FDS and Hees et al. [73] using FDS to simulate confined fires in mechanically ventilated scenarios, testing the Heat Ventilation Air Conditioning (HVAC) calculations.

1.2.1 Review of Tunnel fire research

As it has been remarked the tunnel fires research, and the fire research in general, has been evolving in the past decades. Several literature works have added fragments of knowledge to the understanding that we have in this moment of tunnel fires, its characteristics and the effect of the different variables related to them. Several of these works have been reviewed during my research to get a grasp on the nature of tunnel fires and the methods to simulate them.

Literature with experimental and scaled tunnel tests

An important part of these works use tunnel fire data to compare with CFD or develop physical models. Among these works figure the contributions from prof. Ingason an other authors:

Ingason et al. [38], in 2012, used data obtained in fire test at the runehamar tunnel to study the flow reduction in a tunnel caused by the fire effect, a 1D model was developed that matches the experimental data for low HRR fires, but is less accurate as the HRR increases. This inaccuracy is concluded to be due to the difficulties to calculate all the 3D effects of the fire in a 1D model.

Ingason et al. [37], in 2015, used data from 5 experimental tests in the runehamar tunnel, and previous researches, to build simple theoretical models to estimate parameters of tunnel fires like the back-layering, visibility, among others.

Ingason et al.[48], in 2016, studied the influence of the tunnel geometry in the HRR of tunnel fires, finding that, for heptane pools, the HRR rises if the tunnel has a lower height, until it arrives to a limit value, and that for solid fires it has barely no effect.

Also, Ingason et al.[46], in 2017, studied the relationship between a tunnel cross section and the critical velocity, providing a formula to calculate the critical velocity. In addition, this research compared model scale tests with FDS simulations obtaining agreement for small fires and some overestimation for bigger fires.

Hwang [35], in 2005, compared experimental tests and FDS simulations for tunnel fires, focusing in the back-layering length, the research also focused in the parameters that influence the back-layering length and found a good degree of agreement between FDS and the available test results.

McGrattan et al. [52], in 2006, used FDS to simulate a reconstruction of the Howard street tunnel fire, first the model was compared to some experimental tests, agreeing with them, and afterwards the results of the simulations were capable of indicating the values of the temperatures inside the Howard street tunnel in the time of the fire.

Kim et al. [45], in 2008, tested FDS 4.0 using a sensibility analysis and comparing the results to a 100MW tunnel fire test, the conclusion of the research points out that the FDS results are qualitatively accurate but that they lack some precision under certain circumstances.

Binbin et al. [5], in 2011, used Fluent and FDS in simulations of smoke spread in subway tunnels, comparing the simulation results to measured data, the results indicate that the FDS simulations are closer to the measured data than the fluent simulations, even if the geometries FDS is capable to create is not as accurate.

Guo et al. [26], in 2014, presents a 1D model for tunnel fire calculations, and compares its results to FDS and experimental data, concluding that the three data sets agree in the results, still for narrow tunnels FDS shows some inaccuracies.

Wang et al. [75], in 2016, compared Fluent CFD results to experimental tests, finding good agreement between the two results, also the effects of vertical shafts in tunnel fires were researched finding that they have a positive effect fighting the fire consequences.

Chang et al. [7], in 2017, shows a series of tests made in a mock-up tunnel, were a fire of 25MW is suppressed using mist sprinklers placed in the walls of the tunnel, as a result the spray system is capable of reducing the temperature in the tunnel and ceiling and increasing the visibility upstream of the tunnel.

Scaled tunnel are also capable of providing good data sets, but they are far less

common. Some examples of scaled tunnels are in the works of:

Chow et al.[10], in 2015, studied horizontal and tilted tunnels with forced ventilation using both scaled tunnels and CFD calculations, finding equivalent formulas for back-layering distance and a modified expression for the critical velocity of tilted tunnels.

Weng et al. [76], in 2015, proposes an expression that uses the hydraulic diameter to calculate the back-layering length and critical velocity, the expression is found through studying tunnel fires using scaled tunnels tests and FDS simulations.

Tang et al. [64], in 2017, made a scaled tunnel to test the influence of air extractions upstream of the fire, it concluded that increasing the velocity of the extraction made the fire tilting smaller increasing ceiling temperatures, some expressions were modified to account for this.

Wang et al. [74], in 2017, investigated the relationship between the tunnel ventilation, the HRR, and the fire spread in tunnels related to the ventilation velocity, comparing to other empirical relations and testing the spread in a scaled tunnel pool fire.

CFD tunnel modeling literature

The scientific articles presented in the previous section were able to compare their results with full or scaled tunnel tests, using this data to validate the capabilities of the models used. This is a great advantage that, as mentioned before, is not always possible to have. The works in this section focus in the development of CFD tools, by comparing the models among them, to find the advantages and disadvantages of the methods used in regards to others.

The work of Jiang et al. [40], in 2004, validated and compared the results of different models for solving fires in tunnels, he compared RANS (Reynolds Averaged Navier Stokes) and LES (Large Eddy Simulations), obtaining that LES is more accurate but requires a longer amount of calculation time compared to RANS.

Van Maele et al. [69], in 2008, simulated a tunnel of reduced dimensions with RANS, in Fluent, and LES, in FDS, and compared both simulations to experimental tunnel fires, concluding that the data obtained from RANS can be useful for the LES parameters and that LES is more accurate, but much more dependent of the mesh resolution.

But most of the works have used the models directly to understand some characteristics of the tunnel fires in different kinds of tunnels (horizontal or tilted), for different kinds of ventilation system (natural, forced and transversal) and focusing in different phenomena of the fire (heat release rate, back-layering, fire spread and extinction)

Hu et al. [34], in 2008, studied the critical velocities for tunnels when the fire is not centered but close to the walls of the tunnel, his research concluded that for low HRR the critical velocity increases as the fire moves to the sides (based in CFD simulations), but that for higher heat release rates the critical velocity difference between the center and the wall is close to zero.

Lin et al. [49], in 2014, studies numerically tilted tunnels focusing in semi-transversal

ventilation systems, affirming that for this kind of ventilation the amount of air extracted by the ventilation has to increase proportionally to the tunnel tilt angle.

Chow et al. [9], in 2016, continue the study of horizontal and tilted tunnels, now with natural ventilation, using both scaled tunnels and CFD calculations, the tests and simulations agree in their results and the study proposes a relationship to calculate the smoke velocity decay.

Weng et al. [77], in 2016, continues its research in critical velocity and back-layering length, the work focuses in sloped tunnels and describes the geometry of the tunnel using the hydraulic diameter, the area and height of the tunnel.

Li et al. [47], in 2018, tested the effects of fire suppression systems in tunnel fires, the research showed that for late activation or water flows incapable to suppress the fire the effect of the suppression system was negative as the amount of CO increased in the air and the visibility was notably reduced.

1.3 Thesis Goals

The main goals of this thesis are to improve the multiscale model that has been in development in Politecnico di Torino in the last years. This improvement will include:

- Profound changes to the way it is compiled, to reduce greatly the computational time it requires, that it's a multiscale model stronger point.
- Improvement of the handling of pressure, to eliminate pressure errors in tunnel simulations.
- Modification of the boundary handling, to ensure that the model respects the mass, momentum and energy conservation
- Modifications to the data exchange among models to minimize perturbations introduced to the flow by the model due to buoyancy at the boundaries.
- Verification of the 1D and 3D models capabilities to simulate tunnel fires using experimental data and simulations in other models.

1.4 Test cases

The tunnels that will be used as reference for the tests in this research are reported in this section. These have been chosen due to the availability of experimental results, or because their simulations have been of interest during these years. The tunnels used are described in the following subsections (1.3.1 and 1.3.2)

1.4.1 2.6 Km Tunnel

This is a 2600 meters long tunnel that has two separate carriageways, with 3 lanes in each direction. This tunnel has a longitudinal ventilation system, with 24 fans placed in groups of three along the tunnel. Also, there are 27 cameras that are part of an alarm system and 6 smoke detectors along the tunnel.

1.4.2 Dartford tunnel

The Dartford Tunnel is a two carriageway tunnel that crosses the river Thames, and is located approximately at 20km from London. The tunnel is approximately 1.5km long with two lanes in each direction. The tunnel has a semi-transversal ventilation with two vertical extractions, placed close to the tunnel portals, and 14 couples of fans mostly placed close to the portals.

Chapter 2

Multiscale modeling

2.1 Multiscale modeling research review

CFD simulations of tunnels have the tendency to consume large amounts of calculation time. Tunnel tests, in scaled or regular tunnels, have the issue of needing preparation and financing. An option that has been explored in the last decade to optimize in time and cost are the multiscale simulations.

Multiscale modeling are a kind of CFD simulation where the model is divided into two subdomains. One subdomain is simulated using a 3D model and the other using a 1D model. The main reasoning behind this division is to have the 3D model solve the more complex part of the domain, the zone close to the fire, and the 1D model simulate the distant areas, where the flow is almost homogeneous. The main aim of using multiscale modeling is to obtain a model that is as accurate as a 3D CFD model, using the 3D model to simulate the fire area, but needs a fraction of the computational resources, as the rest of the tunnel is simplified through a 1D model. Some examples of Multiscale modeling can be found in the literature.

The research by Colella et al. [12, 14, 13, 19] have focused in a multiscale model built using Fluent as the 3D code and Whitesmoke, a code created at the Politecnico di Torino energy department, as the 1D model. The model has been tested using different kinds of coupling for different kinds of simulations. The direct coupling, where the two models exchange information constantly, was used consuming larger amounts of calculation time. The indirect coupling, where there is no exchange but characteristics curves are used in the boundaries, uses longer set-up time instead. In all of the tests the model showed small error percentages, with large time savings with respect to a full 3D simulation.

The research by Cosentino et al. [16] followed some of the research of Collela et al., changing the 3D model from Fluent to FDS (an open source model). The multiscale model uses Whitesmoke as the 1D, adding a concentration calculation and using only a direct coupling. The model is tested for ventilation and fire scenarios, and compared with experimental fires with errors below 7% in velocity and concentration.

Then the research by Ang et al. [2] used FDS 6.1.1 for tunnel multiscale simulations. First, the FDS was used to simulate the Dartford tunnel, to validate the accuracy of the software when simulating tunnels and its ventilation system. The validation was made using velocity profile comparisons. Then, after validating the FDS the same tunnel was simulated using the FDS HVAC as the 1D in a multiscale simulation. Both of the comparisons showed that FDS is capable of reproducing the velocity profile from 80 m downstream of the fans and onward, but closer to them the velocity profiles do not match the experimental measurements. The discrepancies are said to be mostly related to the lack of information about the on-site fans characteristics, and not due short comings of the software. The tests also show that the HVAC uses close to 1% of the time used by the full-scale simulations, being capable of saving time proportionally to the tunnel length simulated in the 1D.

The work by Vermesi et al.[71] focuses again in FDS and the HVAC function it includes. Through its research Vermesi et al. compared the calculation time spent by the FDS using a full 3D calculation, a multi-mesh calculation and a multiscale approach. The multiscale approach spent the shortest amount of time, reducing the total time in more than a 90% and the multi-mesh managed to reduce the time close to a 50% of time. The results of these simulations show that it is feasible to run multiscale simulations in FDS and also that the results agree with previous Fluent simulations.

Haghighat et al.[27] based his research in a multiscale model using FDS 6.0 as the 3D and VentFIRE as the 1D. VentFIRE is a module capable of simulating the transport of smoke and heat through a discrete sub-cell transport and node mixing methods. The coupling in this model is indirect, meaning there is no constant exchange of information, but that the boundaries are managed by characteristics curves. Using the turbulent kinetic energy (TKE) and a vorticity analysis this model was capable of coupling the boundaries and achieving temperature and velocity error below 5% between a full 3D simulation and a multiscale one.

The research so far has started to show the capabilities of multiscale simulations as a tool that introduces time saving with small losses of accuracy, in comparison mainly to full 3D simulations. Still, some multiscale models have some issues, in the works of Colella the main issue was using Fluent, as it would make it difficult to develop a tool having limited access to the code, and being incapable of introducing deeper changes. In the FDS+HVAC cases the issue is mainly that the HVAC model is not intended for this purpose and, therefore, it has shortcomings when it comes to the functionalities it offers of the kind of communication it has between the 3D and HVAC models. At last, the third model shown has FDS linked to Vent-fire being its issue the longer setup time required by indirect couplings, making the model less flexible when changes have to be introduced in the simulation to test more scenarios or make sensitivity analysis around different variables. The aim of our research is to continue developing a multiscale model with direct coupling that is capable of a high degree of time saving, a low degree of error and a 1D model capable of introducing different kinds of boundary conditions.

2.2 Fundamentals of Domain Decomposition Methods and Multiscale Modeling

Multiscale models fall into the category of domain decomposition methods. This kind of methods are mostly used to solve partial differential equations in large domains by dividing said domain in smaller pieces that can be solved in parallel or, in this specific case, that can be simplified and solved faster. According to Tang et. al. [65], The idea of domain decomposition was proposed more than one hundred years ago, but has been attracting more and more attention mostly in the last 30 years, with an increasing amount of research published in journals about multi-block or domain decomposition applied to fluid flows.

Domain decomposition methods can be classified in two ways. The first criterion focuses in the sub-domains created by the method, by them being overlapping (if they share parts of the domain) or non-overlapping (if they don't). The other classification regards to the kind of boundary conditions that they use, were we have Dirichlet-Dirichlet methods (or Schwarz methods), Dirichlet-Neumann methods and Neumann-Neumann methods, where Schwarz methods are overlapping and the two latter are non-overlapping.

Dirichlet-Dirichlet

The Dirichlet-Dirichlet method was the first decomposition method that was known to be developed, according to [65, 66, 24], and was published around 1870. It was developed by Schwarz, a german mathematician, to prove a part of the theory of analytic functions introduced by Riemann, named the Dirichlet principle. It is now called the alternating Schwarz method, is used with Overlapping subdomains and works in 2 steps.

As it can be seen in Figure 2.1, for an irregular domain Ω that is divided in Ω_1 and Ω_2 regions, both overlapping, and has a Γ external boundary, and therefore, also a Γ_1 and Γ_2 external boundaries, where a part of Γ_1 is inside Ω_2 and a part of Γ_2 is inside Ω_1.

The first step of the alternating Schwarz method calculates first in Ω_1, with initial conditions over all Γ_1 (including the part inside Ω_2), and then uses the Ω_1 solution to approximate the boundary condition in Γ_2. The second step is the calculation in Ω_2, using the Γ_2 boundary condition, that includes a part defined by the Ω_1 solution, now also the Γ_1 has its region inside Ω_1 approximated by the Ω_1 solution. Then, the calculation continues with one region calculating the boundary for the other, and the intersection zone between the two subdomains Ω_1 and Ω_2 has the same solution for both subdomains upon convergence.

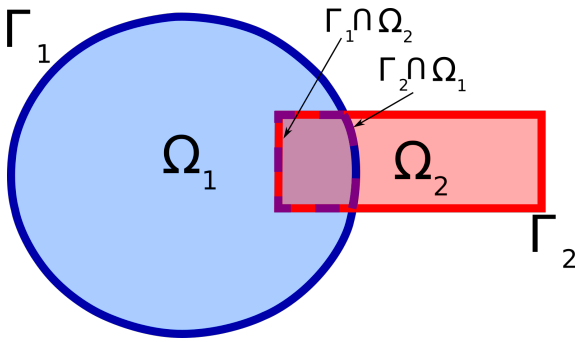

Figure 2.1: Overlapping domains, for a Dirichlet-Dirichlet domain decomposition

This method afterwards was developed to be used in parallel calculation, the parallel schwarz method, and other similar methods.

Dirichlet-Neumann

Dirichlet-Neumann Domain decompositions are non-overlaping and work in 2 stages. The setup is similar to the one of the Schwarz method, but in a non-overlapping domain as seen in Figure 2.2. For a domain Ω that is divided in Ω_1 and Ω_2 regions, non-overlapping, and has a Γ external boundary, and therefore, also a Γ_1 and Γ_2 external boundaries, that share a Γ_{12} boundary.

The first step of the Dirichlet-Neumann method calculates first in Ω_1, with an initial Dirichlet conditions in Γ_{12}, and then uses the Ω_1 solution to approximate the Neumann boundary condition in Γ_{12}. Then, the Γ_{12} solution obtained in the first subdomain is used as a Neumann boundary condition on the second subdomain, namely Ω_2, the solution for the second subdomain is obtained and a new Γ_{12} value can be approximated and, afterwards, used as a Dirichlet boundary condition in the calculation of Ω_1.

This exchange of boundaries continues among the 2 subdomains. For bigger domains, if there are more than 2 subdomains they have to be organized in a chess pattern to match the boundary conditions.

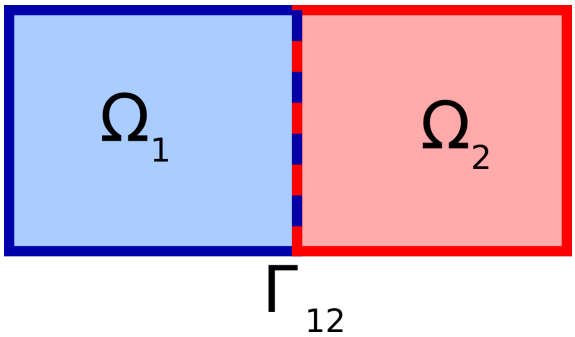

Figure 2.2: Non-Overlapping domains, for Neumann domain decompositions

Neumann-Neumann

Neumann-Neumann domain decomposition methods also use non-overlapping domains. Here the subdomain distribution is similar to the Dirichlet-Neumann decomposition.

The procedure is different, both of the subdomains are solved simultaneously, Ω_1 and Ω_2, using a Dirichlet initial value in the shared boundary, Γ_{12} . In the second step the problem is solved in both of the subdomains, but using the difference of the derivatives in the normal direction to the shared boundary Γ_{12} as the Neumann condition in Γ_{12} for both of the subdomains. As a result a new initial Dirichlet value can be calculated in Γ_{12} , used to continue the iterations.

The method used in the multiscale model developed in this work is the Dirichlet - Neumann domain decomposition. The domain for the multiscale simulations is mainly divided in a 3D subdomain including the fire, and 2 or more 1D subdomains that communicate the 3D simulation to the environment (through the portals or exhausts, etc.). The boundary conditions used for the flow problem are mainly two. The pressure is imposed in some boundaries as a Dirichlet boundary condition, and the mass flow is imposed in other boundaries as a Neumann boundary condition; more details will be given in the discussion of the coupling among the sub-models.

2.3 Multiscale Model in Development

This work follows the development of the multiscale model started by Sara Cosentino [16], mentioned earlier. The multiscale model combines FDS as the 3D algorithm and Whitesmoke as the 1D algorithm. The model exploits the best capabilities of each one of the two sub-models, first, the 3D (FDS) is used to simulate the areas close to the fire, providing more accurate and detailed results for the flow, temperature and other properties, in the vicinity of the fire. Then, the 1D (Whitesmoke) is used to reduce the calculation time, by simplifying the more homogeneous areas of the tunnel to a 1D model, reducing the time taken by the 1D part of the domain greatly.

The algorithm follows the steps shown in Figure 2.3. The first step is a 1D iteration, called 1D guess, with initial conditions over the boundaries that it shares with the 3D. Posterior to this 1D guess the 1D model is capable of calculating the boundary conditions that it has to pass to the 3D calculation. Then, the 3D calculation is solved and the algorithm checks whether it has to stop (If it has arrived to the time end) or if it has to pass info for a 1D iteration (If the total 3D iteration count is higher than 50). Once arrived to the iteration number 50 all the subsequent iterations of the model will include a 1D calculation until the 3D reaches the end time of the simulation. The first 50 iterations are left to the 3D alone to ensure that the steady flow conditions in the cold tunnel has been reached, and that the pressure field is stable. Furthermore, to guarantee this stability the pressure boundary condition imposed from the 3D to the 1D is averaged over 50 iterations, in this way it is possible to reduce the impact of possible

pressure peaks or pressure oscillations.

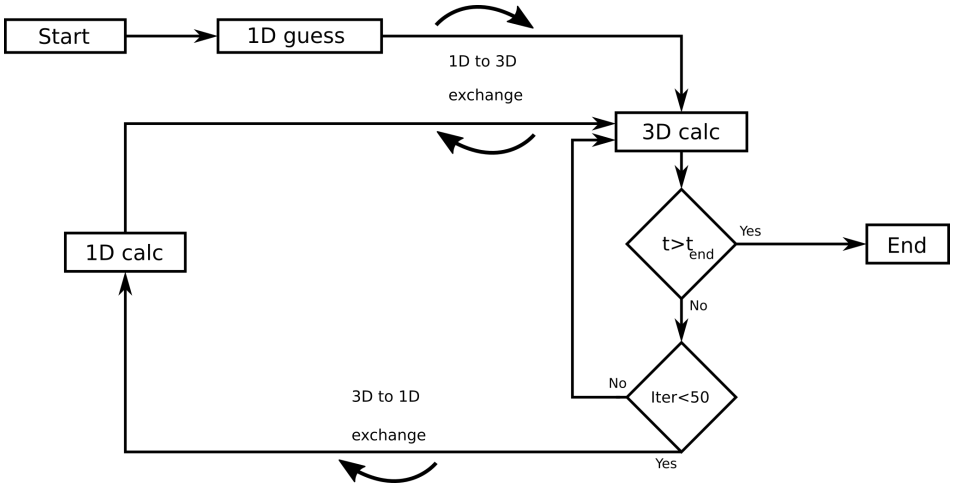

Figure 2.3: Modified multiscale algorithm representation

The multiscale model is divided in two sub-models, and the simplest way to explain the multiscale would be to focus first in its two parts, and at last in the link between them.

2.3.1 Three Dimensional Modeling

The FDS is used as the 3D model of the multiscale, it is a software developed by the NIST (National institute of Standards and Technology) in collaboration with the VTT institute in Finland. FDS was released publicly in February of 2000, after some years of development at the NIST. It has not been the only fire dynamics model developed at NIST, as the institute has a long history related to the fire research from it's beginnings and the development of other fire models as CFAST (Consolidated Fire And Smoke Transport), among others. FDS is a computational fluid dynamics software capable of a wide range of fire and fluid flow simulations under diverse conditions and can be characterized by some of its major and most used features:

Turbulence modeling, Large-eddy Simulation

Turbulence can be described as an spontaneous instability in the flow properties, causing these values to behave in an statistical (chaotic) way, as explained in the book Numerical computation of internal and external flows [29]. The values of the flow properties fluctuate around a mean value, with fluctuations that can be around a 10%, or more in the case of separated zones of the flow. This turbulent fluctuations appear when the Reynolds number of the flow goes beyond the critical number, which happens even at low speeds for most of the CFD applications.

Different methods are used to numerically describe the properties of a turbulent flow. First, DNS (Direct Numerical Simulation), where the complete spectrum of energy due to the turbulence is simulated, as it is shown in figure 2.4. This means that all of the eddies produced by the turbulent flow are numerically calculated, obtaining an accurate simulation that has the downside of requiring unreasonable amounts of time and resources, in most of the cases.

Second, another method used often in the literature is RANS (Reynolds average Navier-Stokes). This method aims to average out, in time, most of the turbulent effects in the flow, requiring some knowledge regarding the turbulence and its relation to the average flow [29]. Explanations regarding RANS are outside of the scope of this work more information can be found in [29].

At last, the LES (Large-eddy simulation) is a method that belongs in complexity of the calculation in the middle between the RANS solutions and the direct numerical simulations, as seen in figure 2.4. In this method, the contribution of the large, energy carrying structures of momentum and energy transfer, are calculated exactly. Meanwhile, the smaller scales of turbulence are modeled through different sub-grid-scale models, as these eddies behave in an universal way and modeling them requires less complex models than similar RANS solvers [58].

FDS is capable of using both the LES and the DNS approach during its calculations. To use LES in the calculations FDS introduces a low-pass filter using the grid size as filtering size, as mentioned in the FDS technical reference guide [33]. The eddies with sizes bigger than the grid are then solved exactly and the rest are modeled by different sub-grid scale models, as the Deardorff model, that is the default, the Smagorinsky model and the Wall-Adapting Local Eddy-viscosity (WALE) model, among others.

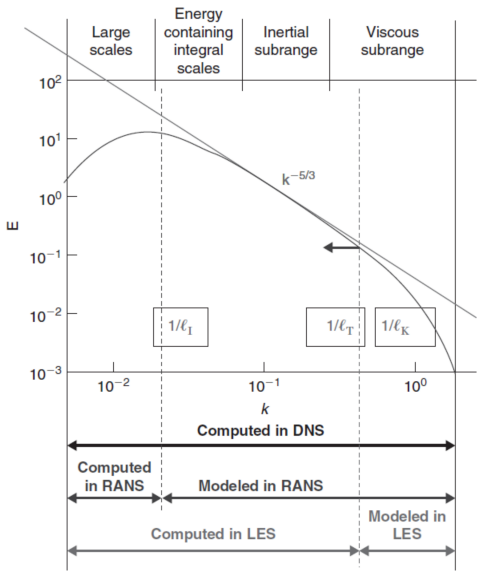

Figure 2.4: Turbulence energy spectrums, and the parts calculated by each turbulence model, extracted from [29]

Low Mach number approximation

The pressure in FDS is handled as the sum of two terms, the background pressure $\bar{p}(z,t)$ and the perturbation pressure $\tilde{p}(x,y,z,t)$, following the observations published in [59]. Using this definition of pressure, the background pressure is used for the calculations with the ideal gas law, the HVAC calculations among different compartments and the proportionality between internal energy and enthalpy in the energy conservation equation. Therefore, the background pressure works as a sort of thermodynamic pressure that remains mostly constant, while the temperature and density vary, as it happens in fires under normal conditions. Conversely, the perturbation pressure is used in the momentum calculations, being closely linked to the fluid flow in the simulation and acting as a hydrodynamic pressure. The two term pressure plus the FDS algorithm make it easier to calculate the properties of the flow, but have to compromise with obtaining an infinitely fast sound speed. This compromise means that pressure waves are transported infinitely fast in the simulations. In most of the applications, in relatively small domains or with long enough time-steps, the infinitely fast sound speed assumption is safe, as the sound waves will actually behave as they were infinitely fast arriving to the boundaries of the domain in only 1 time step. Still, if the simulated domain is large enough it may cause some inconsistencies.

Grid

FDS uses rectilinear meshes, uniform or stretched in up to 2 directions. Having an uniform grid spacing makes it more straight-forward to define the LES filtering length. The FDS mesh is a Staggered grid mesh, meaning this that the scalar properties are calculated in the center of the cells, the velocity components in the cell faces, and the vorticity in the cell edges [33]. Staggered grids are opposed to collocated meshes where all the variables are defined in the same grid position. Staggered grids are selected as they are more stable than collocated meshes, as collocated meshes suffer from decoupling between the velocity and pressure in each point (as p_1 does not influence u_1, and vice versa)[29].

Simplified Chemistry and "Lumped species"

Fire is essentially a reaction of fuel and air that has different products, as carbon dioxide, monoxide, and others according to the fuel composition and the completeness of the combustion. This means that completely describing a fire would need several reactions, the same as tracking the species would need a large number of transport equations. To reduce the complexity of the calculations and reduce the amount of variables FDS employs the lumped species approach. Lumped species are groups of substances, at a determined proportion, that are handled as an unique gas species, for example air, being a mix of oxygen and nitrogen. Using this concept, also in the products of the combustion reaction, is possible to simplify this reaction to one where there are only 3

species, fuel, air and products. Furthermore, handling only fuel, air and products also reduces the amount of transport equations solved.

The combustion reaction is also calculated using lumped species. The reaction is limited by the amount of mixing between the fuel and air, and it occurs infinitely fast (meaning that all the fuel-air mix that can burn in a time-step, will burn in that time-step). Other reactions models can be used for combustion, as Arrhenius equations, etc.

Solution Procedure

FDS uses a second-order predictor/corrector algorithm. The basic procedure follows the update of the density, ρ^n, mass density, Z^n, velocity vector, u^n, background pressure $\bar{p}^n$, the Bernoulli integral H^n, and the temperature, T^n. In brief the steps that the solver follows are, for the predictor step:

- The density, ρ^n, mass density, Z^n, and background pressure $\bar{p}$ are updated in time with a explicit Euler step.
- Density, ρ^n and mass density, Z^n are computed.
- The temperature is calculated, using the equation of state.
- The velocity divergence is computed
- The Poisson equation is solved, calculating the Bernoulli integral H^n, main variable related to the momentum and pressure
- The velocity u^n is calculated using the Bernoulli integral.
- The CFL constraint is checked, if it is satisfied the corrector step starts

And then, for the corrector step:

- The density, ρ^n, mass density, Z^n, and background pressure $\bar{p}$ are corrected taking into consideration the predictor value and the previous step value.
- The temperature is calculated, using the equation of state, with the new corrected variables.
- Source term for heat and mass are calculated and stored, as the heat release per unit volume, $\dot{q}'''$.
- The velocity divergence is computed, using the corrected values.
- The value for the Bernoulli integral H^n is also corrected, using the estimates of the last steps.

- The velocity u^n is corrected.

Detailed information regarding the software can be found in each one of the different manuals provided by the developers. The FDS user guide [30] includes information regarding how to use the software and essential formulas used in the software. The FDS technical guide [33] focuses in explaining the mathematical formulation for all the modeling done inside the software. The FDS verification guide [32] explains the procedure to do your own verification cases, and shows all the verification that FDS has so far. And the FDS validation guide [31] exhibits all the validation that FDS has against real tests for a wide variety of scenarios.

2.3.2 One Dimensional Modeling

The 1D part of the Domain is solved using Whitesmoke, a mono-dimensional model developed at Politecnico di Torino. Whitesmoke is mainly used to solve the flow conditions inside networks of tunnels or pipes that can be represented as a combinations of nodes and branches. The main assumption of the model is that for domains where 1 dimension greatly prevails over the other two, as example a tunnel where the length is several times longer than the section, it is possible to solve a mono-dimensional problem instead of the three dimensional problem. Whitesmoke solves a modified version of the Navier-Stokes equations for the momentum and continuity, a transient equation of energy for the thermal properties and a Mass transfer equation that combines the Fick theory and the continuity equation for the mass concentration.

Network Representation

The Graph Theory [6] is used to define the network, meaning that the network is described using nodes and branches. Branches are 1D fragments of the network connected to 2 nodes that are the branch inlet and outlet. In the branches geometrical and physical properties of the tunnel are defined, as: area of the section, perimeter, length of the branch, external temperature, roughness of the walls, thermal resistance and minor losses coefficient. Branches are also the center of momentum calculations, and the zones where vectorial quantities, as flows, are defined. Nodes are the points where one or more branches connect with each other. In nodes it is possible to define the height of the tunnel and external flows. Nodes are used as the center of thermal and concentration calculations, and the points where scalar quantities, as Temperature, Concentration and pressure, are defined.

For networks of this nature is possible to build an incidence matrix to describe their topology. An incidence matrix is a matrix that has as many rows as nodes has the network, and as many columns as branches. The values in the matrix are:

- zero (0) if the row (node) doesn't has contact with the branch (column).

- +1 if the node is the inlet of the branch.
- -1 if the node is the outlet of the branch.

Fluid flow model

The expression used to calculate the fluid flow is based in the Navier-Stokes equations for continuity and momentum, 2.1.

$$\begin{aligned} &\frac{\partial \rho}{\partial t} + \nabla \cdot \left(\rho \vec{u}\right) = 0 \\ &\frac{\partial \rho \vec{u}}{\partial t} + \nabla \cdot \left(\rho \vec{u}\vec{u}\right) = -\nabla p + \nabla \cdot \boldsymbol{\tau} + \Delta P_{source} \end{aligned} \tag{2.1}$$

In these equations, ρ is the density, $\vec{u}$ is the velocity vector, t is the time, p stands for the pressure and $\nabla \cdot \boldsymbol{\tau}$ is the viscous term. The Navier-Stokes Equations 2.1 have to be modified to be fit to solve the problems presented in this work. To achieve this first the mono-dimensional form of the Navier-Stokes equations are considered, by eliminating the dependence with two of the three dimensions. As a consequence, the term $\nabla \cdot \boldsymbol{\tau}$, present in the momentum equation of Navier-Stokes, losses part of its meaning and is substituted by the source term ΔP_{frict} that takes into consideration the viscous term through semi-empirical correlations. The last term, ΔP_{source}, takes into consideration pressure introduced by fans, buoyancy, piston effect, among others. Introducing these changes in the Navier-Stokes equations 2.1 we obtain the mono-dimensional equations for continuity 2.2 and momentum 2.3.

$$\frac{d\rho}{dt} + \frac{d\rho u}{dx} = 0 \tag{2.2}$$

$$\rho \frac{du}{dt} + \rho u \frac{du}{dx} = -\frac{dp}{dx} + \Delta P_{frict} + \Delta P_{source} \tag{2.3}$$

To adapt the continuity and momentum equations to the network problems they have to be developed considering the topology of the network. Then, the momentum equation 2.3 is developed around a branch j, and the continuity equation 2.2 is developed around a node i. The transient term of the equations is expanded using the backward Euler method, in both of the cases. This changes result in the equations in 2.4, for continuity, and 2.5, for momentum.

$$\frac{\rho_i^t - \rho_i^{t-\Delta t}}{\Delta t} \left(\sum_j \frac{A_j L_j}{2} \right) + \sum_j u_j A_j \rho_j + G_{ext,i} = 0 \tag{2.4}$$

$$\rho_j L_j \frac{u_j^t - u_j^{t-\Delta t}}{\Delta t} + \left(P_{i+1} - Pi\right) + \Delta P_{frict} + \Delta P_{source} = 0 \tag{2.5}$$

$$P_i = p_i + \frac{\rho_i u_i^2}{2} + \rho_i g z_i \tag{2.6}$$

In 2.4, the transient continuity equation around a node is shown. The first term in the left hand side is the time advancing term, and represents the change in mass inside the analyzed node. In this term, ρ_i^t is the density in the node i, for the actual time-step, A_j means the section of the branch j, as L_j stands for the length of the branch j. The second term is the summation of the mass flows entering and leaving the node from connected branches. And the third term represents the external flows entering or leaving the node, and the network.

Equation 2.5 shows the momentum equation, that is developed around a branch. The first term in the momentum equation represents the change of momentum inside the branch, is the transient term. The second term shows the variation of total pressure in the branch. And the last two terms remain as source terms for the losses caused by friction ΔP_{frict} and the pressure introduced by other devices ΔP_{source}. The total pressure, used in the second term, is defined as in 2.6, it groups the static pressure, the dynamic pressure and extracts the buoyancy term from the ΔP_{source}.

$$\Delta P_{frict} = \frac{1}{2}\left(f_j \frac{L_j}{D_{h,j}} + \sum \beta j\right) \rho_j u_j^2 \tag{2.7}$$

The expression 2.7 shows the empirical relation used to calculate the losses due to friction. The first term inside the parenthesis calculates the losses along the tunnel, using f_j that is the friction coefficient of the branch j, and the hydraulic diameter $D_{h,j}$. The second term in the parenthesis makes a summation of the βj concentrated losses coefficients of the branch.

Regarding the term in the ΔP_{source}, the equations 2.8 are the two expressions used to calculate the pressure change introduced by fans. The first expression calculates $\Delta P_{fan,j}$ using a third grade polynomial, where the constants a, b, c and d have to be either provided by the manufacturer or calculated to fit the operation curve of the fan. The second expression uses the fan discharge velocity u_f, area A_f and the pressure rise coefficient K_f, with properties of the branch and the amount of fans in the branch to calculate the pressure change due to the fan action.

$$\begin{aligned} \Delta P_{fan,j} &= a u_j^3 + b u_j^2 + c u_j + d \\ \Delta P_{fan,j} &= n_j \rho_j \frac{A_f}{A_j} K_f u_f \left(u_f - u_j\right) \end{aligned} \tag{2.8}$$

The piston effect of the tunnel can also be considered in the calculation. The expression used to calculate it is shown in 2.9, in the formula ϵ_v is the aerodynamic factor of the vehicle, A_v is the cross section area of the car and N_1 and N_2 are the number of vehicles in the two directions of the tunnel, and u_1 and u_2 the velocities in these directions.

$$\Delta P_{piston,j} = \epsilon_v \frac{A_v}{A_j} \frac{\rho_j}{2} \left(N_1 \left(u_1 - u_j \right)^2 - N_2 \left(u_2 - u_j \right)^2 \right) \tag{2.9}$$

Thermal model

The thermal calculation of the model is based in the transient form of the energy equation, 2.10. In this equation the c_p stands for the specific heat capacity of the flow, T is the temperature of the species, k is the thermal conductivity and φ_s corresponds to a volumetric source term.

$$\frac{\partial \left(\rho c_p T \right)}{\partial t} + \nabla \cdot \left(\rho c_p \vec{u} T \right) = \nabla \cdot \left(k \nabla T \right) + \varphi_s \tag{2.10}$$

The equation in 2.10 is then developed in its 1D form, by neglecting the 2 dimensions that are perpendicular to the tunnel length. Also the volumetric heat source term is divided in two terms for equation 2.11.

$$\rho c_p \frac{dT}{dt} + \rho c_p u \frac{dT}{dx} = k \frac{d^2 T}{dx^2} + \varphi_v - \varphi_l \tag{2.11}$$

Then, the energy equation is applied to control volumes that surround each node and half of the connecting branches and the backward Euler step is employed to develop the transient term, resulting in the equation 2.12. The first term, of this expression, corresponds to the transient term, containing the time rate change of energy in the control volume, of volume ΔV [70]. The second term represents the energy flow due to mass flow entering or leaving the control volume through the connected branches. The temperature of the flows is defined using the upwind scheme [70], meaning that the temperature of the fluids in each branch corresponds to the temperature of the inlet node of the branch. The first term in the right hand side calculates the heat conduction through the connected branches, it tends to be negligible as it is orders of magnitude smaller in comparison to the mass flow term [70]. The last two terms in the right hand side are the volumetric heat source term φ_v and the losses sink term φ_l. This last term contains the information regarding the losses of energy from the tunnel caused by the non-adiabatic walls of the tunnel [70].

$$\rho_i^t c_{p,i} \frac{T_i^t - T_i^{t-\Delta t}}{\Delta t} \Delta V + \sum_j \rho_j^t c_{p,i} u_j^t A_j T_j^t = \sum_j k_j \frac{dT^t}{dx} A_j + \phi_{v,i} - \phi_{l,i} \tag{2.12}$$

The two source terms in equation 2.12 are calculated through empirical relations. The volumetric heat term usually would include energy contributions due to fire, that will be not considered as the Multiscale tool aim is to simulate this kind of complex reactions in its 3D part. The losses sink term is evaluated using the expression in 2.13.

$$\phi_{l,i} = \sum_j \left(\frac{L_j}{2} \Omega_j U_j \left(T_i - T_{\infty,j} \right) \right) \tag{2.13}$$

In Equation 2.13 the losses through the walls are calculated using the length, L_j, the perimeter, Ω_j, the global heat transfer coefficient U_j and the temperature difference with the external temperature, T_j^∞ of the branch. These losses are calculated on half of the connected branches as it is the portion of the branches that belongs to each, node centered, control volume. The losses are calculated using a global heat transfer coefficient obtained using the equations 2.14 and 2.15. First, the convective heat transfer coefficient h_j is calculated using the velocity, the specific heat and the friction coefficient of the branch, as in 2.15. Then, the global heat transfer is calculated following equation 2.14, using the, $R_{RR,j}$, thermal rock resistance of the wall.

$$U_j = \left(\frac{1}{h_j} + R_{RR,j} \right)^{-1} \tag{2.14}$$

$$h_j = \frac{1}{8} f_j c_{p,j} \frac{G_j}{A_j} \tag{2.15}$$

Mass composition model

The concentration is described using the Convection-Diffusion form of the conservation law [29] with concentration , or density, as the scalar variable. Therefore, the model uses an expression that is similar to the continuity equation, but adds the term for the diffusion of the species, 2.16.

$$\frac{\partial C}{\partial t} + \nabla \cdot \left(\vec{v} C \right) = \nabla \cdot D \nabla C + S_p \tag{2.16}$$

Here C is the concentration, D is the diffusion coefficient, and is considered constant in space, and S_p is a source term for species entering and leaving the network. This equation then has to be passed to its one dimensional form, in 2.17.

$$\frac{dC}{dt} + u\frac{dC}{dx} = D\frac{d^2C}{dx^2} + S_p \tag{2.17}$$

In the one dimensional form only one of the three terms of laplacian of the diffusion remains, in the right hand side with the source term. In the left hand side the first term represents the change of concentration over time, and the second term the concentration change due to advection. As a last step the equation is developed in a control volume around a node, using the backwards Euler method as the time advancing scheme, resulting in equation 2.18.

$$\frac{C_i^t - C_i^{t-\Delta t}}{\Delta t} + \sum_j u_j^t A_j C_j^t = \sum_j D_j A_j \frac{C_i^t - C_j^t}{L_j} + S_{p,i} \tag{2.18}$$

Matrix formulation

The expressions in equations 2.4, 2.5, 2.12 and 2.18 are passed to matricial form, to describe the entire network topology, using the incidence matrix. In equation 2.19 the continuity equation is expressed in matricial form. The first term contains the mass flow entering and exiting the node control volume, as the product of the incidence matrix, $A_{(i,j)}$, and the column vector containing the mass flow in each branch, $G^t_{(j)}$. The second term contains the external mass flows into the control volume and the third term the transient component.

$$A_{(i,j)}G^t_{(j)} + G^t_{ext(i)} + r_{(i)} = 0 \tag{2.19}$$

In the case of the matricial form of the momentum equation 2.20 in the left hand side the total pressure change is written as the product of the transpose of the incidence matrix, $A^T_{(j,i)}$, and the Total pressure pressure column vector, $P^t_{(i)}$. In the right hand side the first term groups the hydraulic resistance, $R^t_{(j,j)}$, and part of the unsteady term, $C^t_{(j,j)}$, multiplied by the mass flow. The second term stands for the pressure sources introduced in the branch, $t^t_{(j)}$, and the third term is the second half of the unsteady term created with the backward Euler scheme when developing the equation.

$$A^T_{(j,i)}P^t_{(i)} = \left(R^t_{(j,j)} + C^t_{(j,j)}\right) \cdot G^t_{(j)} - t^t_{(j)} - s^t_{(j)} \tag{2.20}$$

Equation 2.21 corresponds to the thermal model matricial form. In this equation, the matrix $\boldsymbol{M}$, called the mass matrix, is a square matrix containing the $\frac{\rho_i^t c_{p,i}}{\Delta t}$ of the

unsteady term in 2.12. Also, matrix K, called the stiffness matrix, contains data related to the energy flow due to convection and half of the losses source term. The other half of the source term is in the term $f^t_{(i)}$, that corresponds to the half that contains the external temperature, the known part of the term. The term $\Phi_{v(i)}$ contains volumetric energy sources introduced in the networks, if there are any. And the last term in the right hand side contains half of the unsteady term, referred to the previous time-step.

$$\left(M^t_{(i,i)} + K^t_{(i,i)}\right) T^t_{(i)} = f^t_{(i)} + \Phi_{v(i)} + M^{t-\Delta t}_{(i,i)} T^{t-\Delta t}_{(i)} \tag{2.21}$$

The structure of the mass transport equation in matricial form, 2.22, is also similar to the thermal model equation. The values contained by the M_C matrix adjusts to the equation and are now $\frac{1}{\Delta t}$. The matrix K_C in this equation contains the advective terms and part of the diffusive term, of the form $\frac{D_j A_j}{L_j}$. The first term in the right hand side $f^t_{(i)}$ contains known terms, mostly in the boundaries. The second right hand term contains the species source term. The third term contains half of the transient term, due to the Backward Euler time advancing scheme.

$$\left(M^t_{C(i,i)} + K^t_{C(i,i)}\right) C^t_{(i)} = f^t_{C(i)} + S_{p(i)} + M^{t-\Delta t}_{C(i,i)} C^{t-\Delta t}_{(i)} \tag{2.22}$$

Solution procedure

The system of equations is solved iteratively using a SIMPLE (Semi-Implicit Method for Pressure Linked Equations), as it was proposed in [56]. The steps followed for the solutions are shown in the figure 2.5.

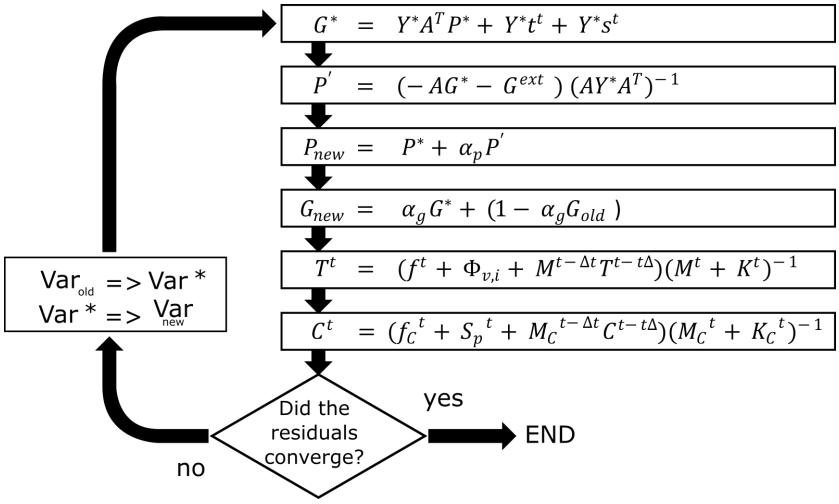

Figure 2.5: SIMPLE Algorithm Representation

The procedure in the figure 2.5 starts with the calculation of the flow using the momentum equation. In the momentum equation, Y^* is the inverse of the hydraulic resistance and it is a function of the mass flow, making the problem non linear introducing the need to solve the problem iteratively. After obtaining this mass flow guess it is used to calculate the pressure change, this is done using the second expression in the right. This expression is the result of assuming that the difference between $Y(G)$ and $Y(G^*)$ is negligible; a complete explanation of this process can be found in [70]. Then, the values of the new pressure P_{new} and new mass flow G_{new} are obtained, using under relaxation factors α_p and α_G, respectively. The last two formulas are the thermal model and mass transport model, they calculate the temperature and concentration of species, respectively. After this iterations the residuals of the continuity, momentum, energy and concentration equations are evaluated, and if they are below a tolerance the iterative process ends. Otherwise, the process enters a new iteration were the values of G_{old} and P_{old} are substituted by G^* and P^* , and these last two are substituted by G_{new} and P_{new}.

2.3.3 Coupling method

The coupling method used corresponds to a Dirichlet-Neumann method, according to the domain decomposition literature. The coupling information is exchanged in non-overlapping boundaries using 2 kinds of boundaries that exchange pressure and mass flow data frequently between the 3D and 1D models. The coupling of the 3D and 1D models is done using Fortran, the same language in which both FDS and Whitesmoke are written. The exchange of information happens at the end of the 3D (FDS) calculation, where the properties that exit the corrector phase of the FDS are passed to the 1D (Whitesmoke), the 1D step takes place and new boundaries for the FDS simulation are obtained. The 2 kinds of boundaries used in the exchange are opposite in the kind of information that they pass from one sub-model to the other, and are necessary to ensure that the problem can be solved adequately.

”PRES” Boundary

In this boundary the 3D model passes pressure information to the 1D, and the 1D passes the mass flow information back to the 3D model, as seen in the left part of 2.6. The pressure in the 3D boundary is averaged across the boundary surface. The average is weighted by the mass flow, so the information in every cell of the 3D is multiplied by the local density and velocity, and then divided accordingly. The averaged value obtained is then assigned to the 1D node that is connected to the boundary surface of the 3D simulations. In the opposite direction, after the 1D finishes its iteration the value of the mass flow in the 1D node is assigned to the whole boundary surface that it connects to, distributing the flow homogeneously in the 3D boundary section.

This boundary is used in tunnels simulations for the upstream boundary condition,

a boundary where the conditions are barely affected by the fire and introducing an uniform mass flow over all of the boundary does not create instabilities. The only point to take into consideration is to keep this boundary away from the back-layering or any other bidirectional flow. The back-layering is the name that receives the smoke that manages to return upstream of the fire. It is closely related to the critical velocity, which is the ventilation velocity in the tunnel for which the smoke is unable to return upstream. The boundary should be kept away from bidirectional flows as it acts as a sort of wall that introduces a mass flow rate at a set velocity in only one direction. Bidirectional flows close to this boundary would create zones with artificially higher or lower pressures. When it comes to the back-layering, expressions can be used to predict the back-layering length in a fire scenario and place accordingly the boundary surface.

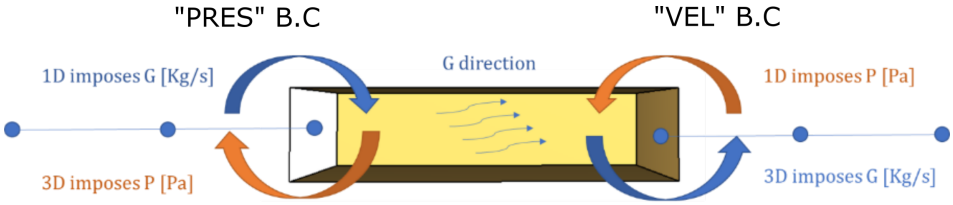

Figure 2.6: Boundary conditions between the 1D and 3D models

”VEL” Boundary

The ”VEL” boundary complements the ”PRES” boundaries by passing the pressure information from the 1D to the 3D model, and the mass flow information from the 3D to the 1D model, as seen in the right side of 2.6. The passage of the mass flow is done through an average of it over the 3D boundary surface; the value is then passed to the node connected to the boundary as an external mass flow rate.

In the opposite direction, the 1D imposes the pressure boundary condition to the 3D. The pressure is calculated in the node connected to the boundary surface, this pressure is assigned to the mean pressure of the 3D surface. Using an uniform pressure distribution in the 3D surface causes instabilities in the flow and the simulation, as shown in Figure 2.7. To avoid these instabilities a new distribution is made each iteration, the distribution represents an average of the pressure behavior in the last 5% of the domain in the direction perpendicular to the boundary. At last, the boundary imposed combines the average pressure provided by the 1D with a distribution provided by the 3D, calculating as in Figure 2.8.

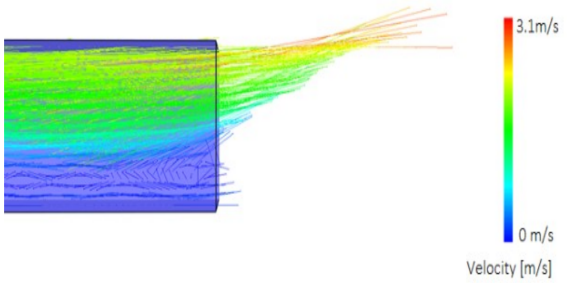

Figure 2.7: Downstream instabilities, due to uniform pressure boundary

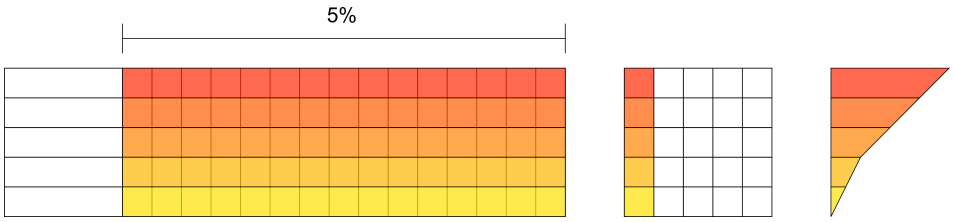

Figure 2.8: Pressure distribution calculation

Regarding the placement of this boundary it should be placed far from the fire, at a distance that should compromise having flow conditions that are close to homogeneous and keeping the 3D as small as possible to save time. The capability of the fire of disrupting the flow is proportional mainly to the fire heat release rate, so for fires of higher intensities the domain will have to be bigger to ensure more stability.

Temperature and Concentration Boundary Conditions

The temperature and concentration boundary conditions are exchanged in the boundaries following the upwind scheme. Therefore the mass weighted temperature and concentration average are calculated in all the 3D boundary conditions, and in all the 1D nodes, and they are passed in the direction that the mass flows follow. The variables are calculated using mass weighted means to ensure the conservation of momentum, energy and mass concentration

2.3.4 Network Representation

The network must not only represent the tunnel, but also the ventilation system composed of different devices across the tunnel length. These devices aim to simulate precisely the presence of fans inside the tunnel and in transversal ducts systems. To achieve this the fans are modeled according to a pair of expressions, the degradation of their operation is considered by recalculating their contribution each time-step and other effects are also simulated if they would exist, like the piston effect.

Ducts are mainly used in transversal and semi-transversal systems. These systems use networks of ducts parallel to the tunnel that exhaust vitiated air and introduce

clean air across the tunnel. They can be linked in the same way extractions are, even in multiple points of the tunnel.

Extractions and Networks

Extractions are used in ventilation systems of long tunnels, mainly. For the 3D domain it is possible to place extractions using FDS vents, to fix the volumetric or mass flow that is inserted or extracted of the tunnel. It is also possible to use the multiscale algorithm to place transversal ducts in 3D domains, and in the 1D part, the boundary conditions that they use has to be adjusted accordingly to the properties known of the extraction, all of the options are shown in 2.9.

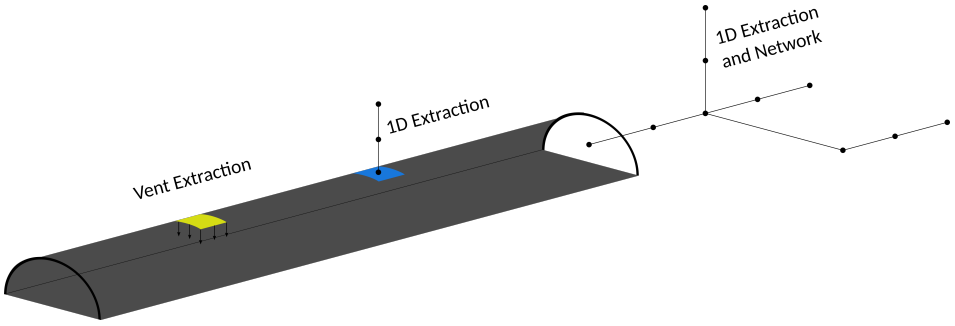

Figure 2.9: Network and Extraction configurations

Fans

Jet fans are used mostly in longitudinal and semi-transversal ventilation systems. They can be modeled inside the 3D model by adding an obstruction with two vents in each side, one working as a flow sink and the other as a flow source. The 1D model has expressions to simulate the presence of fans inside the branches, one expression calculates the pressure difference introduced based in the characteristic curve of the fan, and the other based in the change of kinetic energy, as mentioned in previous sections of this chapter. Both of the options to introduce fans are illustrated in 2.10.

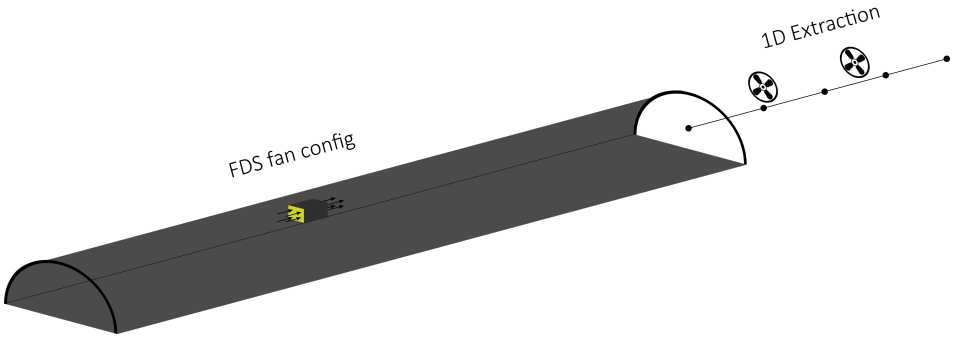

Figure 2.10: Fans configurations

Chapter 3

Calculation time considerations

The reduction of the calculation time is one of the main objectives of multiscale simulations. Therefore, it is very important to evaluate the factors that raise the calculation time in a CFD simulation, and more importantly the methods available to reduce this time cost.

Focusing the study in the case of the proposed multiscale model it is possible to mention different factors. These are described in section 3.1.

3.1 FDS single process factors

First, we will be considering a simple FDS simulation, ran using only 1 mesh and leaving aside the different tools available to parallelize the workload. In the case of this simple simulation some important factors that have an influence in the calculation time of the simulation are the following:

Domain and Meshing

The amount of cells to simulate, and therefore the domain size and meshing, are one of the main factors regarding the duration of an FDS simulation. For an FDS simulation the total amount of mathematical operations that have to be solved is directly related to the number of cells and equations that are needed to calculate the properties in these cells.

Heat release rate

Still, the domain and meshing are constrained by different physical aspects of the simulation to be solved. Among them, the heat release rate of the fire simulated is important as it needs the mesh resolution to be small enough to calculate the properties of the fire precisely. If the mesh resolution is too coarse a part of the information might be lost inside the cell average values. The mesh resolution can be compared to the characteristic

fire diameter to obtain a degree of the capability of the mesh to calculate the properties of the flow [33]. This equation and other parameters shown in the guides are still references and do not guarantee the quality of the mesh, therefore making a sensitivity analysis is still recommended.

Maximum velocities

The Courant–Friedrichs–Lewy condition is an important stability condition for explicit schemes solving wave and convection equations. The condition expresses that the distance that can cover any disturbance at a velocity v during a time period Δt has to be inferior to the distance between two grid points [29], also other similar constraints are used and explained in [33]. As FDS has to ensure that this condition is applied to all the domain the limitant is the highest velocity in the simulation. This constraint has to be taken into consideration as this means that refining the mesh will not only raise the amount of cells but also shorten the time-steps, consequently making the calculation time longer.

Models Used

The physics involved and their modeling also affect the computational time. Some examples of modeling that can change the simulation time are: complex reactions, changing the near-wall model, introducing particles or sprinklers, changing the pressure solver, among others. Optimizing the calculation time also requires the capability to decide which models are needed in a simulation, as in several cases like preliminary simulations it is heavily advised to simplify the physics used. How to simplify the physics depends on the simulated case, but regularly it means to eliminate the radiation calculation, using volumetric heat release sources instead of fires, etc.

Hardware available

The computational time is also affected by the computer used to perform the simulation. Here we consider the amount of cores to simulate in parallel, of ram space to handle large numbers of cells, among others.

3.2 FDS Multiple process factors

Reducing the time it takes to finish a simulation is important. It is one of the main concerns of this work and has been an important focus through the development of FDS as a CFD model. In FDS a method that has been developed to reduce the computation time of the simulations has been to exploit the paralellization of work through OpenMP and MPI.

OpenMP

OpenMP, that is a short name for Open Multi-Processing, is a set of language extensions that can be implemented as compiler directives. Its implementation is available in Fortran, C and C++, and is used to increase parallelism in a sequential code. It adds directives in the loops in the code to be executed in parallel, being the compiler itself the responsible of creating and managing the threads that make it possible, as explained in [51].

OpenMP is implemented in FDS and allows the usage of multiple cores of a computer or computer cluster to parallelize the FDS calculations. The number of cores that will be used are defined before the simulation, and are more effective if they are physically associated, for example in multi-core processors [30]. A study in OpenMP efficiency is available in the FDS guide [30].

MPI

MPI stands for ''Message Passing Interface" and is a set of library routines that allow process management, message passing (among processes) and other communication operations. In contrast to OpenMP, the division of the program at hand in multiple processes is more responsibility of the developer and makes it more difficult to write and manage.

FDS allows the creation of multiple meshes, this meshes can be distributed among several processes to be calculated in parallel, MPI handles the communication among the processes that happens at the boundaries. A study in the efficiency of the usage of the MPI is shown in [30] in this studies is appreciable how the time saving is proportional to the amount of meshes in which the domain is divided, but it introduces a new process that consumes time, that is the communication of data among the meshes.

OpenMP + MPI

It is possible to use both methods together, with the program parallelized in different processes (MPI) and the internal loops working in parallel in different threads. Still, using MPI is recommended over using openMP, as the capacity of MPI to reduce the calculation time is higher [30].

3.3 Multiscale factors

Multiscale models offer a different alternative, here the usage of a 1D model can substitute regions of the 3D domain, lowering the calculation time consumed by those regions greatly, not compromising the precision of other zones of the domain and not needing higher amounts of computation power to manage parallelized work. The comparison between the FDS paralellization methods and using the HVAC model with FDS to make

Multiscale simulations has been observed in the work by Vermesi et. al. [71], showing that multiscale models achieve higher degrees of time saving.

3.4 Comparison Multiscale and Full-3D simulations

To compare the full-scale and multiscale models a hypothetical tunnel was simulated using both of the methods to compare the amount of time they spend. The tunnel used has a 4.8 m x 4.8 m section and a length of 600m. Inside this tunnel, a pool fire of 2MW is started, placed at 300 m from each portal, in the middle of the roadway. In the upstream portal of the tunnel the air speed is imposed to be 1 m/s, equivalent to 28.23 kg/s, of mass flow, for the ambient density of the air. Conversely, in the downstream portal the pressure is set to be ambient.

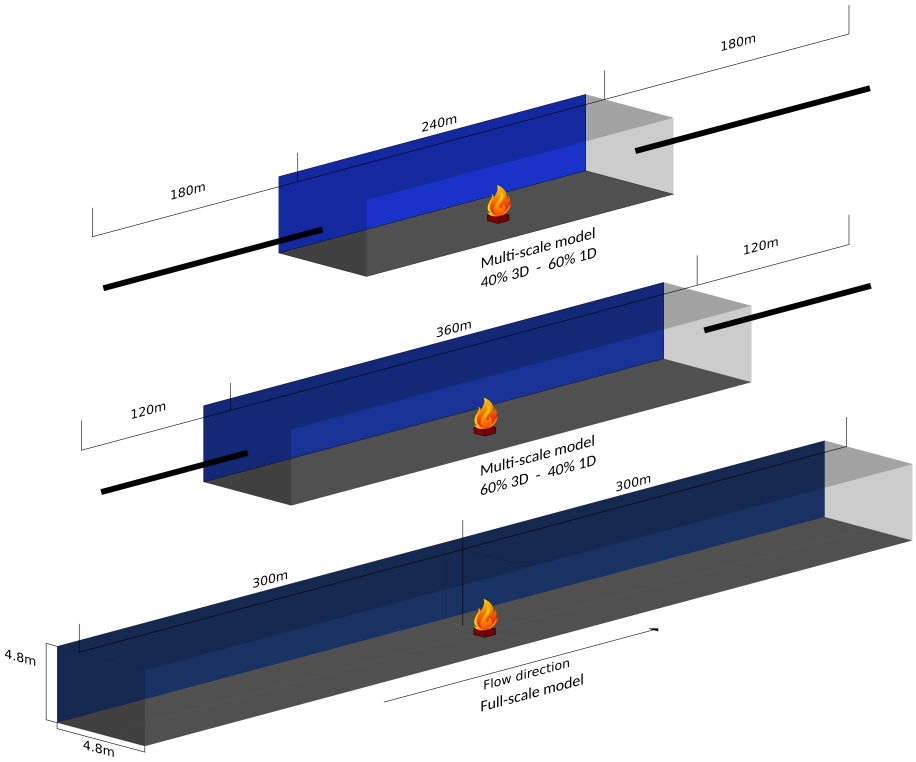

Figure 3.1: Simulated Tunnels for Multi-scale and Full-scale comparison (Full, n°2 and n°4, from the lower to the higher)

The Table 3.4 contains information regarding the 5 cases that will be compared in this section, 1 Full scale test of the tunnel and 4 multiscale tests with different 1D-3D domain distributions. Three out of this five test cases are shown in Figure 3.1, making evident their different domain distributions.

Case	3D length	3D%	1D length	1D%
Full	600m	100%	0m	0%
n°1	420m	70%	180m	30%
n°2	360m	60%	240m	40%
n°3	300m	50%	300m	50%
n°4	240m	40%	360m	60%

Table 3.1: Cases comparing multi-scale and full-scale simulations

The exchange boundaries between the two models are placed at the same distance before and after the fire, in these test cases. Still, the boundary upstream of the fire is always placed at a distance higher than the expected back-layering length, that is calculated to be of 54m (Li formula) or 63m (Weng formula) [76].

All the tests were executed in the same computer, an Intel Xeon Gold 6230R, with 96gb of Ram, running linux Ubuntu 20.04. The tests use the multiscale and OpenMP setting, using 4 cores for the OpenMP calculation. Further time reduction can be obtained by using MPI instead of OpenMP, as it was seen in the literature [71], still the script used to link the 1D and 3D models has to be adapted to be used in an MPI calculation.

3.4.1 Test Results

The five tests simulated the flow in the tunnel for 1000 seconds. The flow inside the tunnel reaches the downstream portal of the tunnel after 300 seconds, as seen in the Figure 3.2. From that point onward the flow inside the tunnel gradually reaches steady state. The flow is stratified, with higher velocities and temperatures in the upper part of the tunnel downstream of the fire. In the Upstream area of the fire some back-layering is present, with a length of 65 meters approximately, not very far from the values previously approximated.

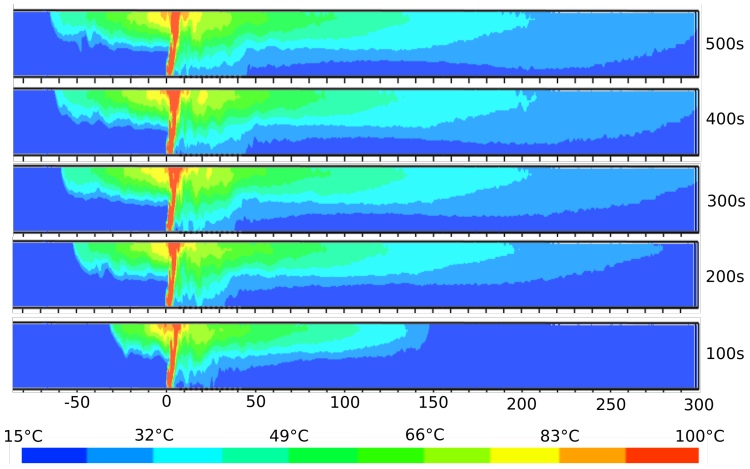

Figure 3.2: Temperature across the longitudinal section of the tunnel after 100s, 200s, 300s, 400s and 500s of the fire start

Calculation times

Completing the test took different amounts of time for the different setups, mostly influenced by the distribution of the domain among the 1D and 3D model. The Figure 3.3 shows the time each one of the five test cases needed through the simulations, until they end at the 1000 seconds. The time curves for every simulation are mostly lineal, only the first 50 seconds of the simulation are computed a little faster as the fire starts gradually after some seconds of cold flow, which implies a simpler flow with a longer time step.

The time reduction obtained for every 10% of the domain simulated using the 1D model of the multiscale has a linear trend, suggesting that the simulation time reduces linearly with the increase of the proportion of the domain modeled in 1D. In the Figure 3.4, the calculation times for the different setups are compared to a straight line from the full scale simulation time to 0 seconds. This Figure makes it evident that the time reduction is almost linear for the presented cases. Still, the 1D portion uses a smaller, and not null, amount of time and introduces time expenditure in the form of boundary conditions calculation, data exchange and data output, that is reflected in the deviation from the straight line.

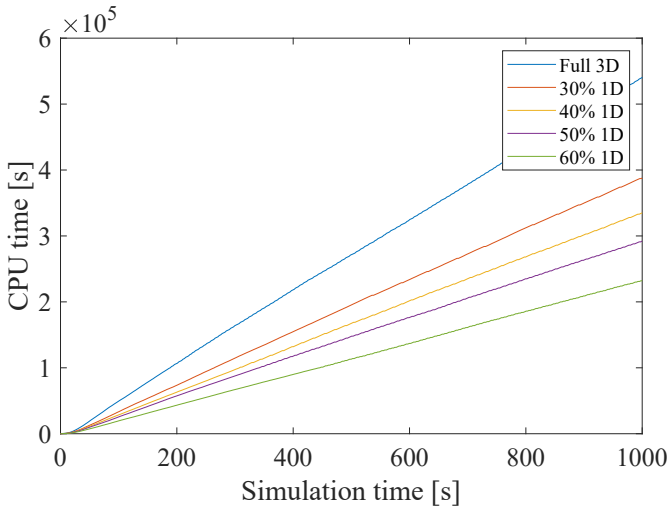

Figure 3.3: Simulation time against CPU time in full and multi-scale simulations

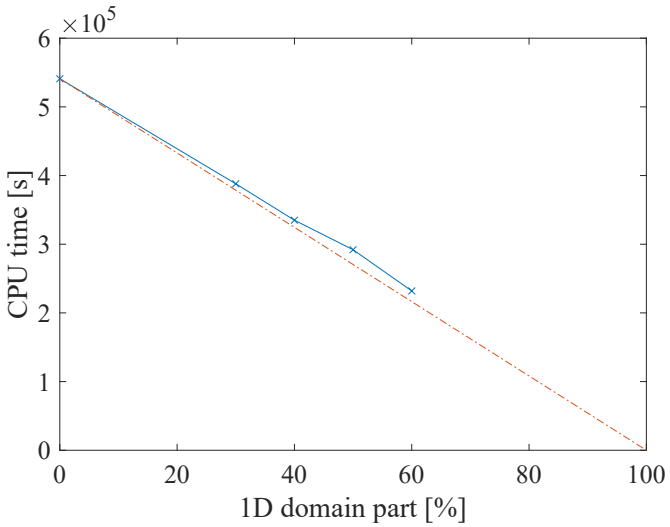

Figure 3.4: CPU time reduction for different 1D-3D distributions

Fluid dynamic Behavior (Pressure)

Other properties of the flow are compared to ensure that the simulation is not only faster, but also accurate. The Figure 3.5 shows the pressure for the five cases, averaged over the 400 to the 900 second of simulation. The behavior of all of the curves is similar in qualitative terms, as they have similar shapes and averages. Still, the curve with the higher 1D portion of the domain introduces higher pressures close to the fire and in the upstream part of the domain. The remaining curves maintain their errors, with respect to the full 3D simulation, around the 10%, being lower in the case of the 50% 1D and 3D curve, where the error remains close to the 5%.

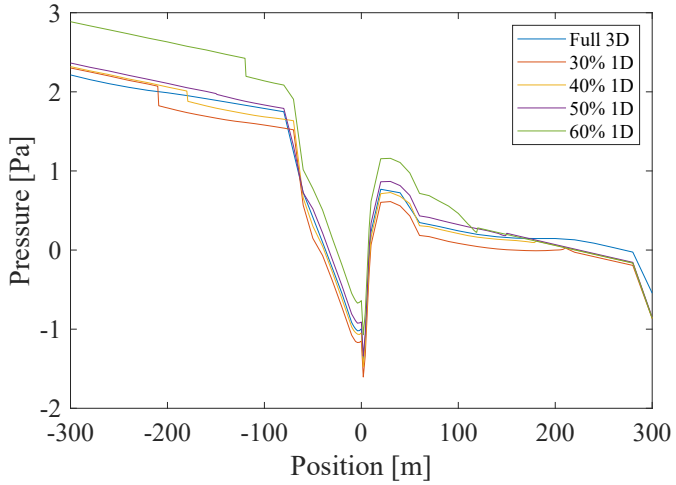

Figure 3.5: Pressure along the tunnel in full and multi-scale simulations

Fluid dynamic Behavior (Velocity)

Following the analysis, the velocity is shown in Figure 3.6. The differences in the velocities are smaller, most of the multiscale simulations keep their velocities within small deviations from the full-scale simulation. The deviations are concentrated in two points, the downstream portal and the back-layering length. In the case of the back-layering area the difference is introduced by small variations in the back-layering length, which changes the conditions in the area noticeably. In the case of the downstream portal, the deviation comes from a different exit flow interaction where the 3D makes an ambient exit with bidirectional flow (exiting at high speed in the upper part and entering at low speed in the lower part to keep the same mass flow, and a pressure drop due to the increase in velocity) and the 1D model only introduces a localized loss (to match the pressure behavior of the 3D). Among the showed test cases the only one which includes higher differences between the 3D and multi-scale simulation is the case n°4 (with 60% of 1D domain). This difference is caused by the error introduced close to the boundary between the models, when the flow passes from the 3D to the 1D domain. This error is lower as the boundary is farther from the fire and the flow is more homogeneous, and represents a limitant factor for the domains used in the multiscale.

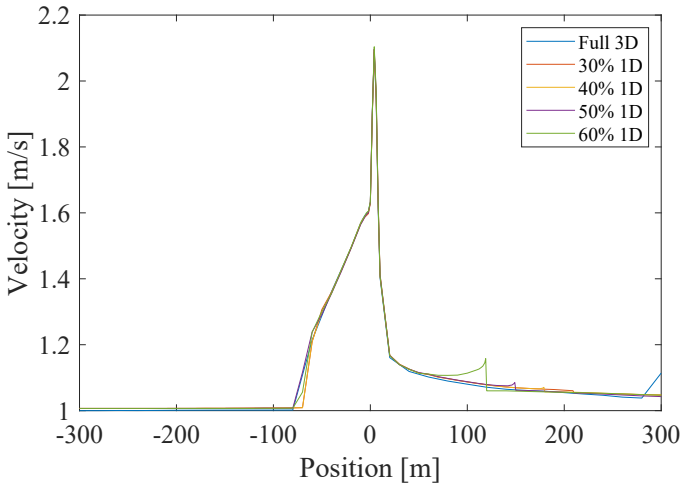

Figure 3.6: Velocity along the tunnel in full and multi-scale simulations

Thermal Behavior (Temperature)

The behavior inside the thermal model is shown in the Figure 3.7. The thermal model errors center in the same spots as in the velocity, Figure 3.6, being the points the downstream portal and the back-layering length. In the case of the downstream portal the sudden raise in velocity includes air that enters, at environment temperature, from the outside, lowering the temperature of the area. And in the case of the back-layering length the small difference in the total back-layering length produce differences among

the simulations. Here the divergent behavior of the temperature case n°4 is caused by the same boundary problems mentioned in the velocity section, as colder air enters from the boundary and lowers the temperature of the vicinity.

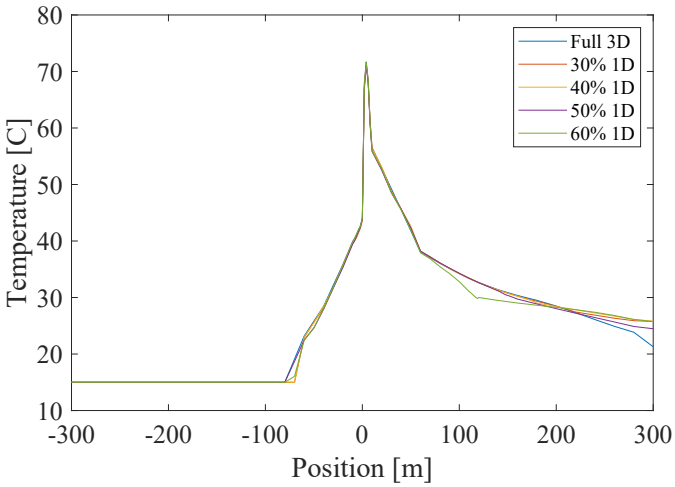

Figure 3.7: Temperature along the tunnel in full and multi-scale simulations

3.5 Observations

The results in the cases from the n°1 to the n°3, meaning from 30% up to 50% of the domain in the 1D, accumulate low amounts of error in both the velocity and temperature, and acceptable amounts of errors in the case of the pressure. Still, raising the 1D domain to a 60%, in this case, introduces higher errors in the pressure, temperature and velocity. The reason is that being closer to the fire the downstream exchange boundary is placed in an area with a non-homogeneous flow. And in this non-homogeneous flow the 1D assumption is not suitable, introducing errors into the simulation.

Regardless of this issue, the multi-scale model has achieved time savings proportional to the amount of domain simulated through the 1D in all the cases, with limited amounts of errors in most of them. The calculation time reductions will be more pronounced as the tunnels simulated are longer. This can be seen in Figure 3.8, where the Dartford tunnel, a 1.5 km long tunnel, is simulated using a 3D 250 m long and a 1D 1250 m long. As a result the time needed for the multi-scale simulation is lower than a sixth of the time necessary to complete the same full 3D simulation.

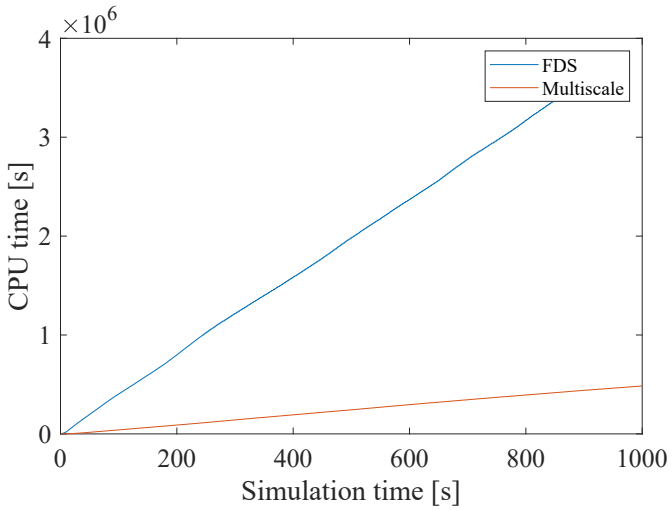

Figure 3.8: Simulation time against CPU time in full and multi-scale simulations in the Dartford tunnel

It is known that MPI simulations dividing the domain in several meshes can match or improve the results shown; however the computational capacity required for those simulations would also raise. To provide an equilibrated comparison the multiscale was matched with a regular 3D simulation. The model must still be developed to be capable of adding multimesh calculations and provide even faster simulations.

Chapter 4

Pressure Equivalent Model

The software and programs used for fire research are under constant testing and development thanks to the input given by the different researchers of the fire research community. Among these software, FDS is a good example where the frequent testing finds different issues that are then tracked by the FDS developers to be solved, with the objective to continue improving the FDS overall accuracy and speed.

Some attention has been focused, in the forums and issue tracker, in the pressure and mass flow distribution along tunnels in FDS [22, 20, 21]. The issues reports showed simulations where inconsistencies were found between different simulations and groups of data extracted from FDS.

Along my research some inconsistencies were seen between the values calculated for pressure in the FDS and some expected values (values obtained from analytical sources and other software). Pressure drops, after the fire, where higher than expected, leading to some doubts regarding the accuracy of the 3D. Still, other variables as the velocity and temperature had small deviations from the reference values, indicating that the problem was probably located in the pressure calculation.

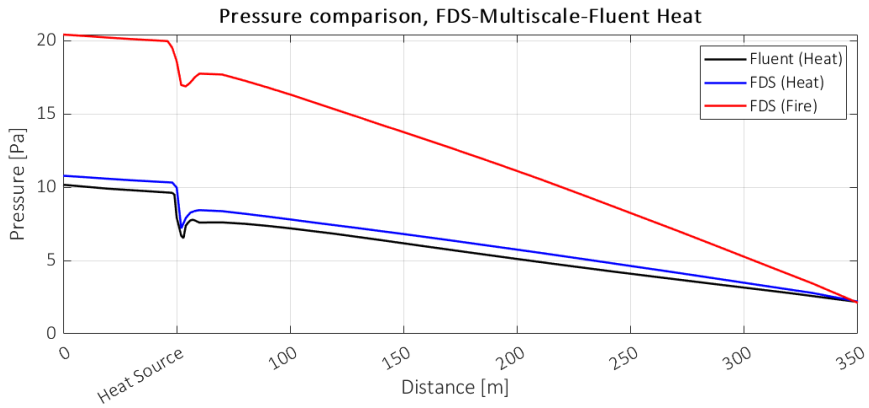

Figure 4.1: Pressure issue graph

In Figure 4.1 the behavior of the pressure across a tunnel of 350 m is observed. The tunnel has a cross-section of 3m x 3m, with a flow speed of 1.5 m/s. A fire or heat source is placed 50 m away from the tunnel upstream portal, with an intensity of 2MW. The behavior observed in the FDS and Fluent simulations, using a heat source, agree in similar values for the pressure upstream and the pressure losses across the tunnel. Nevertheless, the pressure drop observed in FDS cases, with fire, for the downstream area is 3 times the pressure drop observed in heat source cases. The simulation of fire complicates the physics of the problem, still the temperature and velocity conserve similar values in the 3 simulations (FDS fire, FDS heat and Fluent heat), suggesting that there might be some issues in the pressure values obtained in the fire simulation. The values are measured all as mass averages in the sections of the tunnel, discarding issues related to point measurements not being representative of the whole 3D section.

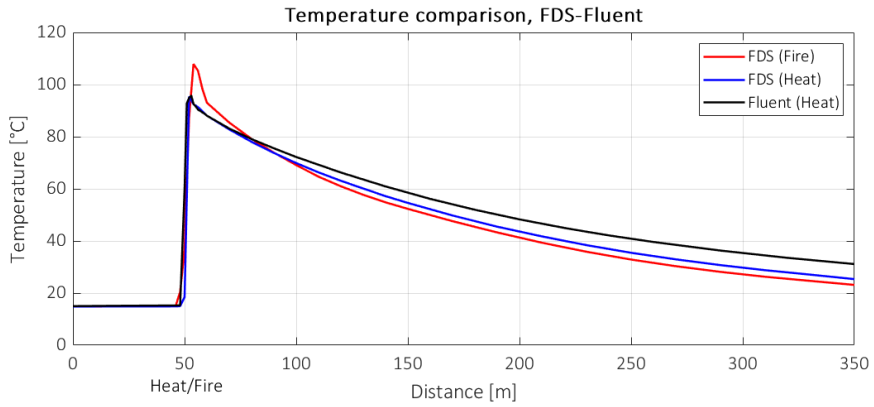

Figure 4.2: Temperature graph, related to the pressure issue

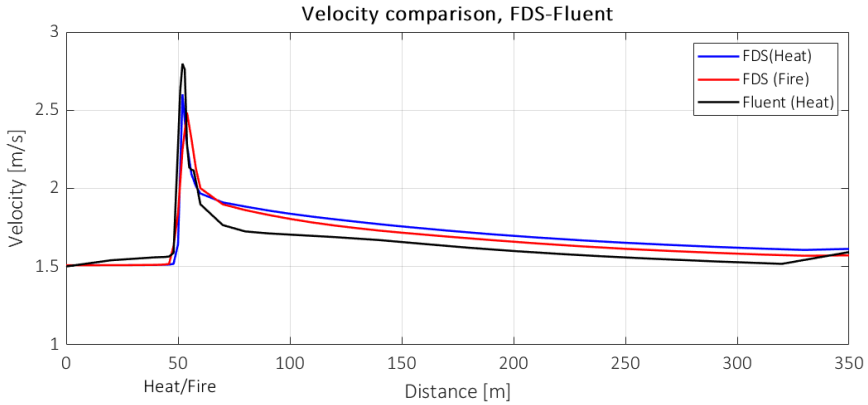

Figure 4.3: Velocity graph, related to the pressure issue

In Figure 4.2 and Figure 4.3 relatively small differences can be observed between the results of the 3 simulations (FDS fire, FDS heat and Fluent heat). The differences are

smaller when the the heat and fire FDS simulations are considered. This small differences do not agree with the large difference in pressure, which is the main motivation to analyze more in depth the pressure calculation and understand if there is any problem. Then, to compare the results of the pressure calculation a 1D model is developed. This 1D model calculates the pressure drop across the tunnel using other properties calculated by the FDS and applying a modified version of the Bernoulli equation. This model is explained in the next section.

4.1 Modelling

The model is developed by dividing the tunnel in sections that are one cell thick in the longitudinal direction, as indicated in the Figure 4.4. The velocity, density and other properties are averaged inside these sections.

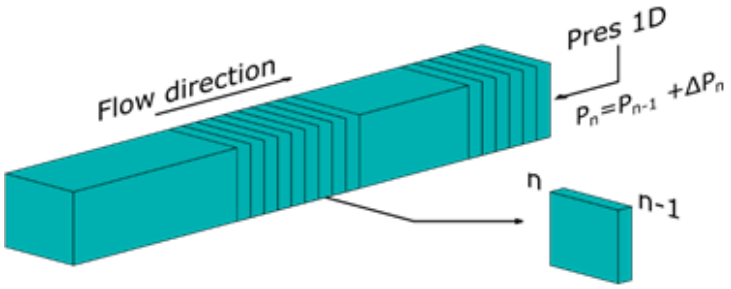

Figure 4.4: Domain discretization for the pressure equivalent model

The Bernoulli equation is applied to each section to obtain the pressure drop across each fragment of the domain. The expression 4.1 shows the bernoulli equation where the sum of the variations in kinetic energy (Δe_c), potential energy (Δe_p) and the pressure term ($\int v\,dP$) is equal to the losses in the portion of the domain. It is assumed that the flow is incompressible inside of each one of the domain sections, making it possible to integrate the pressure term and simplifying the expression. The losses are approximated as the product of the effective viscosity (μ_{Eff}) times the laplacian of the velocity, obtaining the expression 4.2 that can be calculated from data available in FDS.

$$\Delta e_c + \Delta e_p + \int v\,dP = losses \tag{4.1}$$

$$\Delta e_c + \Delta e_p + v\Delta P = \mu_{Eff}\nabla^2 u \tag{4.2}$$

The aim of the model is to calculate the pressure across the longitudinal direction of the tunnel. To achieve this the pressure change is calculated in every section using the Equation 4.3. The pressure in the longitudinal direction is calculated using the pressure

changes, as in Equation 4.4,and fixing the initial pressure in an OPEN portal of the tunnel.

$$\Delta P = \rho \mu_{Eff} \nabla^2 u - \rho \Delta e_c - \rho \Delta e_p \tag{4.3}$$

$$P_n = P_{n-1} + \Delta P_n \tag{4.4}$$

4.1.1 Data Extraction

The data used for the calculations are all extracted or calculated using FDS properties. The data used are specifically the density, velocity, the laplacian of the velocity and the viscosity. First, the values for density are defined in the center of the cells, so the average is obtained over the cells in the section. Instead, the velocities are calculated in the faces of the cells, and the average is calculated as the mid value between the averages of the two faces of the section, this applies to other quantities like the derivatives of the velocity. The laplacian of the velocity is calculated by numerically derivating the velocity using central differences, using the velocity field obtained by the FDS. The viscosity is extracted from FDS, where the effective viscosity represents the sum of the molecular viscosity and the turbulent viscosity that is calculated by the wall-model.

4.2 Testing methodology

The layout of the simulation used in this chapter is composed by a tunnel of 3m per 3m of cross section and a length of 350 meters, like the one used in the figures shown before, Figure 4.1, Figure 4.2 and Figure 4.3. A fire is placed inside the tunnels, 50m away from the upstream portal. The fire is simulated as a heat source that releases hot air that equals the heat produced by a 2MW fire, in (Heat) cases, and as a fire of 2MW fueled by Diesel.

The pressure equivalent model and FDS models use the multiscale with a “PRES” boundary upstream and a “VEL” boundary downstream, meaning that the 1D imposes the velocity upstream and the pressure downstream. The upstream 1D has a mass flow set to get a velocity of 1.5 m/s in the 3D tunnel, at 15°C. In the downstream direction 250 meters of tunnel arrive to an exit to environmental pressure. The focus of the analysis is on the pressure drops inside the 3D, therefore the 1D results are omitted for clarity.

In the Fluent case the upstream portal has a velocity inlet boundary type, imposing 1.5m/s of velocity, of air at 15°C. in the downstream side the boundary condition is a pressure outlet boundary condition set at environmental pressure.

Regarding the Heat source, in both programs it has been modelled as a 1.2m x 1.2m pool of 0.2 m of height. The total air flux is of 1.5933 kg/s at a temperature of 826.85 °C.

To compensate this inflow of air the sides of the pool extract the same amount of air. In this way the amount of air circulating in all the tunnels, with fire or heat, is the same. In the fire scenario it behaves as a surface of the same dimensions with an imposed Heat Release Rate Per Unit Area of 2MW.

Regarding the Meshing, the FDS has a hexahedral mesh, with elements of 0.3m x 0.3m x 0.3m, arranged 10 in the width, 10 in the height and 1167 in the length. In fluent, the mesh is Tetrahedral, using inflation in the walls to obtain a higher density of cells in the walls and achieve higher precision in the losses calculation.

Regarding the physical models used, in FDS the default settings for a LES simulation are used, switching to WALE in the case of the wall model. In Fluent, the physical configuration were changed to include the energy calculations, to simulate turbulence with the k-ω SST model and handle the density of air as a incompressible ideal gas.

4.3 Results comparison Fluent

The results of the different simulations are compared by the trend they show in the longitudinal direction of the tunnel, when averaged on time. Also, cross-sections of the Fluent and FDS simulations are compared to check the similarities in the distribution of temperatures.

4.3.1 Longitudinal

Now, in figures 4.5 and 4.6, it is possible to observe the average, over a 100 seconds of steady state flow, of the pressure. In the case of 4.5 the comparison is between the fluent heat calculation, used as a reference, and the FDS heat calculation, side by side, the pressure equivalent model resulting pressure values. The 3 graphs show a similar trend, with small differences in the losses downstream of the fire and in the presure effect of the heat source.

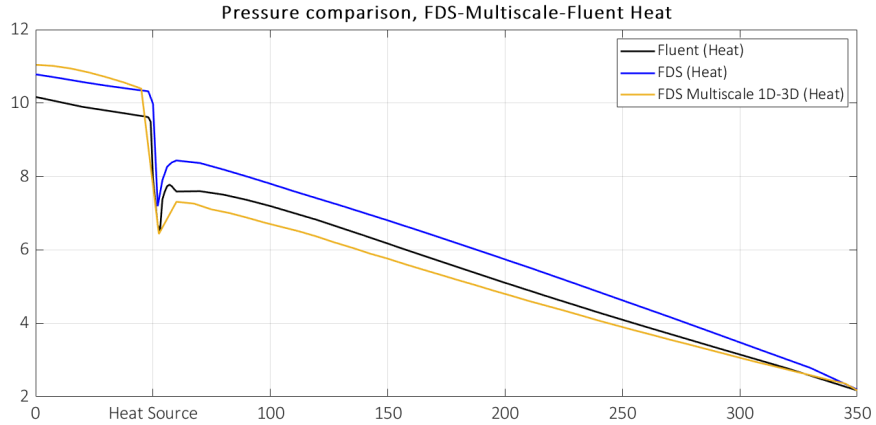

Figure 4.5: Pressure comparison, FDS with pressure equivalent model vs Fluent (Heat)

The most evident difference can be seen in the figure 4.6 where the FDS simulations include fire instead of a hot air flow, as heat source. Here the downstream losses reported by the fire simulation are more than two times higher than the same losses in heat simulations or in the pressure equivalent model. Still, the output of the pressure equivalent model results always close to the same values, regardless of the heat source used, indicating that the expected pressure drops away from the fire should not be influenced severely by the nature of the heat source.

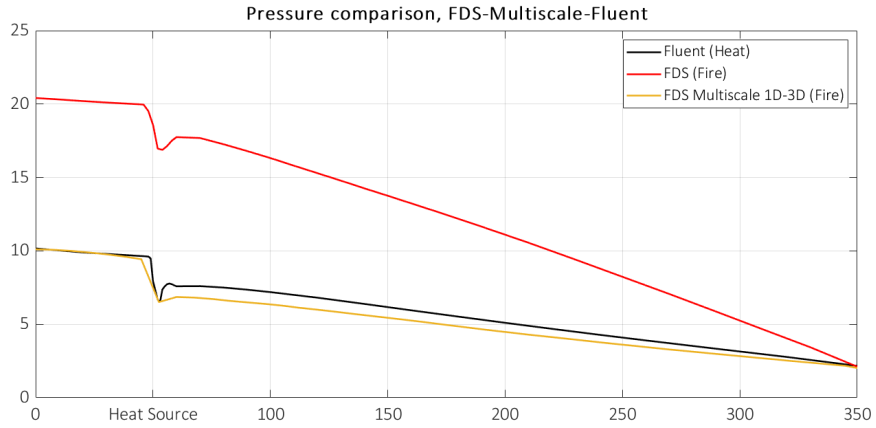

Figure 4.6: Pressure comparison, FDS with pressure equivalent model (Fire) vs Fluent (Heat)

4.3.2 Cross-sections

Figures 4.7 and 4.8 compare the cross-sections distribution of both the temperatures, 4.7, and the velocity, 4.8.

The distributions of temperature in figure 4.7, are taken every 20 m after the first 30 m downstream of the heat source, fire for the FDS and hot air flow for Fluent. Also, they both belong to the same simulations that are described in figure 4.2. The distributions are in agreement with the steady state trend, shown in previous graphs. The temperatures are closer between the two simulations when the sections are closer to the heat source itself, both in the average value and in the distribution across the cross-section. Also, it can be observed that both of the flows are stratified with hotter temperatures in the upper area, due to buoyancy.

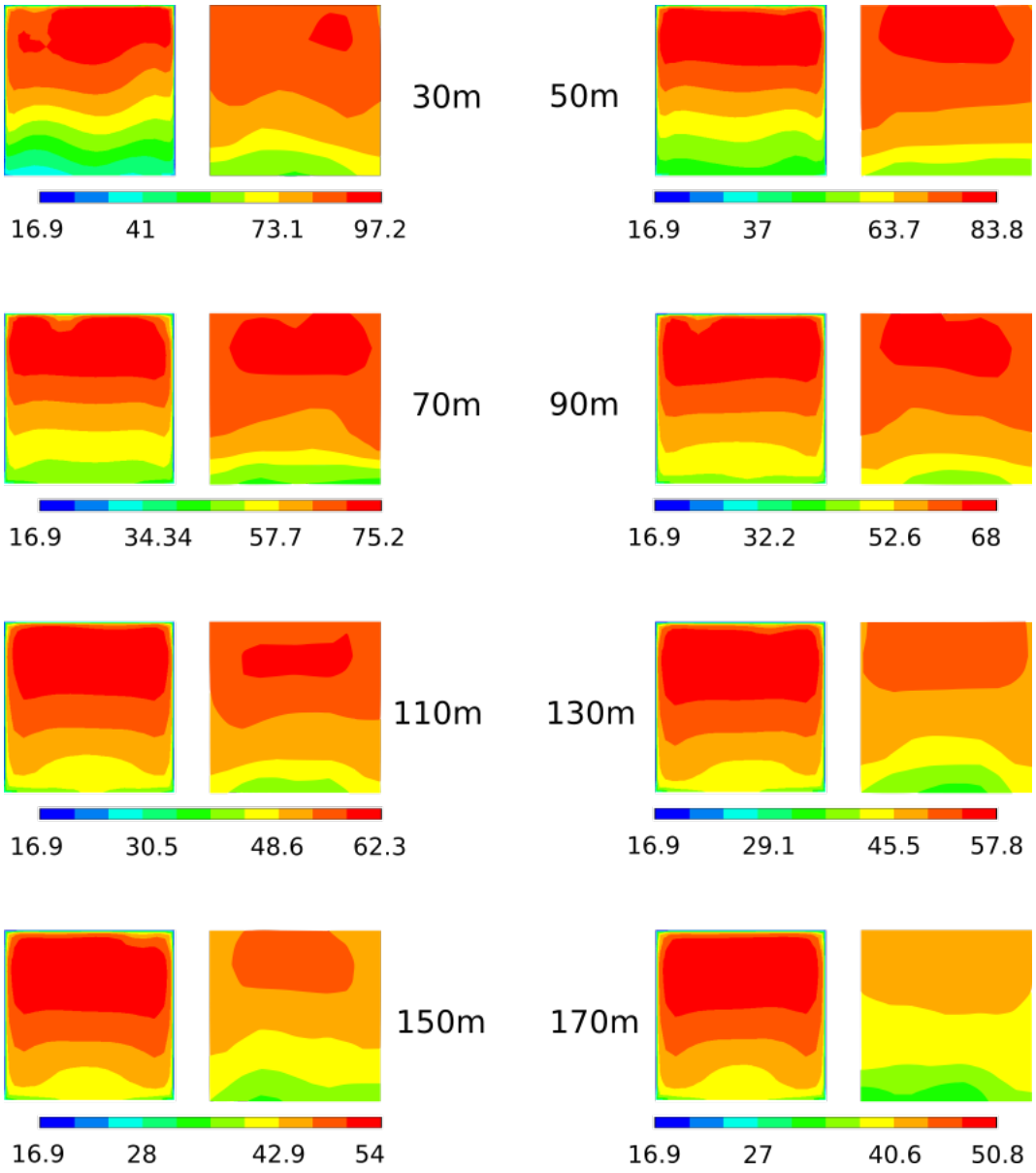

Figure 4.7: Temperature sections downstream of the heat source, Fluent (left) and FDS (right)

The velocity sections, shown in figure 4.8, show a trend where the distributions are more similar when the evaluated section is more distant to the heat source. The flow gets distributed with faster flows in the upper part of the tunnel, and slower close to the floor, due to buoyancy. Still the Fluent graphs seem to need some more distance to arrive to this distribution, when FDS has it immediately after the heat source. Still the distributions and velocity values are very similar, which supports the idea that the temperature and velocity are mostly accurate.

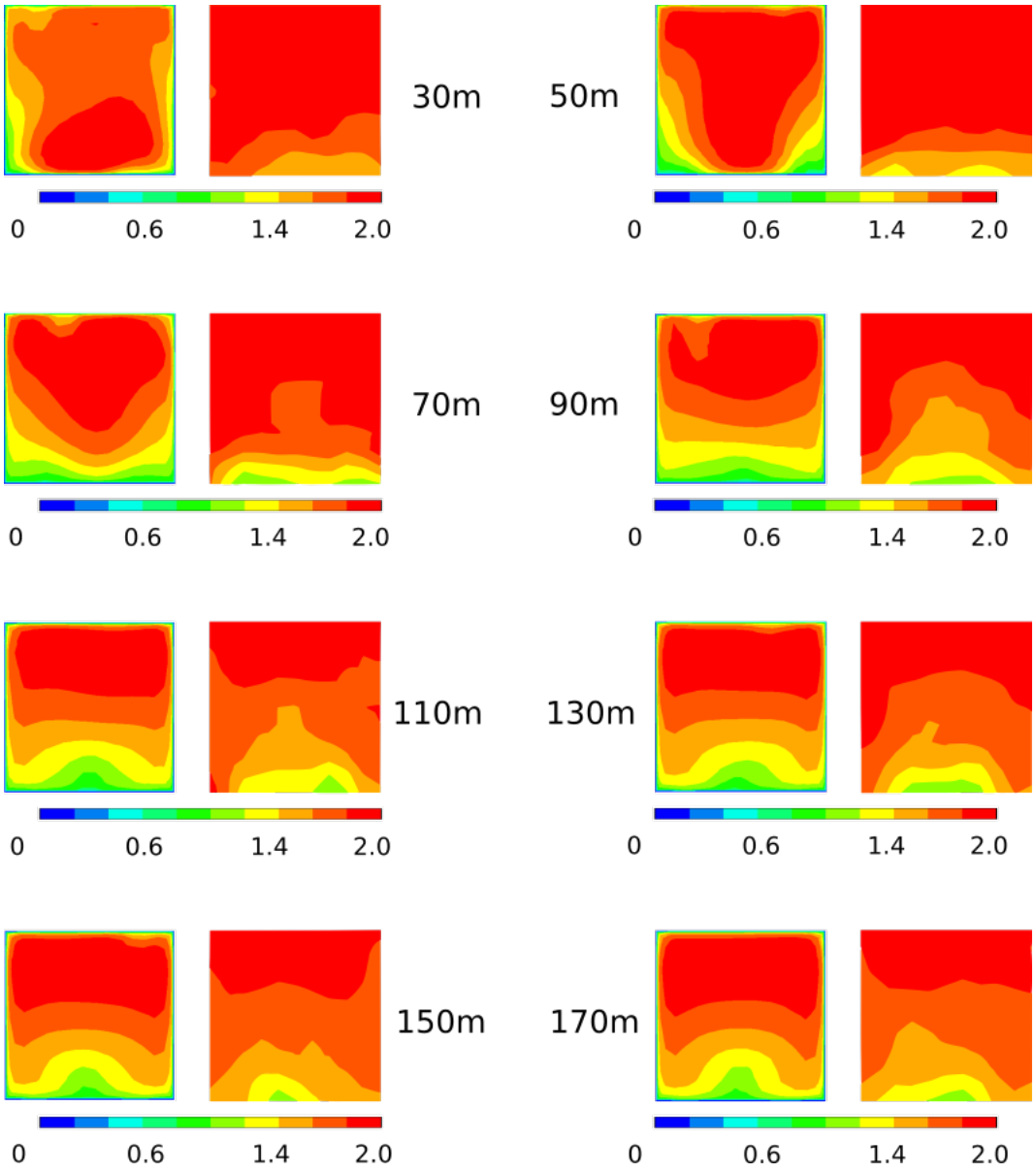

Figure 4.8: Velocity sections downstream of the heat source, Fluent (left) and FDS (right)

4.4 Observations

Taking into consideration the different comparisons that have been shown in this chapter it was possible to determine that:

- There are some slight issues in the pressure output provided by FDS for tunnel simulations.

- The issues present in the pressure seem to have no effect in the calculation of the temperature and velocity, for time-averaged graphs.
- Developing a pressure equivalent model inside FDS confirms the accuracy of the temperature and velocity, as it manages to approximate the values for pressure using the velocity and density as input.
- Further comparison with Fluent confirm agreement not only with the time-averaged values, but also with the cross-section distributions of temperature and velocity.

After this analysis it was decided to keep studying FDS calculation process, in order to find a method to improve the calculation results obtained from the program. The pressure equivalent model allowed us to obtain accurate results to the pressure in the multiscale simulations. Still, as the equivalent pressures are just calculated as an output and are not used inside FDS as part of the calculations it does not represent a definitive solution to the pressure problems, but a good step into finding the actual origin of the pressure issues.

Chapter 5

Tunnel pressure modelling analysis

Following the developments in the previous chapter the next step in the research was to continue the analysis of the pressure calculations inside the FDS. In this occasion it was possible to enter in contact with the developers of the software, both through the issue forums of the FDS and the 2nd Summer School on Fire Dynamics Modeling 2019 (in Juelich, Germany). The research this time was oriented towards testing the outputs provided for tunnels, simplifying the scenarios simulated to find a setup that was capable of providing convergent and reliable results. And therefore, determine the models that could be involved in pressure issues inside the FDS calculation.

5.0.1 Research collaboration

The main part of the collaboration took part from the 29th of September of 2019 through the 29th of February of 2020. During this 5 months constant testing of the program, updating and changing of the code was made.

Through the tests inconsistencies where found when using Fire, instead of Heat, as a source in the tunnel fires. The issue developed as a problem regarding the usage of the specific heat ratio as variable, when placing a fire, opposed to using a constant specific heat ratio, as the latter managed to converge to reasonable values. Following this line of though, it was determined that the main issue should be linked to one of the assumptions that the FDS does in its calculations, that is the Low-Mach number assumption.

During this research process some verification tests for 1D tunnels have been done, checking the validity of calculations in 1D tunnels with both constant and linearly variable specific heat.

Different solutions where proposed at the time, among which the FDS team has continue to develop one that is actually in phase of testing and close to release, the Tunnel pre-conditioning [30].

Still, the solution explored in this work is related to the analysis of the pressure model to find the origin of the problem and the pressure solver more fit to simulate

tunnel fires.

5.1 The pressure calculation

FDS solves the pressure in the whole domain through a Poisson equation. The pressure calculation is made around the assumption of separating the pressure in a background and perturbation pressures, as explained before in Chapter 2. The value calculated referred to the pressure is the Bernoulli equation total pressure H, as in the equation 5.1. Here the first right hand term refers to the dynamic pressure, calculated with the velocity vector $\mathbf{u}$ and the second term is the perturbation pressure $\tilde{p}$ per unit of mass, that is the pressure form used for the fluidinamic part of the calculation.

$$H = \frac{|\mathbf{u}|^2}{2} + \frac{\tilde{p}}{\rho} \tag{5.1}$$

The poisson equation is a form of the momentum equation, that is reached through several simplifications of this latter expression.

5.1.1 Poisson equation for momentum

Starting with the non-conservative form of the momentum equation, as in equation 5.2

$$\frac{\partial(\rho\mathbf{u})}{\partial t} + \nabla \cdot \rho\mathbf{u}\mathbf{u} + \nabla p = \rho\mathbf{g} + \mathbf{f}_b + \nabla \cdot \tau_{ij} \tag{5.2}$$

The first and second term in the left hand side are rearrenged into a form were the velocity divergence appears, equation 5.3.

$$\rho(\frac{\partial\mathbf{u}}{\partial t} + (\mathbf{u} \cdot \nabla)\mathbf{u}) + \nabla p = \rho\mathbf{g} + \mathbf{f}_b + \nabla \cdot \tau_{ij} \tag{5.3}$$

In equation 5.3, the terms in the right hand side are the buoyancy term $\rho\mathbf{g}$, the influence of lagrangian particles $\mathbf{f}_b$ and the viscous term $\nabla \cdot \tau_{ij}$. Now the term $\rho_0\mathbf{g}$ is extracted from the pressure term ∇p, leaving only the variation of perturbation pressure $\nabla\tilde{p}$. Then the equation 5.4 is introduced into the expression, and all the terms are divided by the density.

$$(\mathbf{u} \cdot \nabla)\mathbf{u} = \frac{\nabla|\mathbf{u}|^2}{2} - \mathbf{u} \times \omega \tag{5.4}$$

$$\frac{\partial\mathbf{u}}{\partial t} + \frac{\nabla|\mathbf{u}|^2}{2} - \mathbf{u} \times \omega + \frac{1}{\rho}\nabla\tilde{p} = \frac{1}{\rho}\left((\rho - \rho_0)\mathbf{g} + \mathbf{f}_b + \nabla \cdot \tau_{ij}\right) \tag{5.5}$$

Now in equation 5.5 the pressure perturbation term most be sustituted with equation 5.6 to obtain the divergence of the total pressure ∇H. Then rearrenging equation 5.7 is obtained.

$$\frac{1}{\rho}\nabla\tilde{p} = \nabla\left(\frac{\tilde{p}}{\rho}\right) - \tilde{p}\nabla\left(\frac{1}{\rho}\right) \tag{5.6}$$

$$\frac{\partial \mathbf{u}}{\partial t} - \mathbf{u}\times\omega - \frac{1}{\rho}\left((\rho-\rho_0)\mathbf{g} + \mathbf{f}_b + \nabla\cdot\tau_{ij}\right) - \tilde{p}\nabla\left(\frac{1}{\rho}\right) + \nabla H = 0 \tag{5.7}$$

Now expression 5.7 can be rearrenged and simplified in equation 5.8, and finally applying the divergence operator in both sides the Poisson equation form is achieved, equation 5.9

$$\frac{\partial \mathbf{u}}{\partial t} + \mathbf{F} + \nabla H = 0 \tag{5.8}$$

$$\nabla^2 H = -\frac{\partial \nabla\cdot\mathbf{u}}{\partial t} + \nabla\cdot\mathbf{F} \tag{5.9}$$

A more detailed development of these formulas can be found at the FDS technical guide [33] and some more info in [44].

5.1.2 Solvers

There are different kinds of solvers that can be used to find a solution for the Poisson equation. They can be classified by some of their characteristics as:

- Handling of Internal Obstructions: The domains for the FDS simulations are discretized into rectangular meshes, and obstructions or walls are made to match this grid. These obstructions can be managed through two approaches.
  - Structured: All the grid is incorporated into the resulting discretization, including the gas cells and the solid cells. It makes the form of the matrices very regular, but including solid cells introduces problems with imposing zero penetration velocity conditions.
  - Unstructured: Only includes gas cells and an homogeneus no-flux Neumann boundary condition is specified close to the solid cells. The discretization and resulting matrices are not as regular as structured ones, needing solvers that are more robust .

- Communication among subdomains: Domains in FDS are frequently divided in more than 1 mesh. As the number of meshes in parallel increase the time it takes for the data to arrive from a part to other in the domain depends highly on how the meshes comunicate among them
  - Local: Meshes only comunicate with adjacent meshes. Is a faster approach, but effects might take time to travel by advancing one mesh per time step.
  - Global: Data is not only exchanged with neighboring meshes but with every mesh. As a disadvantage it might take more time to achieve the global comunication, as all the meshes have to exchange info at the same time (some meshes might have to wait for larger meshes to exchange information). Still as all the meshes share the info they are capable to react faster to the data if needed.
- Algorithm approach: Meaning if the algorithm finds the solution directly through one computational cycle, or it does an iterative calculation until it arrives to a desired tolerance.
  - Direct
  - Iterative

Fast-Fourier Transform (FFT)

This is the default solver used by the FDS software. It can be classified as a Direct, structured and Local solver. It is based in the solver package CRAYFISHPACK that solves the pressure in each mesh, then the data is exchanged with the other meshes, locally, to provide an overall solution to the pressure of the whole domain.

The FFT works by finding the eigenvectors and eigenvalues of the matrix A of a system $Ax = B$ that needs to be solved. Knowing them is possible to express A as a combination of said eigenvectors, simplifying the system that has to be solved. Finding these eigenvectors and eigenvalues is generally difficult for any matrix, but is manageable for structured meshes. It must be remarked that the separation of the pressure in background and perturbation pressure, previously mentioned, allows for the calculation of only one Poisson equation through the simulation, otherwise it would be neccesary to rebuild the Poisson matrix every time step.

The solutions of the pressure are continuous in the interior of each boundary, the comunication between boundaries does not ensure that the normal derivatives of the velocity matches at both meshes. Summed to this the characteristics non-zero velocities across solid cells, introduced by the structured discretization, also introduce some problems to the Poisson equation solution. Both of this issues are solved through iteration of the FFT calculation, with the end of reducing this errors down to a certain tolerance, making in the end the method not entirely direct, but reliant in iterations to find a global solution for the pressure.

LU matrix solvers (GLMAT and UGLMAT)

This solver is based in an LU factorization of the A matrix. Therefore, the matrix A is decomposed into the product of two triangular matrices $L \times U$, where L stands for lower as the terms above the main diagonal are all zero, and U stands for upper, as the terms below the main diagonal are all zero. When the problems are highly symmetric it is possible to work with only one of the LU matrices, as the expression 5.10 relates both of the matrices. The solution for the system is found then by progressively sustituing values into the triangular matrices.

$$U = L^T \tag{5.10}$$

Similarly to FFT, it is possible to calculate the necessary matrices once and use them along the simulation, thanks to the pressure division in background and perturbation pressures. But, in contrast, the LU-decompositions are capable of handling structured (GLMAT) and unstructured (UGLMAT) discretizations.

Some advantages of the LU-decompostion are that they are capable of guaranteeing continuity in the normal derivative of the velocity field also between meshes. Furthermore, in the case of UGLMAT, the LU-decomposition can also guarantee zero penetration velocities in internal obstructions, as it is capable of imposing accurate boundaries to these obstructions, because of the unstructured discretization.

Regarding disadvantages of the LU-decomposition, they require higher amounts of memory, as they don't take advantage of the sparcity of the A matrix and by generating the LU matrices it fills the matrices with non-zero values, where the A matrix would have had mainly zero values. Another possible disadvantage is that LU-decompositions comunicate globally the meshes, frequently requiring longer amounts of simulation times than local simulations.

The solver used by FDS for the LU-decomposition is part of the Intel Math Kernel Library (MKL).

Scalable Recursive Clustering (ScaRC)

This last optional solver is an experimental solver called ScaRC. It is characterized mainly by being an iterative solver, instead of direct like the previous options. The calculations executed by iterative methods are more simple, as they rely on the iteration to achieve convergence. Still, the question issue then transforms into how many iterations will it require to converge.

ScaRC is a solver that can be adjusted including characteristics depending on the problem that needs to be solved. It can include the conjugate gradient method, multigrid methods and the McKenny-Greengard-Mayo method.

More information regarding the ScaRC, and the other solvers present in FDS can be found in papers by Susanne Kilian [44][43] and also in the FDS technical guide [33].

5.2 Presented pressure issues

Some issues regarding oscillations in tunnel fire simulations where presented in an Editorial letter by Ang [1]. The article presents issues in simulations with FDS 6.1.1, 6.5.3 and 6.6.0 which initially were made using multiscale simulations of the Dartford tunnel in London, United Kingdom. The problems with oscillations made the researchers rerun the simulation using a simplified case, where the tunnel was simulated using only one mesh, with different subsequent modifications to test the effects of different corrections. The graphs obtained are shown in figure 5.1

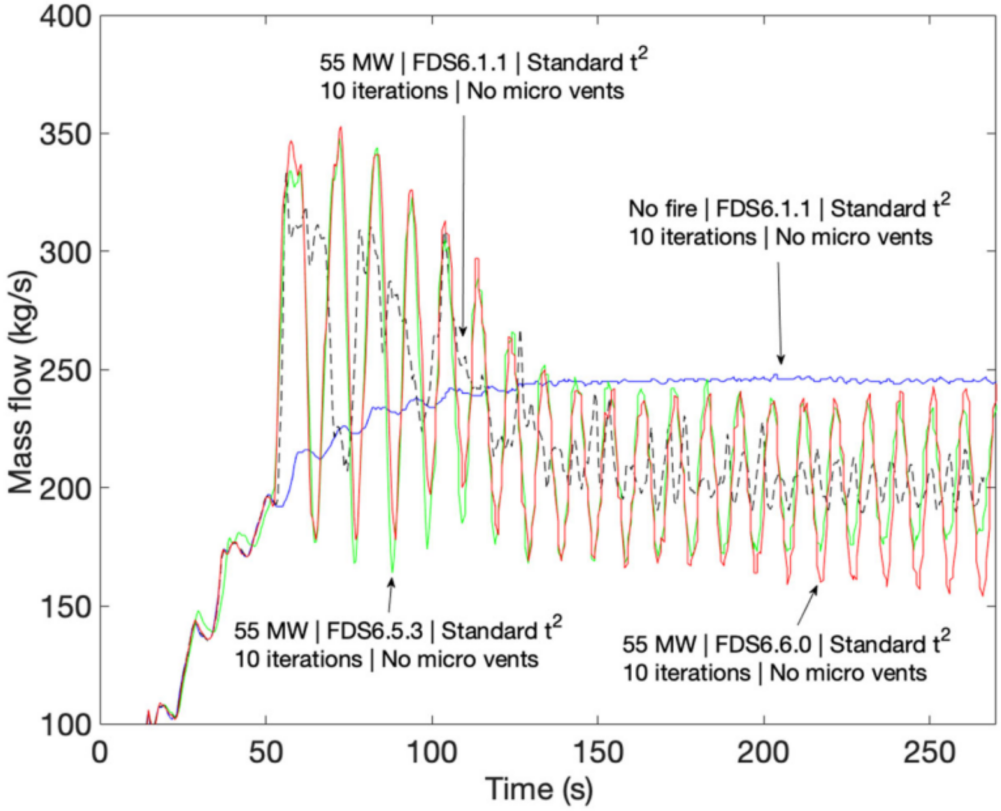

Figure 5.1: Comparison of predicted mass flow out of the tunnel for no fire and 55 MW fire in three FDS versions,[1]

5.2.1 Test layout

The main characteristics of the tunnel are, as mentioned by Ang [1], a 1.5 km tunnel with a cross-section of $40.96m^2$ with 14 pairs of fans distributed equally between the zone upstream and downstream of the fire, as seen in Figure 5.2. Furthermore, there is an open area 10m long in the longitudinal direction after both of the portals, meant to ease the interaction with the OPEN boundaries. The fans are located at 50 and 100

meters from the upstream portal and downstream portal, respectively. And the fan couples are separated 50m, among each other in the longitudinal direction of the tunnel, and 1.2m, among the two fans integrants of the couple. The fire intensity used for the simulation was 55MW.

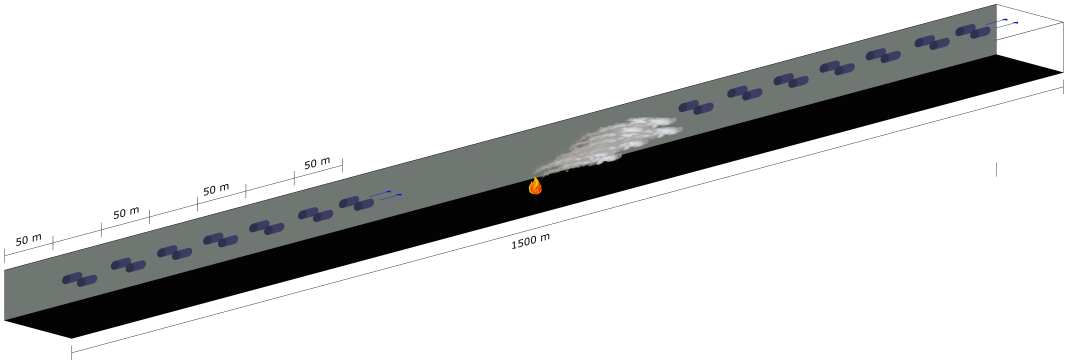

Figure 5.2: Dartford tunnel layout

Some of the data used for the simulation of the Dartford tunnel was also extracted from other articles cited by the source, in [2], [11]. The fans have a flow of 8.9 m^3/s and a discharge surface of 0.8 m per 0.4 m.

5.3 Tests

The first group of tests were made with the idea of finding both the possible influence of the pool size with the existence of oscillations in the flow and, at the same time, to find dimensions similar to those used by the original tests that showed the oscillation issues.

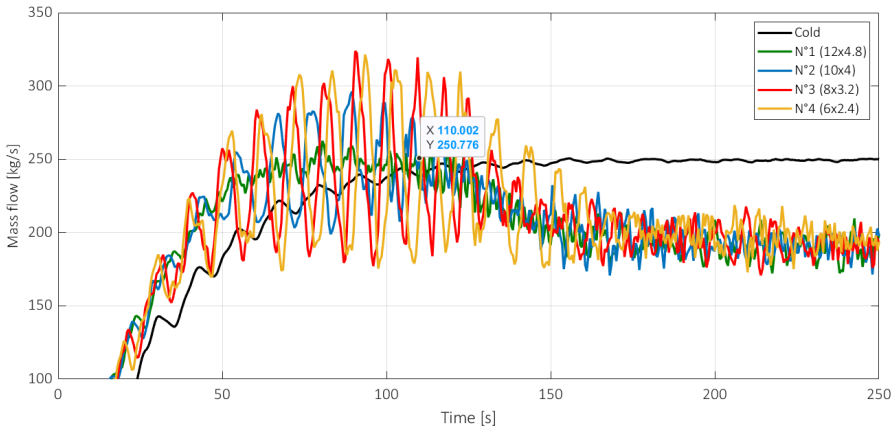

Figure 5.3: Mass flow downstream for different pool dimensions

The Figure 5.3 shows details regarding the mass flow close to the tunnel downstream portal. In Figure 5.3, is possible to observe the trend that the 4 cases follow, for 4 different pool dimensions, as it is also reported in Table 5.1. The four fire graphs, in the figure, follow the same average trend, as the general conditions are the same (same Heat release rate, wind speed, etc.). Still the simulations with smaller pools show bigger oscillations of the mass flow during the first 150 seconds of simulation. This trend on the bigger oscillations is also reported in the table 5.1.

Number	Pool Dimensions [m]	Oscillation Amplitude[kg/s]	Percentage %
1	12 x 4.8	approximately 15 kg/s	6.25
2	10 x 4	approximately 48.68 kg/s	20
3	8 x 3.2	approximately 73.4 kg/s	30
4	6 x 2.4	approximately 73 kg/s	30

Table 5.1: Table on Oscillation for simulations with different pool dimensions

Table 5.1, shows the maximum amplitude of the oscillations in mass flow in each simulation. The effect of the pool size over the issue is made clear, and for smaller pools the mass oscillations are higher. The issue can then be linked to the fire vertical height. Using the Heskestad set of equations for plume properties [42] and using the relations for fire inclination in [62] is possible to calculate the flame vertical high for an inclined fire.

Number	Pool dim. [m]	Mean flame height [m]	Fire angle [°]	Fire vertical height[m]
1	12 x 4.8	8.9	27	4.0
2	10 x 4	10.9	30	5.4
3	8 x 3.2	13.1	33	7.1
4	6 x 2.4	15.4	35	8.8

Table 5.2: Table on Fire height for simulations with different pool dimensions

Now according to the formulas the flame height and inclination are approximated, in Table 5.2. Taking into consideration that the tunnel cross-section measures 6.4 x 6.4 m is evident that both the cases that show the highest amount of oscillations are the cases where the vertical height of the fire should remain in contact with the roof of the tunnel.

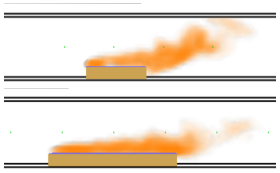

Figure 5.4: Fire height for different pools sizes, (up) 6 x2.4, (down) 12 x 4.8

Figure 5.4 confirms the superior flame height in the case of smaller pools. The dimensions used for the forecoming simulations are 6 x 2.4 m, as these dimensions are capable of reproducing the issue, as seen in figure 5.5, and are close to the theoretical area that would be necessary to produce a fire of the prescribed heat release rate, according to formulas for pool fires [42]. Even though the mass issues could be evaded by distributing the heat release in bigger areas, this does not solve the underlying problem.

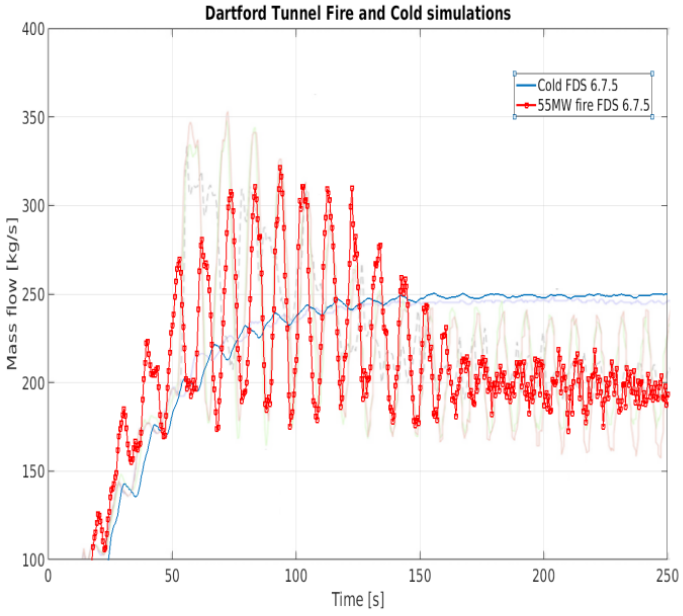

Figure 5.5: Mass flow downstream for different pool dimensions

5.3.1 Solver differences issues

An option that then was explored was the influence of the pressure solver in the behavior of the mass flow through the tunnel. Taking into account the different solvers the simulation was rerun using the GLMAT, with similar results. The next step was using UGLMAT that changes the discretization from the structured, used in both FFT and GLMAT, to unstructured. At first the results appreciated in the pressure downstream

the tunnel show that the pressure that used to be oscillating during the simulation with FFT, now is as stable as the cold simulation pressure, as seen in figure 5.6.

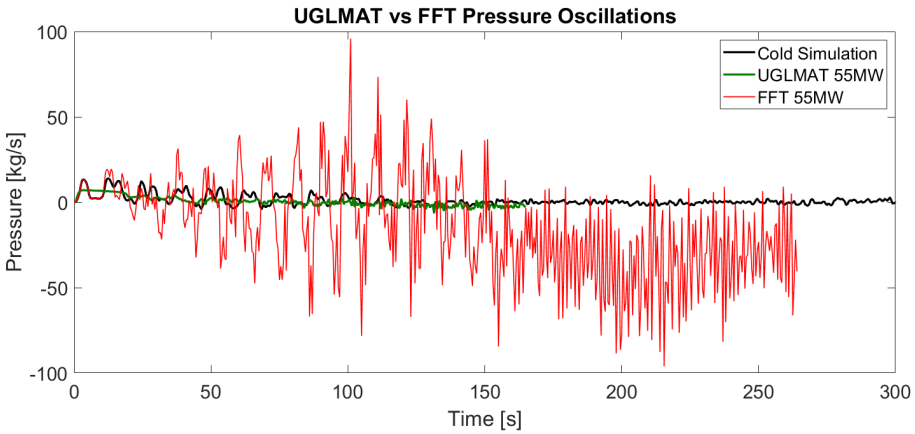

Figure 5.6: Pressure oscillations for different solvers

Furthermore, the mass flow at the downstream portal also seems affected by the change in solver, as shown in figure 5.7. Using UGLMAT reduced the oscillations to a maximum of 5 kg/s, from the 70 kg/s that were observed before.

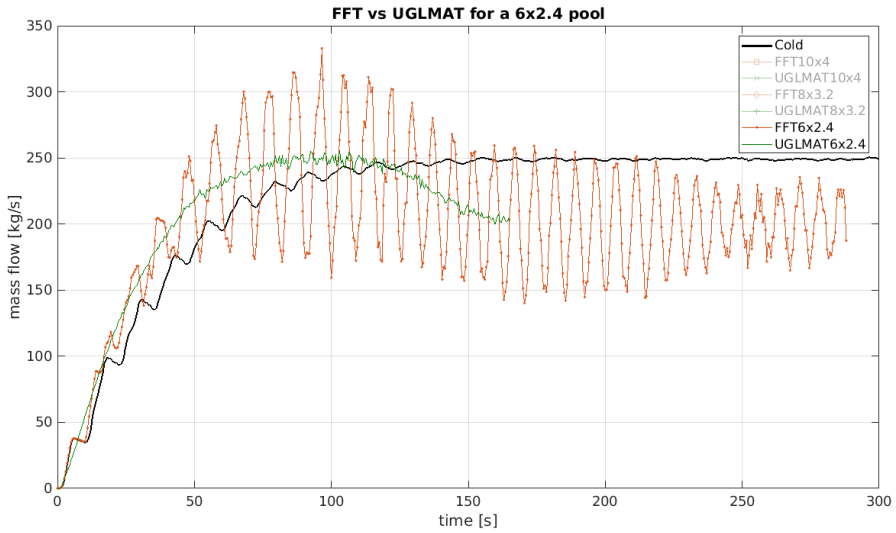

Figure 5.7: Mass flow downstream for different solvers

Further analysis

Further communication with the developers and analysis of the data obtained was required after obtaining these results. The issue observed in the initial simulations is a

combination of the consequences of using the FFT solver with boundaries in one extreme that combine OPEN and solid boundaries, and mass flows that try to penetrate this boundaries. The first part refers to the walls of the tunnel, that are solid through the tunnel length, but at the last and first 10 m of the domain have an OPEN boundary condition.

The FDS code (at the moment of the tests), would use only one kind of boundary condition across the same wall, be it Dirichlet or Neumann. If the whole wall was solid it would have a Dirichlet boundary condition. Still, if even small a region of a solid wall needs a Neumann condition (it's open) the whole wall boundary becomes Neumann, changing also the condition in the solid walls (To a condition similar to that assigned to internal walls). Then this makes the pressure calculation considerably more unstable. The issue was intensified by the flames trying to penetrate the roof, as it's high velocities normal to the wall make the convergence of the Neumann no-flow condition more difficult. This was a factor that increased the instabilities, as only in the cases where the flame height arrives to the roof the oscillations grow up to 70 kg/s, as mentioned in previous graphs and tables.

The developers of FDS have kept working in the pressure solver, creating new solutions for FFT tunnel simulations, as UGLMAT might be more accurate under regular circumstances, but it also consumes more calculation time. Still, the improvements of the FFT solver are highly linked to multimesh calculations, that are a feature not yet implemented into the multiscale.

5.4 Observations

Through this part of the research it was possible to find a pressure solver that would consistently deliver accurate results, at the disadvantage of requiring some more time than the default FFT solver. From this point onward of the research UGLMAT was used in all the multiscale simulations. This exchange is adequate in the case of a multiscale approach, as the 1D already reduces the consumed time, and the time increase due to the change of the 3D solver.

New developments in the FFT solver of FDS has been observed in the last months. This developments are linked to multimesh calculations which makes it necessary to add multimesh capabilities to the multiscale. Adding this feature to the multiscale and working with the Tunnel preconditioner of FDS [30] will yield even lower simulations times in the future.

Chapter 6

Multiscale Tests

Through the research shown in this work it has been possible to change some parts of the Multiscale algorithm, to provide improvements in different capabilities of the model. An essential part of introducing changes is testing them and comparing their results against other sets of data or even measurements in tunnels, when possible. In this opportunity we are capable of using two data sets:

The first test case is based in a 2600 meters long tunnel. A group of in-site tests were made to test the capabilities of the automatic ventilation system, of this tunnel, to react correctly to fires under different circumstances. There were cold tests and fire tests with the objective of analyzing the correct fire detection of the different systems and fan activation to keep the tunnel at certain velocity conditions.

The second test case used are simulations of the Dartford tunnel, comparing the results from the multiscale with a full-scale simulation from this known tunnel, that has been simulated in different publications. Therefore, the data used in the simulation is accurate, and the different outputs obtained are representative of the physics of the real tunnel.

6.1 Test Tunnel

Different kinds of tests took part in the 2.6km tunnel, to test the predictive-adaptative algorithm for the management of the ventilation system. The tests are oriented towards:

- Under regular working conditions, testing the concentration of different contaminants in the tunnel, and the ventilation activation necessary to maintain an acceptable concentration of these contaminants.
- In emergency conditions, ensure safe conditions for the exit of the drivers trapped in the tunnel and, at the same time, preserve the integrity of the tunnel structure.

The types of tests conducted were of two types:

- Cold tests: Tests forcing conditions similar to the ones obtained during regular transit hours of the tunnel, to check the automatic management of the tunnel ventilation.
- Fire tests: To test the management of smoke in the case of emergencies. The procedure includes pools that contain the fuel for the fire, with tests periods superiors or close to the 10 minutes, after the test the fans and extractions are used to exhaust the smoke. Dispositives are placed in the tunnel to measure different properties of the flow. The objective of the tests is to guarantee an air flow higher than 1 m/s during emergencies.

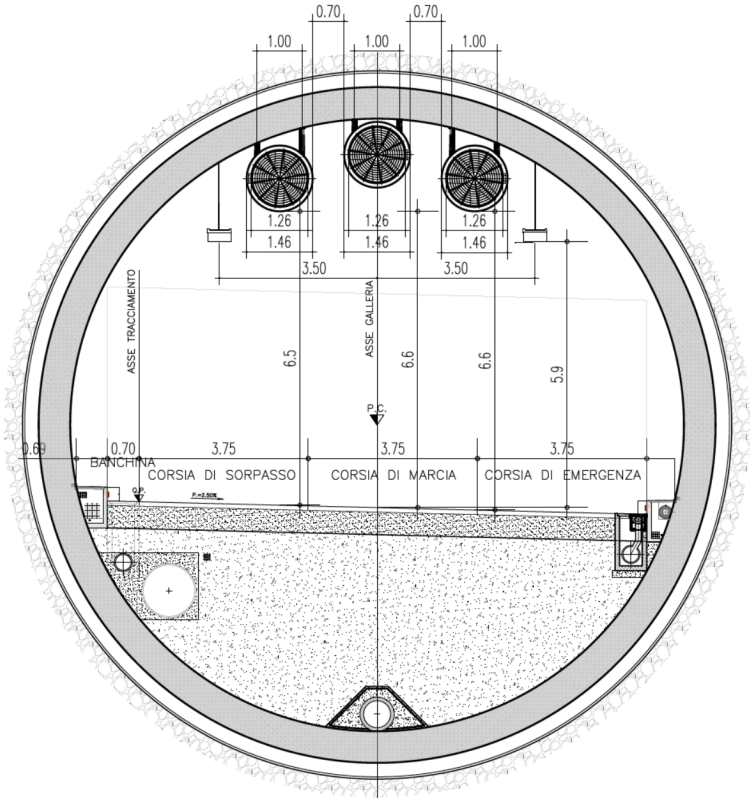

Figure 6.1: Test tunnel section, with dimensions

The analyzed tunnel is 2600m long and has two tubes. The tunnel tubes have an internal diameter of approximately 13.35m and each one of the carriageways are composed of two lanes plus a breakdown lane, as seen in figure 6.1.

The fire test

The fire tests in the tunnel were made using 4 fuel pools, of dimensions 1.3m x 1.3m, placed at approximated 1440 m from the tunnel upstream portal, as shown in the figure 6.2.

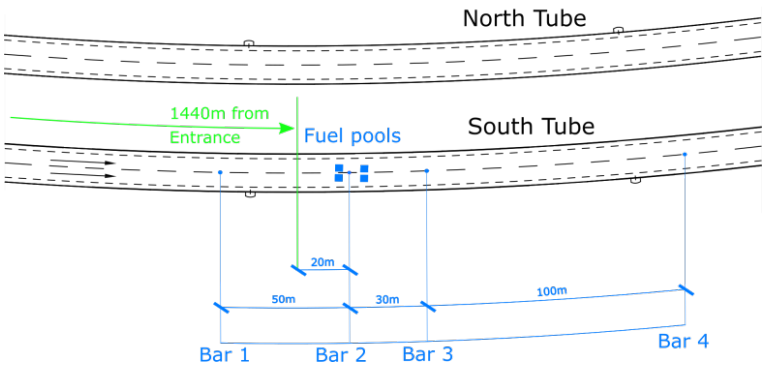

Figure 6.2: Fire test deployment layout

Across the tunnel, and in the vicinities of the fire pools, 4 bars with measuring devices were placed. The devices included are summarized in table 6.1. Essentially there are 6 thermocouples at different heights, at 6m, 5.8m, 5.2m, 4.4m, 3.6m and 2.8m above the ground level, with one more thermocouple in the case of the bar right on top of the fire placed at 2m of height. Instead for anemometers, a serie of 3 devices were placed in the measurement bars at 4.8m of height, except in the bar closer to the fire.

Bar Number	Location [m]	Thermocouples [m]	Anemometer [m]
1	-50	6;5.8;5.2;4.4;3.6;2.8	4.8
2	0	6;5.8;5.2;4.4;3.6;2.8;2.0	none
3	30	6;5.8;5.2;4.4;3.6;2.8	4.8
4	130	6;5.8;5.2;4.4;3.6;2.8	4.8

Table 6.1: Measurement bars location across the tunnel lenght, measured from the fire pools location

Other than the anemometers placed in the measurement bars there are other 4 anemometers across the tunnel, placed in the locations shown in table 6.2.

Sensor Number	Anemometer location [m]
1	100
2	1060
3	2090
4	2350

Table 6.2: Anemometer location measured from the upstream portal of the south tube

The ventilation system, and its management, is the main topic of analysis of the shown tests. The positions of the different fans for the tube of interest are indicated in table 6.3. The fans are placed in the superior part of the tunnel, in groups of 3, as shown

in figure 6.1.

Fan Number	Fan location [m]
1/2/3	150
4/5/6	300
7/8/9	450
10/11/12	2020
13/14/15	2170
16/17/18	2320

Table 6.3: Fans location measured from the upstream portal of the south tube

Regarding the fire the four pools are filled with 1 liter of gasoline and 9 of gasoil. Using expressions for the calculation of heat released by liquid pool fires with fuels similar to the gasoil, as the gasoil is not included in the consulted literature [42], the heat released could be approximated to 10 MW. Still, some factors must be taken into account, as the volume of fuel compared to the surface area of the pools (that allowed only a thin layer of fuel), and the surface quality of the pools itself, as the pools weren't completely plain reducing the possible surface area of the pool.

After some preliminary simulations, and taking these factors into account, the value of the pool heat release rate was imposed to be 4MW, as the value capable to reproduce the temperatures closer to the fire with the higher precision.

The test analyzed starts with the ignition of the 4 pool fires. After some seconds the fire is perceived by the telecameras on the tunnel, starting the emergency procedure. As the air velocity inside the tunnel remains higher than 1m/s, as seen in the anemometer measures in figure 6.3 the system doesn't switch on any other fan at the moment. The fire continues and then after 10 minutes the fire starts reducing in intensity, and the emergency signals stop.

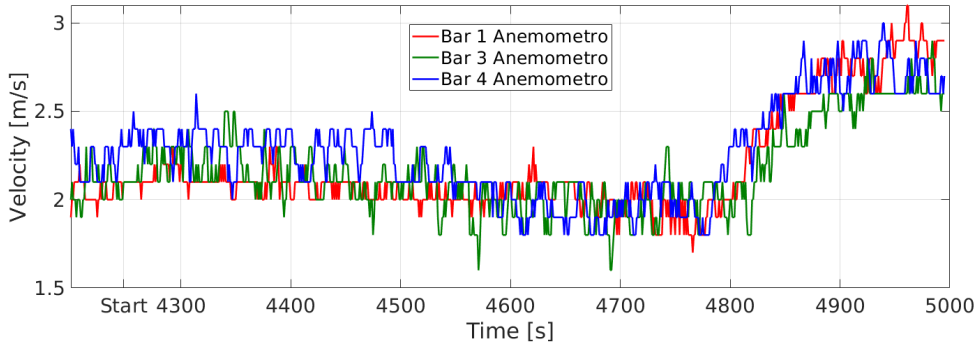

Figure 6.3: Tunnel air velocity during the test (the test starts at 4248 seconds)

The fans that where activated during the test were the fans number 7 and 10, as it can be seen in the figure 6.4. The other fans across the tunnel were used only in the discharge phase, and activated at a lower velocity. The fans numbered from 1 to 6 are not shown as they weren't active during the time period of interest.

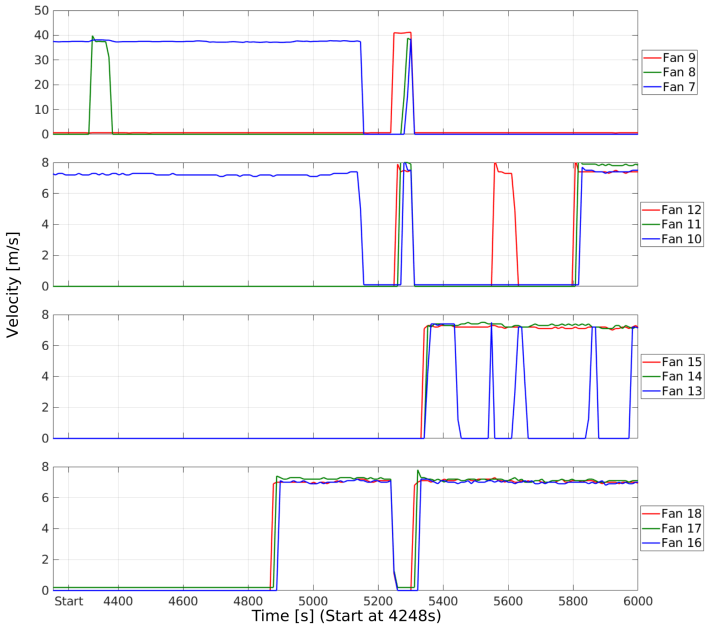

Figure 6.4: Tunnel fan activation during the test (the test starts at 4248 seconds)

The simulation layout

The tunnel was simulated using the multiscale approach, dividing the tunnel simulation into a 3D domain long 250 m and a 1D domain long 2350 m. The fire has an intensity of 4 MW and the heat release curve is modelled in the same shape of the temperature closer to the fire, which corresponds to the thermocouple at 2 m of height above the fire. The fans are modelled using the velocities in the graphs included in figure 6.4 using the formula 6.1 with the values shown in the table 6.4.

$$\Delta P_{fan,j} = n_j \rho_j \frac{A_f}{A_j} K_f u_f \left(u_f - u_j\right) \tag{6.1}$$

Fan discharge velocity u_f	updated each iteration
Fan area A_f	$1.2469m^2$
Pressure rise coefficient K_f	0.8
Branch area A_j	$40.96m^2$
Branch velocity u_j	updated each iteration
Branch density ρ_j	updates each iteration
Number of fans n_j	3

Table 6.4: Data used for the pressure fan calculation

Among the portals of the tunnel there is a pressure difference of 10 Pa. The temperature in the portals is 10.8 °C in the upstream portal and 16 °C in the downstream portal.

Simulation Results (Boundary Analysis)

First the data at the boundaries was analyzed. The exchanged variables between the 1D and 3D model are shown against time in the upstream (Entrance) and downstream (Exit) boundaries of the 3D. The pressure can be seen in figure 6.5, the temperature in figure 6.6 and the velocity in figure 6.7.

First, for the pressure, figure 6.5, the graphs shows the values of the 3D in blue/black and the values of the 1D in red/green. The values are exchanged every timestep, but upstream the pressure is averaged in the last 50 timesteps (to reduce pressure oscillations), which keeps the values obtained by the 1D at the 3D entrance in the mean value of the pressure curve. This only reduces the possible oscillation arriving to the 1D. Still, these oscillations arrive to values of 1 Pa as maximum, which would not be problematic for the simulation. The values in both of the boundaries among the two models match closely, meaning that the constant communication is executed correctly for the pressure.

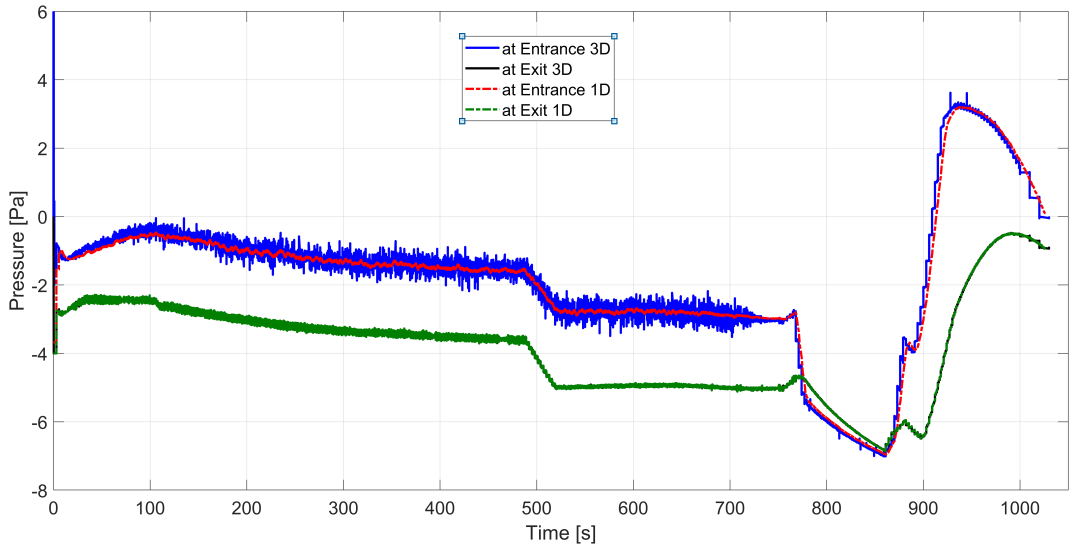

Figure 6.5: Pressure comparison in the boundaries, against time

For the temperature, as shown in figure 6.6. The values upstream of the fire, the cold side of the simulation, are the same through the simulated time. In the case of the exchange downstream there is a small difference, consequence of the different averaging weight used in both of the cases, mass flow for the 1D and only mass in the 3D. Is possible to use the same weight in both, still the mass average is preferred in the 3D as it represents more accurately the temperature in a section and mass flow average is preferred in the 1D as it is the value received from the 3D that ensures mass and energy conservation.

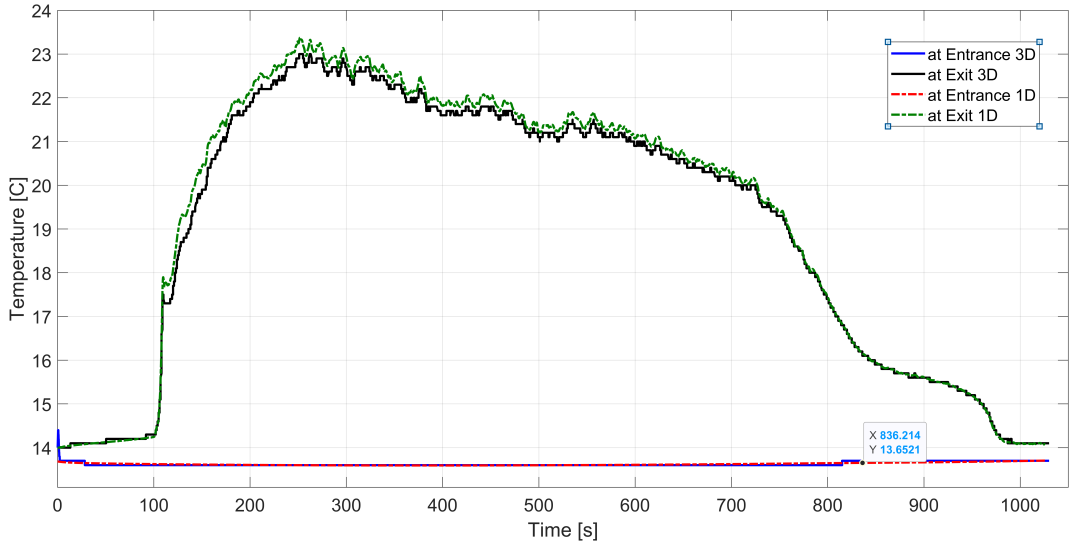

Figure 6.6: Temperature comparison in the boundaries, against time

The last property shown at the boundaries is the velocity. In this case the values are almost identical at both the entrance and exit, as the velocity is averaged using the mass

as the weight in both models. The mass flow average used in the sections, is capable of ensuring the conservation of mass. Therefore, the numbers obtained at each side of the boundary match almost perfectly.

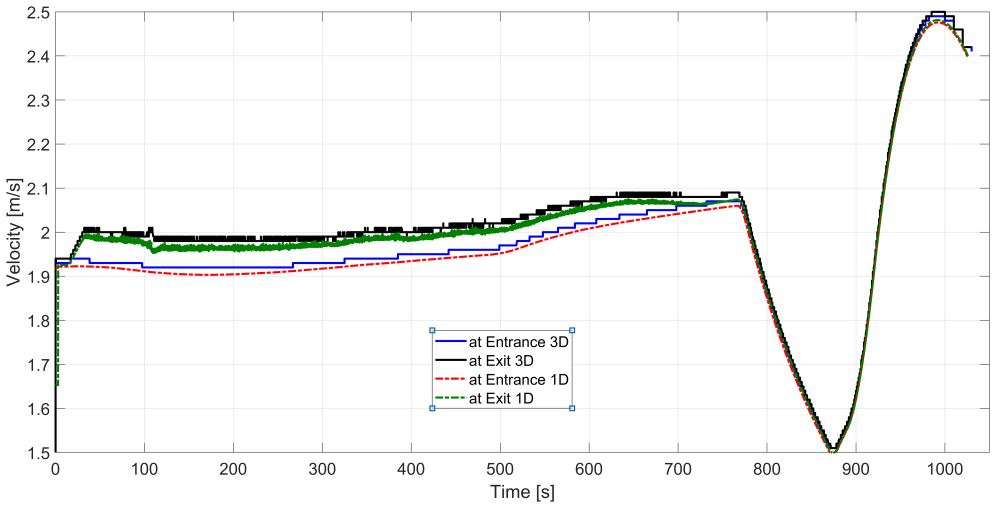

Figure 6.7: Velocity comparison in the boundaries, against time

Comparison of tests and simulation results

After checking the proper exchange of data across the boundaries the results of the simulations are compared to the data measured in site at the tunnel. First, the velocities at 4.8 meters of height, in three of the measurement bars, are compared. The data measured in the tunnels is compared to the output of the simulation in figure 6.8. The agreement between the values is good, and is mostly influenced by the accuracy of the fans operation, the pressure difference between the portals and the fire heat release rate.

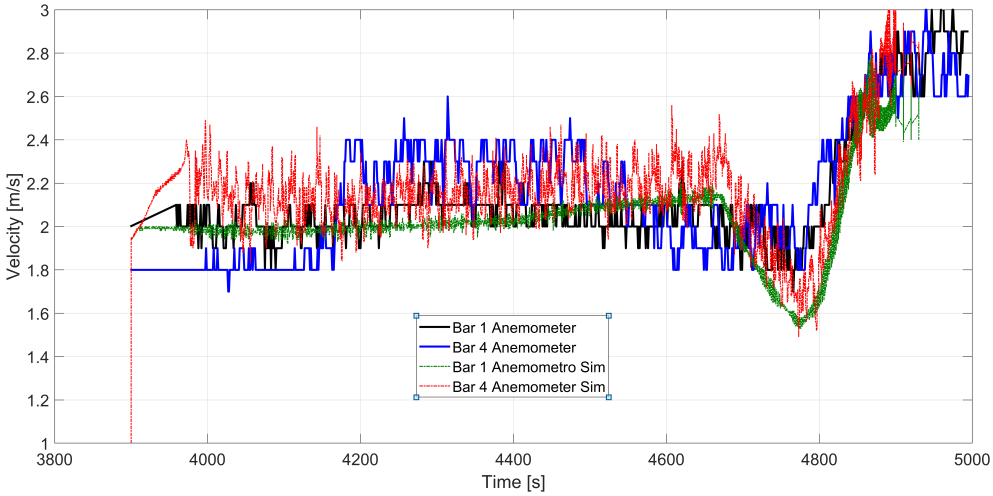

Figure 6.8: Velocity comparison at the anemometers, against time

The first temperature measurement, shown in figure 6.9, reports the temperature above the fire, at 2 meters of height above the ground. This thermocouple belongs to the bar 2 and, the heat release rate over time was modelled taking into consideration the shape of this curve. In the graph it can be seen that the simulated temperature remains lower than the measured one. The difference between the two temperature values are related to the difference between the point measurement of the thermocouple, in the field, against the averaged temperature in a 0.5m x 0.5m cell, in the simulation.

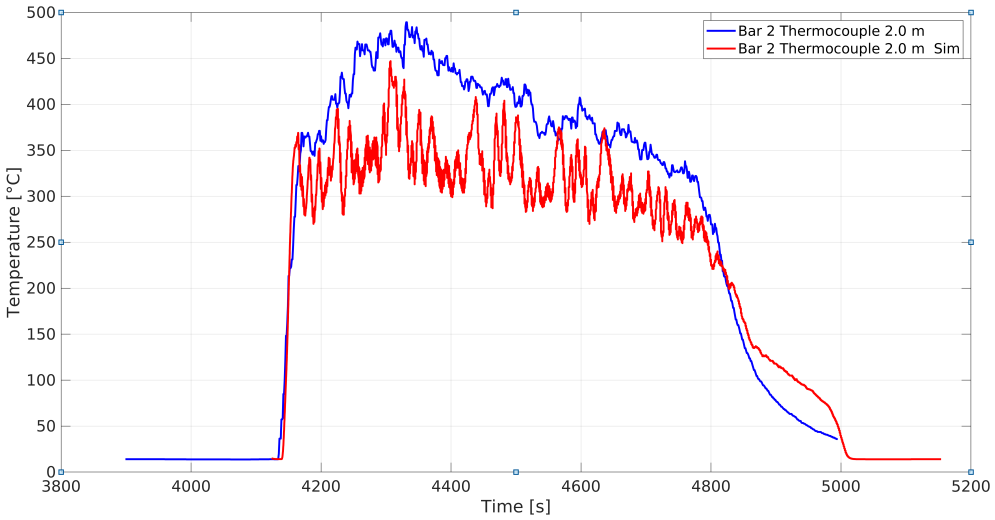

Figure 6.9: Comparison in the lowest thermocouple in the second bar

The temperatures for the measurement bars 2 to 4 are now compared. The graphs for the second bar are shown in figure 6.10 and figure 6.11. Figure 6.10 contains the values of the three lower thermocouples and figure 6.11 has the values of the three upper ones (the graphs were divided into 2 figures for clarity).

In figure 6.10 the thermocouples measurements are compared with the values obtained from the simulation. The values of temperature agree well for the upper (4.4m) and lower (2.8m) thermocouples of the group, still the values for the middle on (3.6m) have a difference of a maximum of 6 degrees, which considering the temperatures of the area is relatively high.

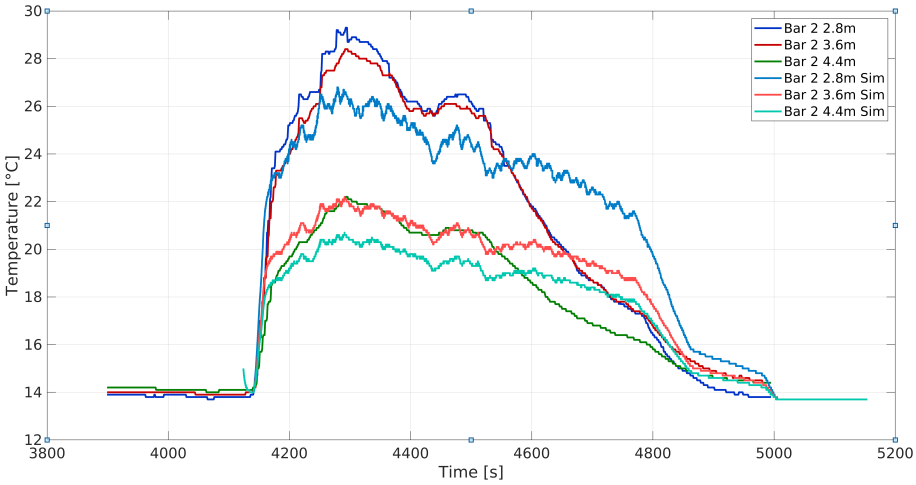

Figure 6.10: Comparison in the lower thermocouples of the second bar

In figure 6.11 the 3 higher thermocouples are compared; here the difference in temperature grows as the thermocouples are farther from the fire. This thermocouple is very sensible to the positioning of the bar itself, and the interaction between the fire and the ventilation system. This because the bar is placed on top of the fire, therefore a change in its position of centimeters would change the cell the thermocouples measure, this added to the possible cell averages between hot and cold zones close to the fire makes it particularly difficult to match the values in this point. Still, the trend of the temperature in figure 6.11 matches the trend of the measurements, regardless of the temperature value.

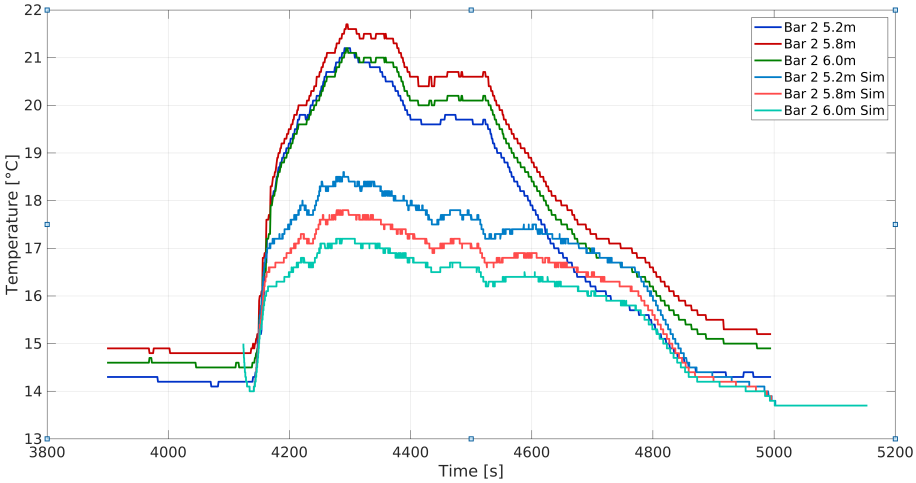

Figure 6.11: Comparison in the higher thermocouples of the second bar

The division in two figures is also applied to the two remaining measurement bars. Therefore, for the bar 3, at 30 meters of distance of the fire, the figure 6.12 and figure 6.13 show the temperature values for the lower and upper parts respectively.

In figure 6.12, the temperature values for the three lower thermocouples are shown. The difference in values among the simulation and measurement reduces as the height of the thermocouple placement increases. It is appreciated here that the error reaches a maximum of 5 degrees for the lowest thermocouple, and then reduces to 3 or 4 degrees at the 4.4 m thermocouple. This trend continues in figure 6.13; here it is possible to see that the temperature differences decrease more with the height. For the thermocouple at 5.2 m of height the difference surrounds the 2 degrees, reducing further for the temperature at the top of the measuring bar, were for the first 500 seconds of simulation the average of the temperatures in the simulation agrees very well with the temperature measured by the thermocouple in the field.

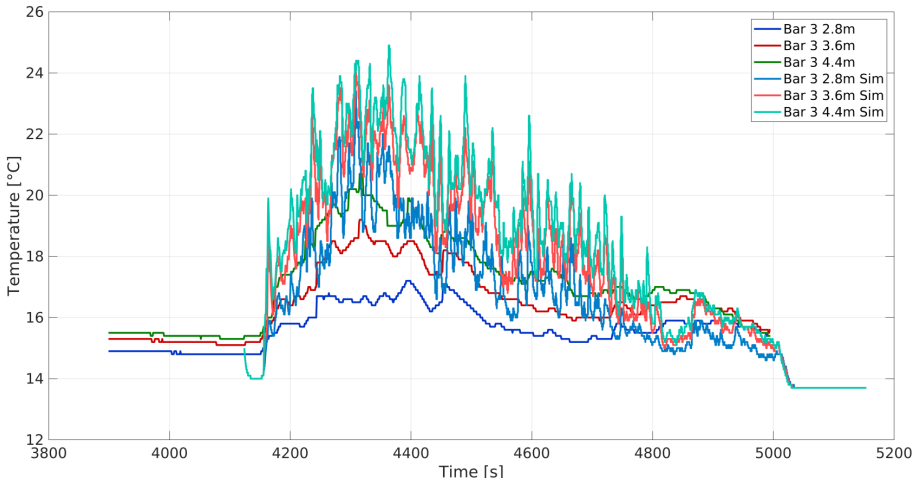

Figure 6.12: Comparison in the lower thermocouples of the third bar

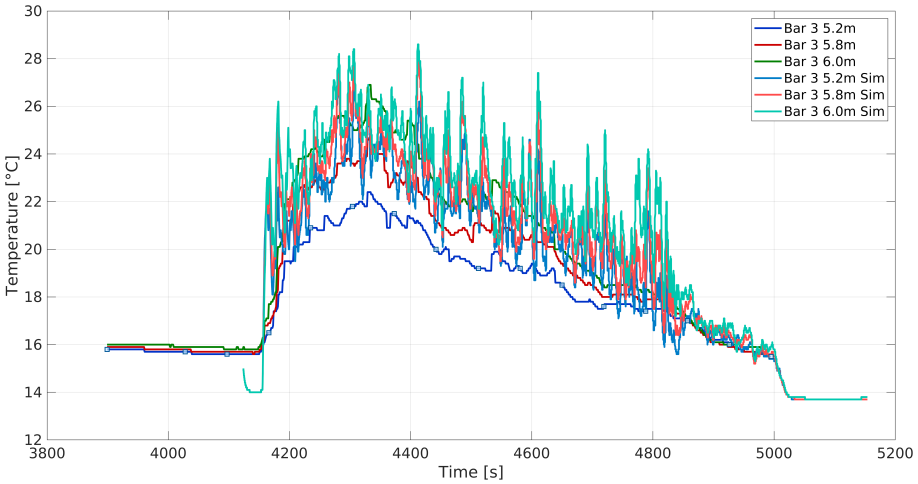

Figure 6.13: Comparison in the higher thermocouples of the third bar

The last measuring bar, placed at 130 meters from the fire is the fourth bar.

In figure 6.14 we can see the values for the lower thermocouples of the fourth bar, for this three thermocouples the error remains below the 3 degrees, in the first 500 seconds of simulation, then the cooling down of the tunnel takes longer in the simulation than it does in the real tunnel, introducing a difference between the values of temperature later in the simulation.

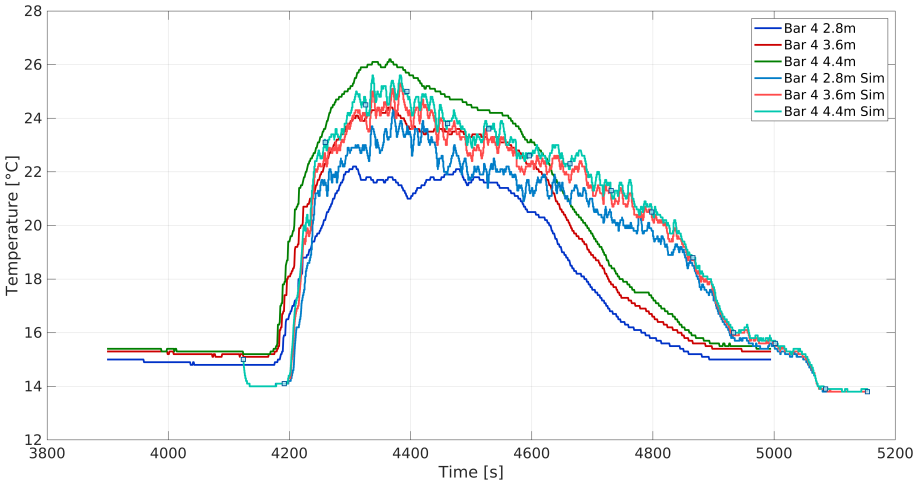

Figure 6.14: Comparison in the lower thermocouples of the fourth bar

The figure 6.15 shows the temperatures measured and simulated for the thermocouples in the higher part of the fourth bar. The trends from the lower thermocouple are kept, as the differences between measured and simulated values remain low. Another particularity is that both the simulation and measured values ranges become more compact in the upper part of this section of the tunnel, as the distribution of temperatures become more homogeneus as it moves away from the fire.

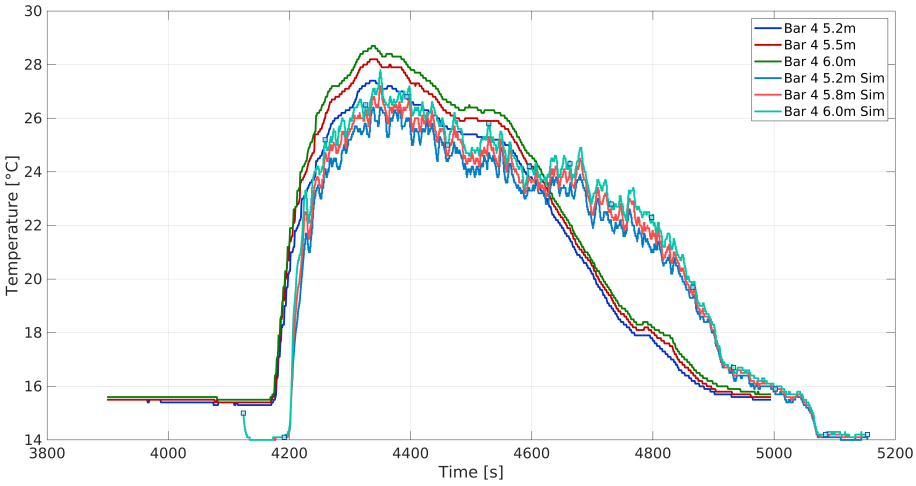

Figure 6.15: Comparison in the higher thermocouples of the fourth bar

6.2 Dartford Tunnel

In the case of the Dartford tunnel, a layout similar to the one explained in chapter 5 is used. Therefore, a 1.5 km tunnel with a square cross-section of 40.96 m^2, 6.4 m x 6.4 m high and width. There are 7 pairs of fans upstream and downstream of the fire, as seen in figure 6.16. Now, there is no open area after the portals, as it was part of the cause of the issues in the previous simulations. The first fan couple is separated 50m from the upstream portal and the last fan couple is 100 meters before the downstream portal. The remaining 12 pairs of fans, 6 in each direction of the fire, are placed with 50m of distance among them. The fire intensity used for the simulation was 55MW.

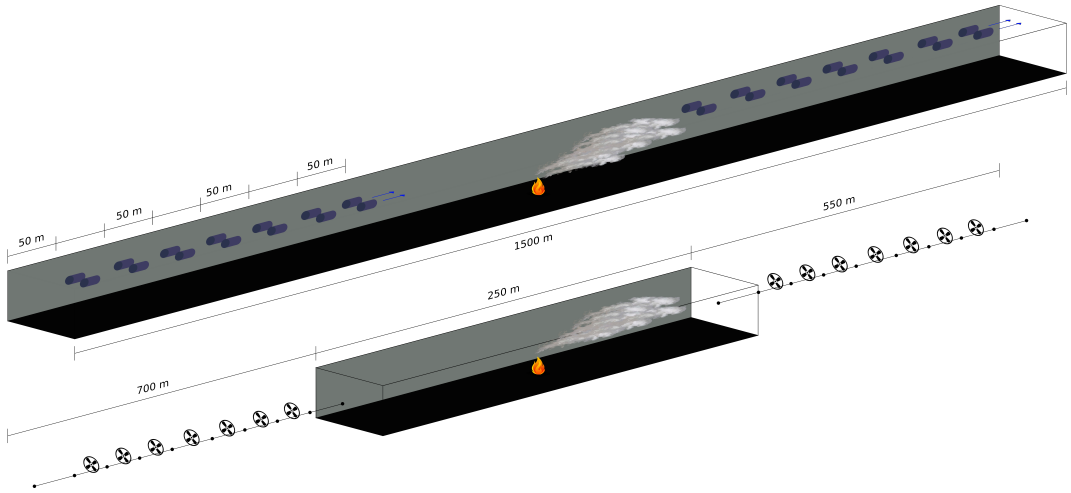

Figure 6.16: Dartford tunnel layout

The fans have a flow of 8.9 m^3/s and a discharge surface of 0.8 m per 0.4 m. The pool of fire is set to be of 6m by 2.4m.

In the case of the Multiscale simulation the domain is divided in 1250m of 1D domain and the remaining 250m of 3D domain. The 3D domain has 50m before the fire and 200m after the fire. The length upstream the fire is rather short because the speed the ventilation system reaches when all the fans are on is superior to the critical velocity of the tunnel. More precisely, the critical speed according Wu Bakar [78] is 4.2 m/s, and the wind speed in the tunnel surpasses this velocity. The simulations agree with this, as there is no backlayering in any of the simulated cases.

Comparison of FDS and Multiscale simulations

Two simulations are compared in this section. An FDS simulation, of the whole tunnel with the 3D approach provided by the fire dynamics simulator. And, a multiscale simulation with 250 m of 3D simulation, and the remaining length simulated using the 1D model.

The first graphs analyzed will be the figure 6.17, figure 6.18 and figure 6.19, showing the pressure, velocity and temperature across the tunnel, respectively, averaged in time.

In figure 6.17 the curve for pressure for both the FDS and multiscale simulations are shown. The trend of both of the curves is similar where the pressure increases in the two zones with fans, from length 50 to 400 meters and 1150 to 1400 meters, and decreases in the rest of the tunnel length. The rise in pressure is continuous in the case of the FDS simulation as only sections without fans are included in the output (ommiting the instantenous jump of pressure because of the fans), and has a saw shape in the case of the multiscale as the pressure difference introduced by the fans is inserted as the pressure difference between two nodes (making the pressure rise in the branch with the fan and decrease afterwards). There is a small difference between the FDS and multiscale curves in the central zone of the tunnel, between the 450 and 1050 meters of length. The difference is lower than 7 Pa in the whole tunnel and is similar to the amount of pressure difference introduced by a fan. Taking into consideration that the pressure difference between the entrances is maintained, and the trend of the curves, it is assumed that the difference is related to the domain decomposition in different parts. Still, it doesn't harm the behavior of the flow in the tunnel.

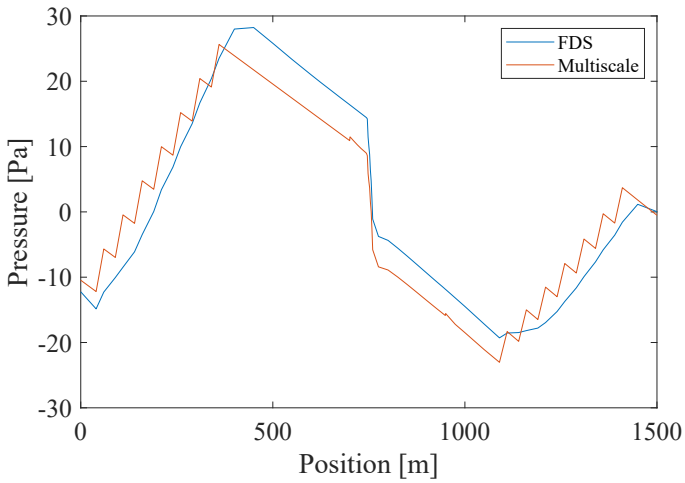

Figure 6.17: Dartford pressure across the tunnel

The second graph, figure 6.18, shows the velocity trend across the tunnel. Both the graphs share the same trend. Still, the small difference in pressure change in the upstream 1D part of the multiscale simulation, from 0 to 700 meters of length, appreciated in the figure 6.17 also introduces a velocity difference in this part of the domain. But, this difference is reduced when the flow advances towards the downstream area, as the multiscale simulation takes into account the fire and the remaining fans.

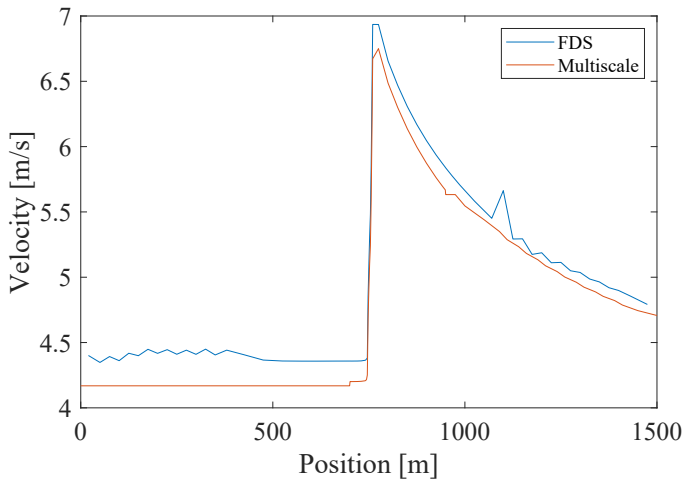

Figure 6.18: Dartford velocity across the tunnel

The third graph, in figure 6.19, shows the trend in the temperature across the tunnel. Upstream of the fire, in the first 750 m of the tunnel, the temperature is constant and equal to 20 °C in both of the simulations, as there is no backlayering or any other thermal interaction in this part of the tunnel. Then, from the mid point, where the fire is placed, towards the end of the tunnel the temperature is higher, falling from 180 degrees close to 50 at the end of the tunnel. Both the multiscale and the FDS are configured to lose heat against walls at environment temperature. But the temperature loss in the case of the 3D is higher that in the 1D region of the simulation. This is related to 3D effects that are not taken into consideration inside the 1D, as the radiation.

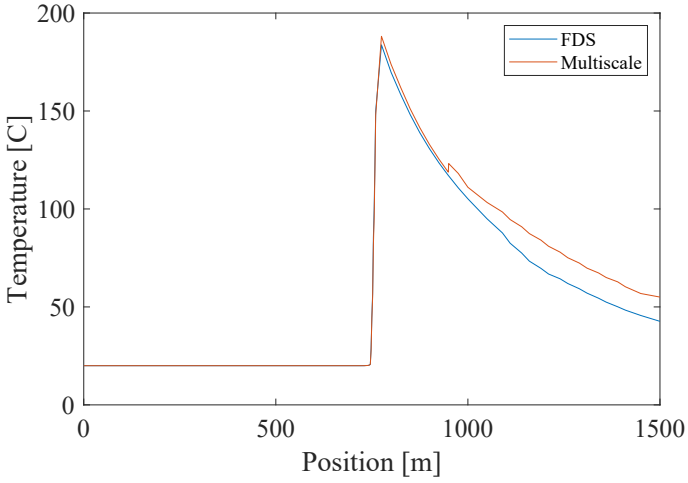

Figure 6.19: Dartford temperature across the tunnel

Now different points across the tunnel are analyzed over time, to observe if the behavior across the tunnel is similar in both the FDS and multiscale simulation. The points analyzed are at 500, 700, 900, 950 and 1050 m from the upstream portal. The points had been selected to compare the multiscale and the FDS simulation in all the possible combinations. Therefore, the FDS is compared to:

- The 1D part of the domain upstream of the fire (500m)
- The 1D-3D boundary upstream of the fire (700m)
- The 3D part of the domain, 150m downstream of the fire (900m)
- The 3D-1D boundary downstream of the fire (950m)
- The 1D part of the domain downstream of the fire (1050m)

First, the graphs for the section placed 500m from the upstream portal are in figures 6.20 and 6.21.

Figure 6.20 shows the trend of the pressure through time in the section at 500m from the upstream portal. In this figure the pressure can be seen to oscillate for the FDS calculation, as inside the FDS simulation all the perturbations are felt infinitely fast across the entire domain (Low mach assumption). Therefore, all the fire perturbation cause changes across the whole tunnel. Differently, in the 1D calculation the value is more stable and almost constant. The reason of this steadiness is that the 1D receives an averaged pressure value from the 3D at the exchange boundary (at 700m), then this value is used in the 1D code interacting mostly with the fan pressure differences and the losses across the tunnel, that don't introduce any volatility. The multiscale simulation has a pressure value close to the average pressure in the section, as also seen in figure 6.17 having a difference of 7 Pa.

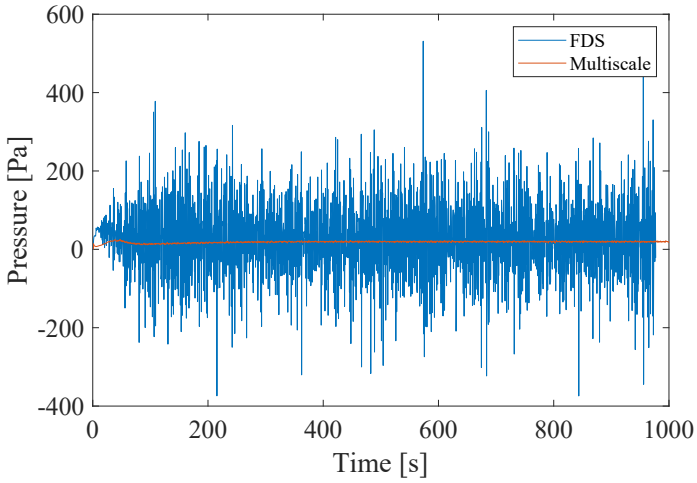

Figure 6.20: Dartford pressure at 500m distance to the tunnel upstream portal

Figure 6.21 shows the velocity trend through time in the section at 500m of distance from the upstream portal. The graph shows a similar steady state value for both of the simulations (FDS and Multiscale). The multiscale simulation starts at 5.2 m/s of velocity, that corresponds to the velocity that reaches the air in the tunnel when all the fans are activated and there is no fire. In contrast, FDS starts the simulation at 0 m/s, this as starting the FDS simulations in no-flow conditions is a well established good practice. Both reach steady state condition between 200 and 300 seconds from the simulation start, with a small difference in velocity close to the 0.2 m/s, as seen in figure 6.17.

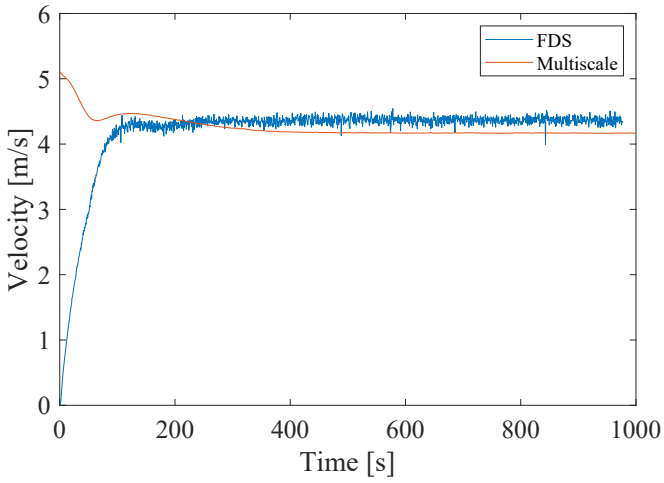

Figure 6.21: Dartford velocity at 475m distance to the tunnel upstream portal

The third graph, regarding the temperature in the 500m section is omitted. The reason is because, as seen in figure 6.19, both of the temperatures are equal to 20 degrees with no changes in time.

The second section analyzed is placed 700 m from the entrance portal, the graphs are in figures 6.20 and 6.21. This section corresponds to the boundary between the 1D and 3D models inside the multiscale, and will therefore include 2 values for the multiscale, one per each part of the domain (3D and 1D).

The figure 6.22 shows the pressure in the boundary section at 700 m. The pressure behavior at this point is similar to the one observed for the section at 500 m, showing oscillations in the pressure ranging mostly the 200 Pa and -200 Pa. The oscillations are shared by the FDS and 3D-multiscale, as expected, as both of them use the FDS and the same solver (UGLMAT) to obtain the pressure field. The pressure used by the 1D model in the multiscale is a 50 timesteps average of the pressure, which helps the value to remain steady in the average value of the 3D curves (both FDS and multiscale 3D)

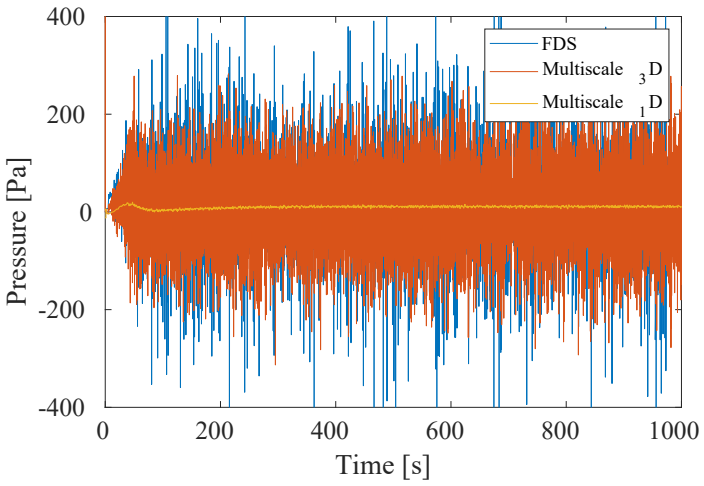

Figure 6.22: Dartford pressure at 700m distance to the tunnel upstream portal

Figure 6.23 shows the velocity in the boundary section at 687 m. Here the trend is similar to the one seen in the section at 475 m with both of the velocities starting from different conditions, cold tunnel flow for the multiscale and no-flow conditions for the FDS. Still, the main purpose of this figure is to show that the exchange of velocity data among the two multiscale domains (3D and 1D) is carried on correctly, with low or no error in the exchange, across all the simulation.

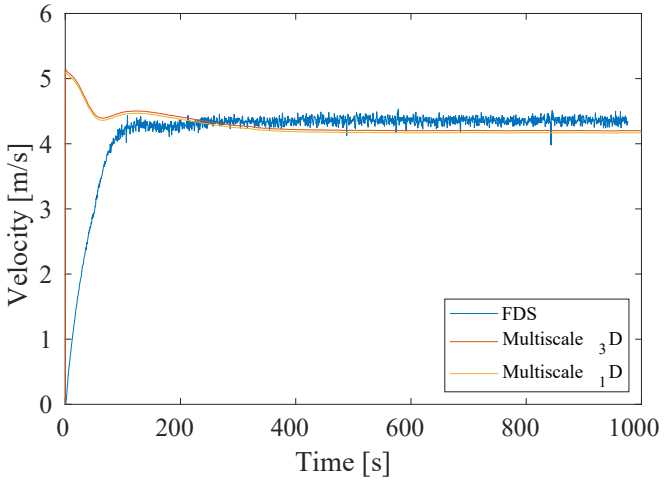

Figure 6.23: Dartford velocity at 687m distance to the tunnel upstream portal

The third point is placed 900m from the entrance portal. This point compares the FDS simulation with the 3D domain inside the multiscale. The main objective is to observe the differences of using FDS alone and coupled inside the multiscale model. The graphs are in figures 6.24, 6.25 and 6.26.

Figure 6.24 shows the pressure across the time 150 meters downstream of the fire. The oscillations in the pressure have appeared through the figures 6.20 and 6.22 for the FDS and 3D-multiscale. In this case the oscillations shown by the 3D domain in the multiscale are lower in amplitude than the oscillations of the FDS simulation. The reduction in the oscillations is related to the shorter region that most be simulated by the FDS inside the multiscale model. This reduced oscillations represent an improvement and they indicate that the simulation is steadier inside the multiscale.

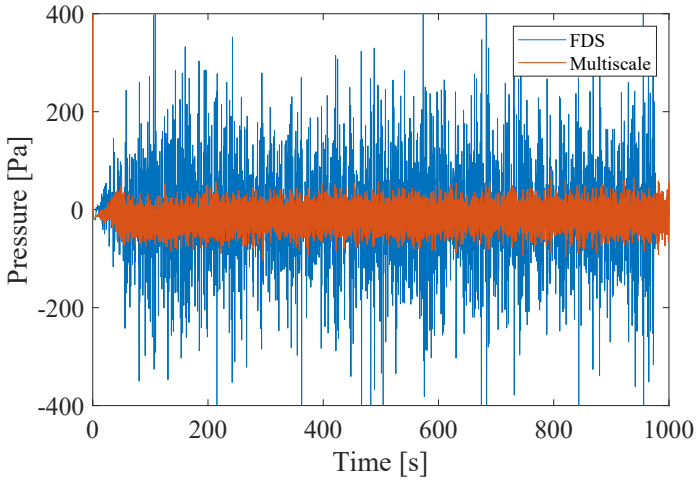

Figure 6.24: Dartford pressure at 900m distance to the tunnel upstream portal

The figure 6.25 shows the velocity at 150m downstream of the fire. Here the starting point of both graphs has the same trend as before but now both of them increase as the velocity downstream of the fire is higher than the cold flow velocity, for most of the downstream region. Both the velocities reach steady state after 300 seconds and settle in values similar to each other, with the FDS velocity being 0.2 to 0.3 m/s higher than the multiscale velocity.

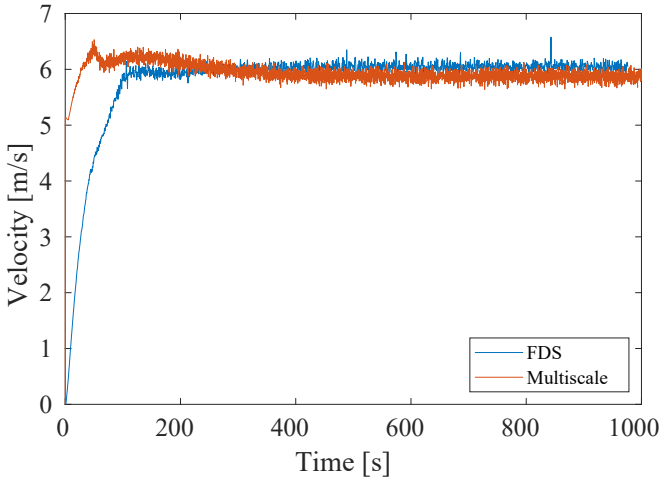

Figure 6.25: Dartford velocity at 900m distance to the tunnel upstream portal

The last graph for the section at 900m from the entrance portal of the tunnel is the figure 6.26 showing the temperature trend. Both of the curves start at environmental temperature, then as the fire starts the temperature grows up to 140 °C, getting its steady state in 130 °C with a difference among them of 3 to 5 °C. The temperature in this point is very accurate in the multiscale, with reference to the FDS simulation.

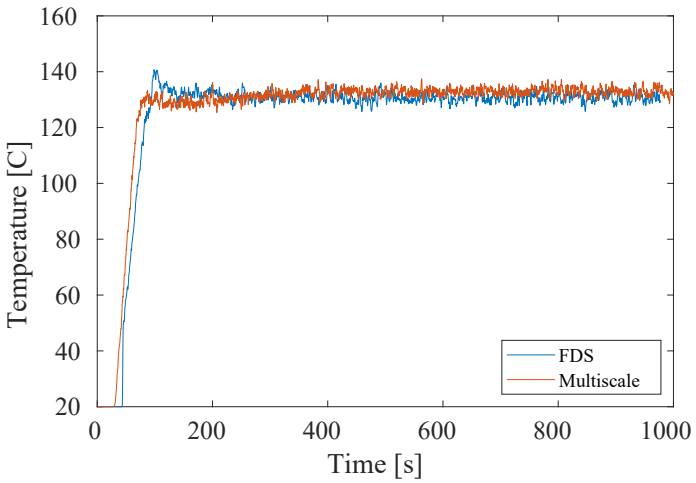

Figure 6.26: Dartford temperature at 900m distance to the tunnel upstream portal

The fourth point analyzed for this tunnel is the boundary between the 1D and 3D, in the multiscale, downstream of the fire. This point is placed 950 m downstream from the tunnel upstream portal and 200m downstream of the fire.

The figure 6.27 reports the pressure in the section against time. Here the trend of oscillating FDS simulations remains. In contrast, the pressure in the multiscale, both in the

1D and 3D, is steady and remains in the -10 Pa after 300 seconds. This figure confirms that the pressure exchange works correctly and without errors inside the multiscale.

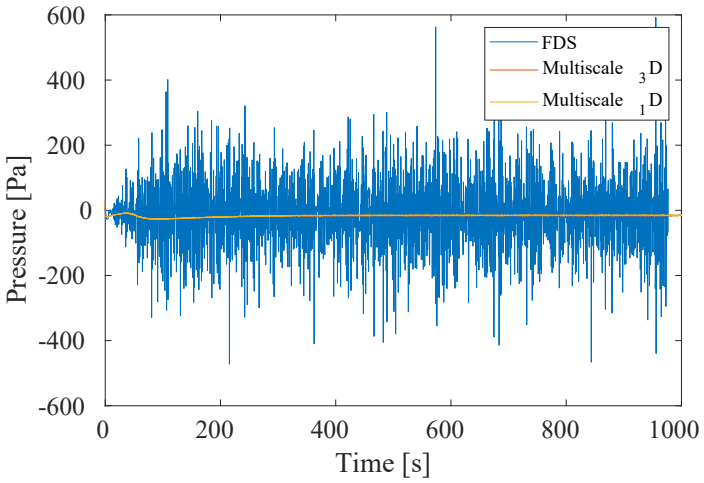

Figure 6.27: Dartford pressure at 950m distance to the tunnel upstream portal

Figure 6.28 shows the velocity. Two values are shown for the multiscale, the value in the 3D domain and the 1D domain, as they encounter in this boundary section. The velocities from the multiscale are superimposed one of top of the other, confirming that the exchange of flow conditions is managed in a correct way. With regards to the FDS velocity the multiscale velocity in this section is slightly lower, 0.2 to 0.4 m/s.

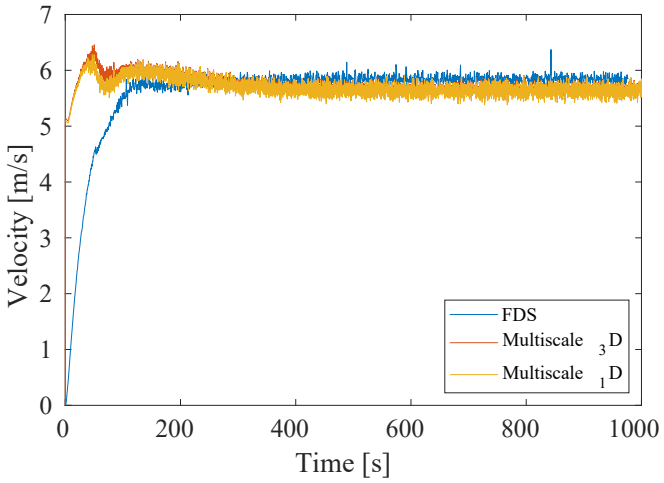

Figure 6.28: Dartford velocity at 949m distance to the tunnel upstream portal

The last comparison in the section 950 m away from the tunnel portal is in figure 6.29, and compares the temperature. In this case there is a small temperature difference

between the two multiscale domains (1D and 3D) lower than 5 °C. The origin of the difference, as mentioned in other boundary sections, is that the exchanged temperature, from the multiscale 3D to its 1D, is the mass flow averaged temperature and the temperature shown in graph (for the FDS and multiscale-3D) is the mass averaged temperature. The difference exists as there is more mass flow of hot air in the boundary (as the density is lower and, therefore, the velocity faster) than of cold air, making the average more influenced by the hotter temperatures of the upper area, than the other temperatures of the section.

Regarding the difference between the FDS and multiscale models, the FDS temperature has a difference of 2 or 3 °C with the multiscale-3D and 6 to 7 °C with the 1D multiscale temperature, maintaining the error low enough to still be considered equivalent.

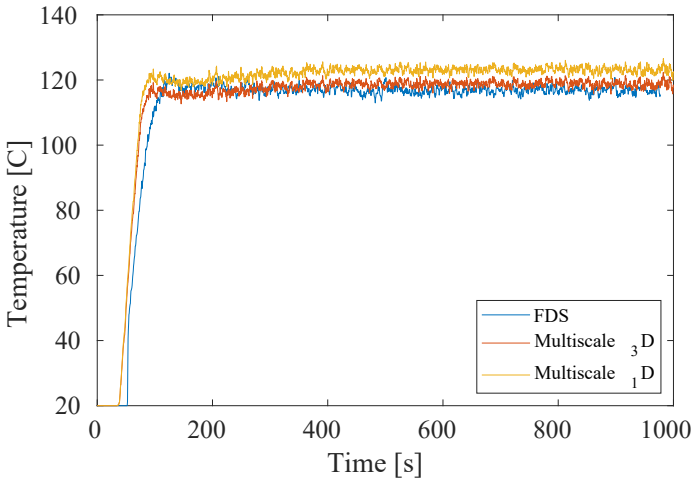

Figure 6.29: Dartford temperature at 950m distance to the tunnel upstream portal

The last analyzed point is placed 1050m from the upstream portal and 300m downstream of the fire. The figures compare the behavior of the 1D multiscale and the FDS in terms of pressure, temperature and velocity.

The figure 6.30 shows the pressure at 1050m from the tunnel entrance. Here the behavior is very similar to the equivalent graph in the first point (500m from the entrance), shown in figure 6.20. The FDS pressure oscillates with an amplitude of 400Pa around the 0, and the multiscale maintains a constant value that is always close to the average of the FDS pressure.

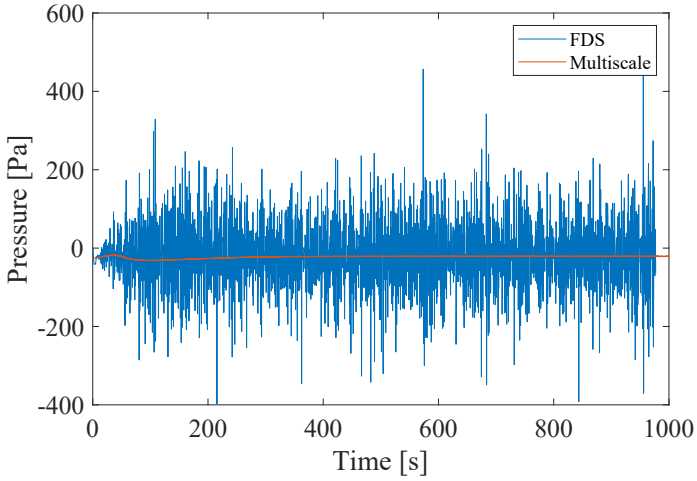

Figure 6.30: Dartford pressure at 1050m distance to the tunnel upstream portal

In terms of velocity, in figure 6.31, is possible to observe that the speed of the air in both of the cases remains within a 0.1 m/s of error. The error among this two can be considered neglectable.

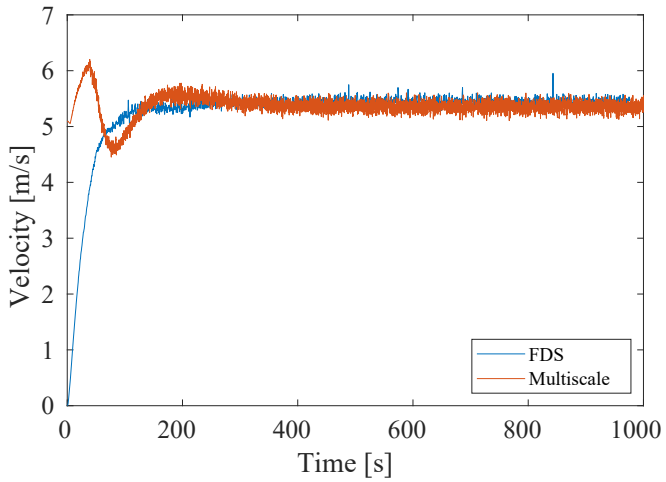

Figure 6.31: Dartford velocity at 1070m distance to the tunnel upstream portal

The last graph analyzed for the Dartford tunnel, figure 6.32, compares the temperature of the two simulations (FDS and multiscale). In this case, as seen in figure 6.19, the difference is more relevant, remaining close but below the 10 °C. This increased difference is related in part to the temperature difference that is introduced in the boundary, as explained before figure 6.29, and also to effects that are not taken into account in the 1D simulation. This because both of the wall configurations are inert walls at environment temperature, therefore, a part of the difference is related to radiation heat transfer

(as it is not turned of in the FDS calculations) or other effects not considered in the 1D model.

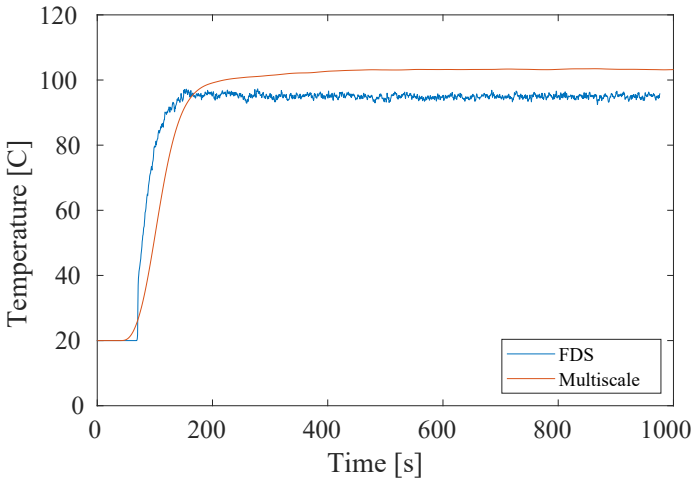

Figure 6.32: Dartford temperature at 1050m distance to the tunnel upstream portal

6.3 Observations

After analyzing the figures shown for both of the tunnels some observations are made.

6.3.1 2.6km test tunnel

First, having experimental data is not a guarantee of accuracy. Still, it helped greatly the setup of the test, by allowing the simulation of cold scenarios and confirming with the measurements that cold simulations for different amounts of fans returned values of velocity very similar to the ones reported by the anemometers through the tunnel.

Then, through the tests the objectives were to prove the capability of the Multiscale model to communicate the 1D and 3D models correctly and, mainly, to reproduce accurately the measurements obtained during the tests.

For the first three figures the discussion is centered in the communication quality. The figures show the values exchanged at the boundaries. For the three graphs the values obtained at each side of the boundaries are very similar among them, specially for the velocity, ensuring the mass conservation across the boundaries. In the case of the pressure values the upstream value is averaged over the last 50 calculations to avoid propagating the small oscilations coming from the 3D simulation into the 1D, therefore the exchanged values remains in close to the average of the 3D values. At last the temperature does have a difference among the curves, mainly caused by the small difference in the averaging of both values. Still the averaging in both is not changed, as the mass flow average in the 1D is used to keep the energy conservation, and in the

3D is used to obtain an output that is representative and easy to understand from the temperature.

The next two figures (figure 6.8 and figure 6.9) serve the purpose of showing the resemblance of the air velocity, measured and simulated, and the Temperature above the fire. In the case of the air velocity, the simulated output is close to the values obtained by the measurements, guaranteeing that the ventilation system works correctly. Then, the values of the temperature above the fire start an issue when it comes to cell averaging of values, as the values calculated in FDS are not interpolated for each point of the cell, and may average cold and hot zones that are close to each other, inside the same cell. Still, the temperatures reached the expected values at some points for figure 6.9 and are accurate in most of the simulations duration for the bars 3 and 4.

In the figures of the bars 3 and 4 (from figure 6.12 to figure 6.15) the temperatures obtained from the simulation resemble closely the values measured on the field. This agreement in values shows that the simulation is representative of the fire phenomena that was measured in the tunnel. Values in bars 3 and 4 are more appropriate to be compared as they are values taken in a zone were the temperature is more homogeneous across the space. These values also show the stratification of the flow at these points of the tunnel which is well reproduced by the test.

The capacity of reproducing the flow and stratification of the fumes in a multiscale simulation helps reaching the conclusion that the multiscale aproach is working correctly by reducing the time required to simulate the tunnel without increasing appreciably the error in the 3D simulation. The simulation took 33 and a half hour to complete, that for a tunnel 2.6 km long for 1000 seconds is not an excessive amount of time. Further reducing this calculation time is possible, and will be a point discussed for future developments.

6.3.2 ”Dartford Tunnel”

The Dartford tunnel shows a comparison between a simulation made completely with FDS, and a simulation made using the multiscale algorithm, that uses FDS close to the fire and a 1D algorithm in the rest of the tunnel. The objective of this test is demonstrating that it is reasonable to use the multiscale instead of a FDS simulation for long tunnels, as it will reduce the time needed (as seen in previous chapters), and not introduce relevant amounts of error with respect to the FDS simulation. To prove this the two simulations are first compared in the trend across the tunnel and then compared in different points. The sections that will be compared are 5 and each one of them compare a different part of the multiscale with the FDS.

Comparison across the tunnel

The three figures that compare the FDS and the multiscale with averaged values across the tunnel (from figure 6.17 to figure 6.19). Figure 6.17 shows that the pressure has the

same trend and a difference below 7Pa. Then, Figure 6.18 with again the same trend and a difference in velocity that passes from 0.3m/s (in the upstream portal) to 0.1 m/s (in the downstream portal). And at last, Figure 6.19 with the same trend in temperature, the first half of the domain with a negligible error and then an error accumulated from the difference in temperature average used in the exchange inside the multiscale and 3D effects non taken into account.

As a sum, the results over the tunnel are satisfactory for the multiscale. In the three variables the error is small, when compared with the FDS, and the temperature error can be fixed in the future by introducing the radiation or finding a way to relate the total losses in 3D with the losses in 1D.

Pressure sections across the tunnel

The pressure graphs are in figures 6.20, 6.22, 6.24, 6.27 and 6.30. The pressure across the tunnel shows two trends when it is in a graph against time. First, the FDS pressure oscillates between 200 and -200 Pa in all the points across the tunnel, changing the average value as seen in the pressure graph averaged in time. Second, the multiscale in the 1D shows steady values of pressure through the tunnel that are always close to the pressure average.

As a sum, the pressure provided by the multiscale, section by section, is always close to the FDS value, and has a steadier behavior in the 1D domain and downstream of the fire in the 3D.

Velocity sections across the tunnel

The velocity sections across the tunnel show simulations starting in 2 opposing conditions, one in no flow (FDS), and the other in cold flow (multiscale) conditions, and converging after 250 to 300 seconds to their steady value. This is satisfactory as the initial condition shows to be irrelevant for the comparison among the simulations. Also, the steady values of the FDS and the multiscale always remain between a small error of 0.4 m/s at max.

Temperature sections across the tunnel

The first two temperature sections are omitted as the curves remain constant in 20 °C during all the simulation. The three remaining analyzed section are the 900 m (figure 6.26), 950 m (figure 6.29) and 1050 m (figure 6.32). The temperature trends in the cases rise from 20 °C, the environment temperature, and reach steady temperature around 300 seconds into the simulation. The multiscale temperatures while inside the 3D domain are almost the same as in the FDS simulation. The differences between the FDS simulation and the multiscale are focused in the 1D area, as the losses of the multiscale are lower than the losses in FDS, obtaining as a result an overshoot in temperature of

around of 10 degrees Celsius. The reason of the difference in losses is vinculated to 3D effects not included into the 1D model, mainly.

Boundary interfaces of the multiscale

The boundaries between the 1D and 3D domains of the multiscale are analyzed in the sections at 700m from the upstream portal and 950m from the upstream portal. Both of the boundaries show agreeance between the values in the two sub-domains of the multiscale (the 1D and the 3D). The only exchanged value that shows a difference between the two domains is the downstream temperature, related to the difference in averages. As the temperature obtained through a mass weighted average (3D) and a mass flow weighted average (1D) are hardly equal if the flow is not homogeneous.

Chapter 7

Conclusions

7.1 Conclusions

During this work the main focus has been demonstrating the improvements introduced to the multiscale model that I have been developing over the last years.

The multiscale model that is under development presented several challenges along the research. The issues were faced, first, by improving the compilation of the software, modifying the group of files to be compilated in a MPI Gnu linux environment, achieving time reductions in both compilation and execution. Then, the pressure issues were confronted by developing a pressure equivalent method that demonstrated that the FDS calculations issues were focused in the pressure and that the other properties of the flow could be used to calculate the pressure to compensate this problem. Then, a collaboration, with the FDS developers, was initiated during which different strategies were tried to fix the pressure problems. As a result the FDS pressure solver used was changed, obtaining reasonable pressure results. At last, problems in the boundary exchange between the 3D and 1D domains of the simulations were solved by upgrading the exchange between the models. The method used to pass the pressure information from the 1D to the 3D was changed, achieving a boundary that lets the flow continue unperturbed.

To show these improvements different simulation results have been included in the last four chapters of this work. The chapter 3 demonstrates the improvement regarding the simulation times needed to obtain results from the tunnel simulations. The chapter 4 focuses in the research that verifies the output of the 3D part of the simulation, given by FDS. The chapter 5, focuses in studying the pressure calculation across tunnels and the particularities of the different solvers, determining a solver capable of finding the most accurate solution for tunnel simulations. The chapter 6 focuses in tests that compare the multiscale results against measurements (and simulations) to evidence that it is an alternative that will reduce simulation times without inserting relevant amounts of errors into the calculation.

7.1.1 Calculation time reduction

This chapter showed the capabilities of the multiscale to reduce the calculation time needed to complete tunnel fire simulations. The tests in the chapter use a small theoretical tunnel as test case and simulate a small fire (2 MW) inside of it to compare the time needed to simulate it. The tunnel is divided in a 3D domain placed in the center, containing the fire, and two 1D domains placed upstream and downstream of the first domain. Four multiscale cases are simulated, with different proportions of 1D and 3D domain to observe the sensitivity that the results and simulation time have to the 1D-3D proportions of the tunnel.

The tests results exhibit a simulation time reduction that is proportional to the percentage simulated into the 1D. Furthermore, connecting the simulation times needed and the percentages of 1D in the simulations is possible to observe that the time reduction is mostly linear. And, if this reduction is compared to a linear time reduction trend going from the maximum simulation time length (100% 3D) to a theoretical minimum of 0 (100% 1D), both of the curves are closely related and only separated by a small amount of time that groups the 1D model execution and communication among the models.

This confirms that the multiscale simulation is capable of providing a simulation time reduction. Then, comparing the pressure, velocity and temperature trends across the tunnel we can also affirm that the error introduced in the flow properties is acceptable. Only one of the simulations shows high amounts of error, caused by a multiscale simulation that has an excessively short 3D domain, placing the downstream boundary in a zone that is not homogeneous enough to support this boundary.

In conclusion, the multiscale manages to reduce the simulation time without being an important source of error.

7.1.2 Pressure equivalent model

From the start of my research pressure modelling, in tunnel fires, has always been a tough topic to take on. The research regarding tunnel fires mainly focuses on velocity and temperature tests. It is understandable, as the measurements from thermocouples and anemometers are more common and related to the main topics researched in tunnels, heat release rate of the fires and backlayering. Still, some attention was put into the pressure trend through the tunnels.

Examining FDS tunnel fire simulations and comparing them to Fluent and FDS heat source simulations we found that the velocity and temperature were similar and even have the same trends in their distribution, but that the pressure presented some inconsistencies. Pressure drops were reported to double the expected values for areas downstream of the fires using the default FDS configuration in fire simulations.

An equivalent model was developed to calculate an accurate pressure field using the other properties provided by the FDS. The model is based in the Bernoulli equation and uses velocity derivatives, densities and viscosity to approximate the pressure losses

across the tunnel. The pressure results of this model where compared with the other reference simulations proving that the properties obtained from FDS were correct, but there was some source of error accumulating in the pressure that made the pressure output unfeasible.

Therefore, at the end of this chapter the reliability of the FDS results was proved for most of its output properties, but the pressure.

7.1.3 Pressure modelling analysis

More research and testing was carried out, now with the help of the FDS developers, to find an answer to the pressure problems in tunnels that the FDS was presenting. Different settings were evaluated to observe their influence in the pressure results, as the divergence, the specific heat ratio, among others. But the setting showing an alternative to improve the pressure results was the change of pressure solver.

The simulations of Ang in [1], served as a good case study to keep researching the pressure issues and finding that the change in pressure solver offered an alternative that reduced pressure and mass flow oscillations along the tunnel. Using UGLMAT from this point onwards guarantees reasonable pressure trends with the downside of slightly longer simulations, disadvantage that the multiscale simulation inherently reduces.

7.1.4 Multiscale tests

After solving the issues surrounding the pressure and duration of the multiscale simulations modifications were applied to the data exchange in the multiscale boundaries.

The distribution of the pressure exchanged downstream of the fire was changed from uniform to a distribution that emulates the pressure layout of the 5% of the tunnel length previous to the boundary. Using a distribution similar to the one that the flow has manages to reduce the perturbations introduced.

The 1D mode changed from being iterated every ”n” seconds of the 3D simulation to being iterated in every 3D iteration. In this way the lag of data between one model and the other is eliminated. Still, and average on time is conserved in the upstream pressure exchange to eliminate pressure oscillations in the 1D region.

Mass flow weighted averages were introduced to respect the conservation of energy, momentum and mass.

Using all the modifications mentioned 2 simulations were realized, 1 comparing the results to measurements from a tunnel test, and the other comparing the results to a FDS simulations.

Test Tunnel

In this case, measurements from a ventilation system test were used to reproduce the test in a simulation and compare the results. The simulation has a 2.6 km long tunnel

with a 4 MW fire close to its center. First, the exchange of data between the two models (3D and 1D) is shown to be accurate by comparing their instantaneous values against time, and then the output of the simulation is compared to the different measuring devices across the tunnel. The tunnel air velocity and temperature in the measurements 30 m and 130 m downstream of the fire are accurate with respect to the measured values. Instead, values in the volume above the fire compared to the measurements on top of the fire pools show the same trends but lower values, in the case of the simulation. This error in the zone close to the fire is caused by the non-uniform distribution of the temperature, where the measurements on the field are capable of measuring a point in the space, and the output in the simulation reflects the average temperature of a whole cell. The results of this test are succesful as they demonstrate that the multiscale model is capable of reproducing a real life fire test.

Dartford tunnel test

Using the Dartford tunnel 2 simulations where done, one with FDS and the other with the multiscale model. The different curves of pressure, temperature and velocity, for the whole tunnel and sections of it where used to compare the results. In the graphs across the tunnel the same trends were observed, with slightly lower pressures in the middle section of the tunnel, low velocities in the first half of the tunnel lenght and temperatures 10 °C higher in the end of the tunnel. Analyzing 5 different sections across the tunnel it is evident that the pressure output for the multiscale is steadier, showing less oscillations in 4 out of 5 spots. In the case of the velocity and temperature the values always took similar times to reach steady state condition and converged to values with small differences among them, that only increased in the case of the temperature towards the end of the tunnel. The differences found in the three variables (Pressure, Velocity and Temperature) are small and the comparison is considered satisfactory as it doesn't introduce important sources of error.

7.2 Future developments

The work developed so far has managed to improve several of the core aspects of the multiscale model. Still, some other aspects, being them of vital importance or more secondary relevance, can still be improved in future version of the model. Among them:

- Multimesh 3D modelling inside the multiscale: so far the multiscale only can manage single mesh calculation inside its 3D (FDS) core calculation. This upgrade would capacitate the multiscale to use the recent developments in tunnel preconditioning in FDS and achieve further time reductions, which is its main goal.

- Improvement of the thermal losses model: as high temperatures enter the tunnel

error accumulates gradually across the tunnel, due to phenomena as radiation. Compensating this losses will yield a much more accurate thermal model.

- Development of a verification set of cases capable of determining if any changes have harmed the model accuracy.
- Script cleaning, optimizing and formatting change to fit FDS code.

Bibliography

[1] C. Ang, G. Rein, and J. Peiro. "Unexpected Oscillations in Fire Modelling Inside a Long Tunnel." In: *Fire Technology* 56.5 (2020), pp. 1931–1941.

[2] Chin Ding (Edmund) Ang et al. "Simulating longitudinal ventilation flows in long tunnels: Comparison of full CFD and multi-scale modelling approaches in FDS6." In: *Tunnelling and Underground Space Technology* 52.Supplement C (Feb. 2016), pp. 119–126. ISSN: 0886-7798. DOI: 10.1016/j.tust.2015.11.003. URL: http://www.sciencedirect.com/science/article/pii/S0886779815302613 (visited on 10/13/2017).

[3] European Automobile Manufacturers Association. *ACEA Report Vehicles in use Europe 2018*. European Automobile Manufacturers Association. Nov. 13, 2018. URL: https://www.acea.be/statistics/article/report-vehicles-in-use-europe-2018.

[4] European Automobile Manufacturers Association. *ACEA Report Vehicles in use Europe 2018*. European Automobile Manufacturers Association. Nov. 13, 2018. URL: https://www.acea.be/statistics/article/report-vehicles-in-use-europe-2018.

[5] Wang Binbin. "Comparative Research on FLUENT and FDS's Numerical Simulation of Smoke Spread in Subway Platform Fire." In: *Procedia Engineering*. ISMSSE2011 26 (Jan. 2011), pp. 1065–1075. ISSN: 1877-7058. DOI: 10.1016/j.proeng.2011.11.2275. URL: http://www.sciencedirect.com/science/article/pii/S1877705811051186 (visited on 05/28/2019).

[6] M. Chandrasekar and F. Wong. "Thermodynamic system analysis - a graph-theorethic approach." In: *Energy* 7.6 (1982), pp. 539–566.

[7] Hue-Pei Chang et al. "Performance of a spray system in a full-scale tunnel fire test." In: *Tunnelling and Underground Space Technology* 67.Supplement C (Aug. 2017), pp. 167–174. ISSN: 0886-7798. DOI: 10.1016/j.tust.2017.04.022. URL: http://www.sciencedirect.com/science/article/pii/S0886779816302474 (visited on 10/06/2017).

[8] L. H. Cheng, T. H. Ueng, and C. W. Liu. "Simulation of Ventilation and fire in the underground facilities." In: *Fire Safety Journal* 36.6 (2001), pp. 597–619.

[9] W. K. Chow et al. "A study on tilted tunnel fire under natural ventilation." In: *Fire Safety Journal* 81.Supplement C (Apr. 2016), pp. 44–57. ISSN: 0379-7112. DOI: 10.1016/j.firesaf.2016.01.014. URL: http://www.sciencedirect.com/science/article/pii/S0379711216300108 (visited on 10/19/2017).

[10] W. K. Chow et al. "Smoke movement in tilted tunnel fires with longitudinal ventilation." In: *Fire Safety Journal* 75 (July 2015), pp. 14–22. ISSN: 0379-7112. DOI: 10.1016/j.firesaf.2015.04.001. URL: http://www.sciencedirect.com/science/article/pii/S0379711215000533 (visited on 05/28/2019).

[11] F. Colella et al. "Calculation and design of tunnel ventilation systems using a two-scale modelling approach." In: *Building and environment* 44.12 (2009), pp. 2357–2367.

[12] Francesco Colella. "Multiscale Modelling of Tunnel Ventilation Flows and Fires." en. In: (May 2010). URL: https://www.era.lib.ed.ac.uk/handle/1842/3528 (visited on 04/07/2019).

[13] Francesco Colella et al. "A Novel Multiscale Methodology for Simulating Tunnel Ventilation Flows During Fires." en. In: *Fire Technology* 47.1 (Jan. 2011), pp. 221–253. ISSN: 0015-2684, 1572-8099. DOI: 10.1007/s10694-010-0144-2. URL: https://link.springer.com/article/10.1007/s10694-010-0144-2 (visited on 10/30/2017).

[14] Francesco Colella et al. "Multiscale modeling of transient flows from fire and ventilation in long tunnels." In: *Computers & Fluids* 51.1 (Dec. 2011), pp. 16–29. ISSN: 0045-7930. DOI: 10.1016/j.compfluid.2011.06.021. URL: http://www.sciencedirect.com/science/article/pii/S004579301100209X (visited on 10/18/2017).

[15] European Commission. *VIRTUAL Real Time Emergency Simulator*. European Commission. June 13, 2005. URL: https://cordis.europa.eu/project/id/IST-2000-29266.

[16] Sara Cosentino. *Innovative Modelling Approaches for the design, operation and control of complex energy systems with applications to underground infrastructures. Ph.D. Thesis*. Torino: Politecnico di Torino, 2016.

[17] Sara Cosentino et al. "Large eddy simulation of compartment fires." In: *International Symposium on Advances in Computational Heat Transfer* (2017).

[18] M.G. Culshaw, V.I. Osipov, and S.J. Booth. *Environmental Security of the European Cross-Border Energy Supply Infrastructure*. Springer, 2016.

[19] Colella F et al. "Time-dependent Multiscale Simulations of Fire Emergencies in Longitudinally Ventilated Tunnels." en. In: *Fire Safety Science* 10 (2011), pp. 359–372. URL: https://www.iafss.org/publications/fss/10/359 (visited on 04/07/2019).

[20] FDS and Smokeview Discussions, eds. *Issues with Pressure in tunnel fires*. Nov. 2018. URL: https://groups.google.com/g/fds-smv/c/ZKrjeLASnQU/m/J_8N4_wABAAJ.

[21] FDS and Smokeview Discussions, eds. *Oscillating mass flow along tunnel*. Aug. 2014. URL: https://groups.google.com/g/fds-smv/c/rCVKP14K8kU/m/ziYUfF9CahYJ.

[22] FDS and Smokeview Discussions, eds. *Pressure rise induced by fires in tunnels*. Aug. 2017. URL: https://groups.google.com/g/fds-smv/c/H5BL3j9j4aM/m/Pwih-19HCAAJ.

[23] J. Floyd, S. Hunt, and F. Williams. "A Network Fire Model for the simulation of fire growth and smoke spread in multiple compartments with complex ventilation." In: *Journal of fire protection engineering* 15.3 (2005), pp. 199–299.

[24] Martin J. Gander. "Schwarz methods over the course of time." In: *Electronic Transactions on Numerical Analysis* 31 (2008).

[25] Christopher Greenshields. *OpenFOAM User Guide*. CFD Direct Ltd., 2020.

[26] Xiaoping Guo and Qihui Zhang. "Analytical solution, experimental data and CFD simulation for longitudinal tunnel fire ventilation." In: *Tunnelling and Underground Space Technology* 42 (May 2014), pp. 307–313. ISSN: 0886-7798. DOI: 10.1016/j.tust.2014.03.011. URL: http://www.sciencedirect.com/science/article/pii/S0886779814000467 (visited on 05/28/2019).

[27] Ali Haghighat, Kray Luxbacher, and Brian Y. Lattimer. "Development of a Methodology for Interface Boundary Selection in the Multiscale Road Tunnel Fire Simulations." en. In: *Fire Technology* 54.4 (July 2018), pp. 1029–1066. ISSN: 1572-8099. DOI: 10.1007/s10694-018-0724-0. URL: https://doi.org/10.1007/s10694-018-0724-0 (visited on 04/05/2019).

[28] Horst Hejny. "The European project UpTun: Results of four years of research to improve the level of fire safety in existing tunnels." In: vol. 94. June 2007, pp. 191–204. ISBN: 9781845640682. DOI: 10.2495/SAFE070191.

[29] Charles Hirsch. *Numerical computation of internal and external flows*. John Wiley and Sons, 2007.

[30] Simo Hostikka et al. *Fire Dynamics Simulator, User Guide*. Gaithersburg, Maryland: National Institute of Standards and Technology, 2020.

[31] Simo Hostikka et al. *Fire Dynamics Simulator, Validation Guide*. Gaithersburg, Maryland: National Institute of Standards and Technology, 2020.

[32] Simo Hostikka et al. *Fire Dynamics Simulator, Verification Guide*. Gaithersburg, Maryland: National Institute of Standards and Technology, 2020.

[33] Simo Hostikka et al. *Fire Dynamics Technical Reference Guide*. Gaithersburg, Maryland: National Institute of Standards and Technology, 2020.

[34] L. H. Hu, W. Peng, and R. Huo. "Critical wind velocity for arresting upwind gas and smoke dispersion induced by near-wall fire in a road tunnel." In: *Journal of Hazardous Materials* 150.1 (Jan. 2008), pp. 68–75. ISSN: 0304-3894. DOI: 10.1016/j.jhazmat.2007.04.094. URL: http://www.sciencedirect.com/science/article/pii/S0304389407005699 (visited on 05/28/2019).

[35] C. C. Hwang and J. C. Edwards. "The critical ventilation velocity in tunnel fires—a computer simulation." In: *Fire Safety Journal* 40.3 (Apr. 2005), pp. 213–244. ISSN: 0379-7112. DOI: 10.1016/j.firesaf.2004.11.001. URL: http://www.sciencedirect.com/science/article/pii/S0379711204001109 (visited on 04/04/2019).

[36] Haukur Ingason, Ying Li, and Anders Lönnermark. *Tunnel Fire Dynamics*. 1st ed. New York: Springer, 2015. DOI: 10.1007/978-1-4939-2199-7.

[37] Haukur Ingason, Ying Zhen Li, and Anders Lönnermark. "Runehamar tunnel fire tests." In: *Fire Safety Journal* 71.Supplement C (Jan. 2015), pp. 134–149. ISSN: 0379-7112. DOI: 10.1016/j.firesaf.2014.11.015. URL: http://www.sciencedirect.com/science/article/pii/S0379711214001660 (visited on 10/06/2017).

[38] Haukur Ingason, Anders Lönnermark, and Ying Zhen Li. "Model of ventilation flows during large tunnel fires." In: *Tunnelling and Underground Space Technology* 30.Supplement C (July 2012), pp. 64–73. ISSN: 0886-7798. DOI: 10.1016/j.tust.2012.02.007. URL: http://www.sciencedirect.com/science/article/pii/S0886779812000399 (visited on 10/20/2017).

[39] A. Jenft et al. "Experimental and numerical study of pool fire suppression using water mist." In: *Fire Safety Journal* 67 (July 2014), pp. 1–12. ISSN: 0379-7112. DOI: 10.1016/j.firesaf.2014.05.003. URL: http://www.sciencedirect.com/science/article/pii/S0379711214000587 (visited on 04/05/2019).

[40] Yi Jiang, Camille Allocca, and Qingyan Chen. "Validation of CFD Simulations for Natural Ventilation." In: *International Journal of Ventilation* 2.4 (Apr. 2004), pp. 359–369. ISSN: 1473-3315. DOI: 10.1080/14733315.2004.11683678. URL: https://doi.org/10.1080/14733315.2004.11683678 (visited on 05/29/2019).

[41] W. Jones and G. Forney. *A programmer's reference manual for CFAST, the useful model of fire growth and smoke transport*. Gaithersburg, Maryland: National Institute of Standards and Technology, 1990.

[42] B. Karlsson and J. Quintiere. *Enclosure fire dynamics*. CRC press, 2000.

[43] Susanne Kilian. "ScaRC is ready for use in FDS." In: *Fire and Evacuation Modeling Technical Conference* (2018).

[44] Susanne Kilian. "The FDS pressure equation: Intuitive understanding and solution strategies." In: *Fire and Evacuation Modeling Technical Conference* (2020).

[45] Esther Kim, John P. Woycheese, and Nicholas A. Dembsey. "Fire Dynamics Simulator (Version 4.0) Simulation for Tunnel Fire Scenarios with Forced, Transient, Longitudinal Ventilation Flows." en. In: *Fire Technology* 44.2 (June 2008), pp. 137–166. ISSN: 1572-8099. DOI: 10.1007/s10694-007-0028-2. URL: https://doi.org/10.1007/s10694-007-0028-2 (visited on 05/29/2019).

[46] Ying Zhen Li and Haukur Ingason. "Effect of cross section on critical velocity in longitudinally ventilated tunnel fires." In: *Fire Safety Journal*. Fire Safety Science: Proceedings of the 12th International Symposium 91.Supplement C (July 2017), pp. 303–311. ISSN: 0379-7112. DOI: 10.1016/j.firesaf.2017.03.069. URL: http://www.sciencedirect.com/science/article/pii/S0379711217300905 (visited on 10/05/2017).

[47] Ying Zhen Li and Haukur Ingason. "Influence of fire suppression on combustion products in tunnel fires." In: *Fire Safety Journal* 97 (Apr. 2018), pp. 96–110. ISSN: 0379-7112. DOI: 10.1016/j.firesaf.2017.06.011. URL: http://www.sciencedirect.com/science/article/pii/S0379711217304757 (visited on 04/05/2019).

[48] Ying Zhen Li et al. "Effect of cross section and ventilation on heat release rates in tunnel fires." In: *Tunnelling and Underground Space Technology* 51.Supplement C (Jan. 2016), pp. 414–423. ISSN: 0886-7798. DOI: 10.1016/j.tust.2015.09.007. URL: http://www.sciencedirect.com/science/article/pii/S0886779815301000 (visited on 10/17/2017).

[49] P. Lin, S. M. Lo, and T. Li. "Numerical study on the impact of gradient on semi-transverse smoke control system in tunnel." In: *Tunnelling and Underground Space Technology* 44 (Sept. 2014), pp. 68–79. ISSN: 0886-7798. DOI: 10.1016/j.tust.2014.07.011. URL: http://www.sciencedirect.com/science/article/pii/S0886779814001096 (visited on 05/28/2019).

[50] Igor Y. Maevski. *Design Fires in Road Tunnels*. Washington, DC: Transportation Research Board, 2011.

[51] T. Mattson, B. Sanders, and B. Massingill. *Patterns for parallel programming*. Addison-Wesley, 2005.

[52] Kevin McGrattan and Anthony Hamins. "Numerical Simulation of the Howard Street Tunnel Fire." en. In: *Fire Technology* 42.4 (Oct. 2006), pp. 273–281. ISSN: 1572-8099. DOI: 10.1007/s10694-006-7506-9. URL: https://doi.org/10.1007/s10694-006-7506-9 (visited on 04/04/2019).

[53] Elizabeth Olson. *128 Missing in Swiss Tunnel Fire; 11 Confirmed Dead*. New York Times. Oct. 26, 2001. URL: https://www.nytimes.com/2001/10/26/world/128-missing-in-swiss-tunnel-fire-11-confirmed-dead.html.

[54] Technical Committee 3.3 Road Tunnel Operation. *Design fire characteristics for road tunnels*. PIARC. 2016.

[55] Technical Committee 3.3 Road Tunnel Operation. *Experience with Significant Incidents in Road Tunnels*. PIARC. 2016.

[56] S. V. Patankar. *Numerical heat transfer and fluid flow*. Hemisphere publishing, 1980.

[57] R. Peacock et al. *CFAST Consolidate Fire and Smoke Transport, Technical Reference Guide*. Gaithersburg, Maryland: National Institute of Standards and Technology, 2019.

[58] U. Piomelli. "Large-eddy simulation: achievements and challenges." In: *Progress in Aerospace sciences* 35.4 (1999), pp. 335–362.

[59] R. G. Rehm and H. R. Baum. "The equations of motion for thermally driven, buoyant flows." In: *Journal of research of the NBS* (1978).

[60] Transport Research, Innovation Monitoring, and Information System. *Safety in tunnels Thematic Network*. Transport Research, Innovation Monitoring, and Information System. May 7, 2006. URL: https://trimis.ec.europa.eu/project/safety-tunnels-thematic-network#tab-docs.

[61] I. Riess, M. Bettelini, and R. Brandt. "SPRINT a desing toll for fire ventilation." In: *Proceedings of aerodynamics and ventilation of vehicle tunnels* (2000).

[62] H. Satoh, H. Kurioka, and O. Sugawa. "Flame Inclination with Induced Wind through Inlet Opening in a Tall and Narrow Atrium." In: *Fire safety science proceedings of the fifth international symposium* (1997), pp. 273–284.

[63] Statista. *Motorway infrastructure in Italy*. Statista. 2018.

[64] F. Tang et al. "Maximum temperature beneath the ceiling in tunnel fires with combination of ceiling mechanical smoke extraction and longitudinal ventilation." In: *Tunnelling and Underground Space Technology* 68.Supplement C (Sept. 2017), pp. 231–237. ISSN: 0886-7798. DOI: 10.1016/j.tust.2017.05.029. URL: http://www.sciencedirect.com/science/article/pii/S0886779816308392 (visited on 10/06/2017).

[65] H. S. Tang, R. D. Haynes, and G. Houzeaux. "A Review of Domain Decomposition Methods for Simulation of Fluid Flows: Concepts, Algorithms, and Applications." In: *Archives of Computational Methods in Engineering* (2020).

[66] Andrea Toselli and Olof Widlund. *Domain Decomposition Methods - Algorithms and Theory*. Springer Berlin Heidelberg, 2005.

[67] A. Trouvé and Y. Wang. "Large eddy simulation of compartment fires." In: *International Journal of computational fluid dynamics* 24.10 (2010), pp. 449–466.

[68] Technical Committee 5 Road Tunnels. *Fire and smoke control in tunnels*. PIARC. 1999.

[69] Karim Van Maele and Bart Merci. "Application of RANS and LES field simulations to predict the critical ventilation velocity in longitudinally ventilated horizontal tunnels." In: *Fire Safety Journal* 43.8 (Nov. 2008), pp. 598–609. ISSN: 0379-7112. DOI: 10.1016/j.firesaf.2008.02.002. URL: http://www.sciencedirect.com/science/article/pii/S0379711208000179 (visited on 05/28/2019).

[70] Vittorio Verda, Adriano Sciacovelli, and Romano Borchiellini. *Numerical design of thermal systems*. C.L.U.T, 2015.

[71] Izabella Vermesi et al. "Reducing the computational requirements for simulating tunnel fires by combining multiscale modelling and multiple processor calculation." In: *Tunnelling and Underground Space Technology* 64 (Apr. 2017), pp. 146–153. ISSN: 0886-7798. DOI: 10.1016/j.tust.2016.12.016. URL: http://www.sciencedirect.com/science/article/pii/S0886779815303400 (visited on 10/12/2017).

[72] C. Wade and J. Barnett. "A Room-Corner Fire Model including fire growth on linings and enclosure smoke-filling." In: *Journal of Fire Protection engineering* 8.4 (1996), pp. 183–193.

[73] Jonathan Wahlqvist and Patrick van Hees. "Validation of FDS for large-scale well-confined mechanically ventilated fire scenarios with emphasis on predicting ventilation system behavior." In: *Fire Safety Journal*. Special Issue on PRISME – Fire Safety in Nuclear Facilities 62 (Nov. 2013), pp. 102–114. ISSN: 0379-7112. DOI: 10.1016/j.firesaf.2013.07.007. URL: http://www.sciencedirect.com/science/article/pii/S0379711213001185 (visited on 05/29/2019).

[74] X. Y. Wang, M. J. Spearpoint, and C. M. Fleischmann. "Investigation of the effect of tunnel ventilation on crib fires through small-scale experiments." In: *Fire Safety Journal* 88.Supplement C (Mar. 2017), pp. 45–55. ISSN: 0379-7112. DOI: 10.1016/j.firesaf.2017.01.002. URL: http://www.sciencedirect.com/science/article/pii/S0379711217300024 (visited on 10/19/2017).

[75] Yan Fu Wang et al. "Full-scale fire experiments and simulation of tunnel with vertical shafts." In: *Applied Thermal Engineering* 105 (July 2016), pp. 243–255. ISSN: 1359-4311. DOI: 10.1016/j.applthermaleng.2016.05.153. URL: http://www.sciencedirect.com/science/article/pii/S1359431116308328 (visited on 04/04/2019).

[76] Miao-cheng Weng et al. "Prediction of backlayering length and critical velocity in metro tunnel fires." In: *Tunnelling and Underground Space Technology* 47 (Mar. 2015), pp. 64–72. ISSN: 0886-7798. DOI: 10.1016/j.tust.2014.12.010. URL: http://www.sciencedirect.com/science/article/pii/S0886779815000048 (visited on 05/28/2019).

[77] Miao-cheng Weng et al. “Study on the critical velocity in a sloping tunnel fire under longitudinal ventilation.” In: *Applied Thermal Engineering* 94 (Feb. 2016), pp. 422–434. ISSN: 1359-4311. DOI: 10.1016/j.applthermaleng.2015.10.059. URL: http://www.sciencedirect.com/science/article/pii/S1359431115011060 (visited on 12/12/2018).

[78] Y. Wu and M. Bakar. “Control of smoke flow in tunnel fires using longitudinal ventilation systems - a study of the critical velocity.” In: *Fire safety journal* 35.4 (2000), pp. 363–390.

This Ph.D. thesis has been typeset by means of the TEX-system facilities. The typesetting engine was LuaLATEX. The document class was `toptesi`, by Claudio Beccari, with option `tipotesi=scudo`. This class is available in every up-to-date and complete TEX-system installation.